

Coordination between cell growth, division and chromosome replication cycles in mycobacteria

Présentée le 30 juillet 2021

Faculté des sciences de la vie
Unité du Prof. McKinney
Programme doctoral en biotechnologie et génie biologique

pour l'obtention du grade de Docteur ès Sciences

par

Gaëlle Madeleine VUARIDEL

Acceptée sur proposition du jury

Prof. A. L. A. Persat, président du jury
Prof. J. McKinney, Dr N. Dhar, directeurs de thèse
Prof. P. Viollier, rapporteur
Prof. J.-W. Veening, rapporteur
Prof. V. Simanis, rapporteur

Acknowledgements

I would like to thank many people without whom this thesis would not have been possible.

I would like to thank my thesis director Prof. **John McKinney**, who believed in me and gave me the opportunity to work in his lab. It was really captivating to try to solve genetic puzzles with you. Thanks a lot for all the time you invested to improve my manuscripts and to reply to reviewers, time during which you taught me tons of valuable things. I also would like to thank you for the freedom you gave me to explore the subjects that I found of interest, while giving me the right pushes and suggestions I needed to make my work more significant. Thank you, John!

Thank you to my thesis co-director, Dr. **Neeraj Dhar** who was always readily there to answer all my questions and helped me with all the “scary” wet lab experiments. I enjoyed our discussions, which often ended up in really interesting brainstorming. Thank you for all your support and kindness Neeraj! I would not have made it this far without you.

Thank you very much to the members of my jury, Prof. **Alexandre Persat**, Prof. **Patrick Viollier**, Prof. **Jan-Willem Veening**, and Prof. **Viesturs Simanis** for their time and interesting feedbacks.

I had the pleasure to meet wonderful people in the McKinney lab and I would like to thank every one of them. They all contributed to make the lab a nice place to work. In particular, I would like to thank Dr. **Katrin Schneider**, for sharing her knowledge and experience with me. Talking with you was always captivating, no matter the subject. I would like to thank Dr. **Paul Murima**, who was my faithful « desk mate». Desk that never found a true owner after you left. Thank you, Paul, for all the constructive discussions! I would also like to thank Dr. **Melanie Hannebelle**, a wonderful person who shares my interest in NETO.

There is also my master thesis lab, which holds a special place in my heart: **the UPSIM lab**. I would like to thank all of you for the regular lunches, your good mood and your good science. A special thank to Dr. **Andréa Krapp** for all your advices and for your friendship.

During my studies, I met a great scientist who became a close friend. A warm thank you to Dr. **Mahé Raccaud** with whom I had nice scientific discussions but with whom I also shared all my states of mind during welcomed tea breaks.

I also thank **my parents** who made me who I am today and who always pushed me to work hard.

Thank you all, my dear **in-laws**, for your support and kindness. Thank you also for all the times you cared for my beloved daughters, Alix and Moïra, while I was working.

Finally, and most importantly, thank you my dear husband **Ambroise**, for your constant and unconditional love and support. I apologize for making α MG, DnaN, ParB, and all their friends a big part of our lives.

Abstract

Propagation of microorganisms is based on three fundamental processes: cell growth, DNA replication, and cell division. Although important for antibacterial drug development, these processes are poorly understood in Actinobacteria, a medically important phylum that includes *Mycobacterium tuberculosis*. Using microfluidic cultures and time-lapse microscopy, we studied single-cell growth, DNA replication, and cell division in the model organism *Mycobacterium smegmatis*.

M. smegmatis is rod-shaped and grows by tip elongation in a biphasic manner due to a “new end take-off” (NETO) event. We find that pole elongation speed is increased and NETO occurs earlier in fast-growing cells than in slow-growing cells. As a consequence of variable timing of NETO, single-cell growth can be monophasic, biphasic, or triphasic. We propose that cells optimize pole growth speed and the timing of NETO to maximize their overall growth.

We show that fast-growing cells initiate DNA replication earlier than slow-growing cells. We also find that single-cell growth speed is linked to cell-cycle progression, which is similar when comparing cells growing at the same speed under different conditions. We also report that multifork replication occurs when the time between DNA replication initiation events is shorter than the C period, which may occur even in slow-growing cells with interdivision times longer than the C period.

Division site selection in many bacteria is governed by the nucleoid occlusion (Noc) and minicell (Min) systems. Mycobacteria do not encode homologs of these proteins and have no known mechanism for division site selection. We found that the DNA replisome and cell division ring colocalize and move together in a biphasic trajectory determined by the chromosome partitioning (Par) system. We propose a model in which Par-dependent movement of the replisome and division ring ultimately determines the site of cell division.

Coordination of cell growth and division is required for cell size homeostasis. Three models of division control have been proposed: *sizer* (cells divide after reaching a critical size), *timer* (cells divide at a certain time after birth), and *adder* (cells add a specific amount of mass before dividing). We show that the single-cell growth model (exponential, linear, or bilinear) constrains the possible division control models. Thus, it is crucial to know the true model of single-cell growth in order to distinguish the true mechanism of cell size homeostasis.

Keywords

single-cell time-lapse microscopy, DnaA, DnaN, FtsZ, ParB, single-cell growth model, cell-cycle progression, cell division, growth speed, cell size homeostasis.

Résumé

La propagation des microorganismes est basée sur trois procédés fondamentaux: la croissance cellulaire, la réplication de l'ADN, et la division cellulaire. Bien que ces procédés soient des cibles idéales pour de développement médicaments antibactériens, peu d'études ont été effectuées chez le phylum des Actinobactéries, qui est néanmoins un groupe médicalement pertinent comprenant *Mycobacterium tuberculosis*. Par l'utilisation de la microscopie fluorescente par time-lapse, j'ai suivi chez *Mycobacterium smegmatis*, la croissance de cellules individuelles, la réplication de leur ADN ainsi que leur division.

M. smegmatis est en forme de bâtonnet allongé et grandit par élongation de ses pôles. Son élongation est biphasique due à l'élongation du nouveau pôle, qui ne commence pas tout de suite après la division de la cellule mère (phénomène connu sous le nom de NETO "new end take-off"). Dans ma thèse j'ai découvert que chez les cellules qui grandissent plus vite, non seulement les pôles s'allongent plus rapidement, mais aussi que NETO se produit plus tôt. En fonction du timing de NETO qui peut parfois être retardé jusqu'à la génération d'après, les cellules peuvent paraître grandir de manière monophasique biphasique ou triphasique. Je propose un modèle selon lequel les cellules optimisent leur vitesse de croissance en optimisant la vitesse de croissance des pôles avec le moment où NETO se produit.

Dans cette thèse je montre également que les cellules qui grandissent plus vite progressent initient plus rapidement la réplication de l'ADN que les cellules qui grandissent plus lentement. Je montre que la vitesse de croissance des cellules individuelles est un bon prédicteur de la progression du cycle cellulaire. Celui-ci est en effet similaire chez les cellules qui grandissent dans différents environnements mais qui ont une vitesse de croissance identique. Je rapporte aussi que l'apparition de fourche de réplifications simultanées se produit lorsque l'intervalle de temps entre les initiations de réplication d'ADN est plus court que la durée de réplication d'ADN, même dans des cellules qui grandissent lentement et dont le temps entre les divisions est plus grand que le temps nécessaire à la réplication de l'ADN.

Chez la plupart des bactéries, la sélection du lieu de division est gouvernée par les systèmes d'occlusion nucléotidique (Noc) et de minicell (Min). Pourtant, dans les mycobactéries, il n'existe pas d'homologue de ces deux systèmes et les mécanismes de placement du lieu de division sont inconnus. J'ai trouvé que le réplisome et l'anneau de division co-localisent et se déplacent ensemble de manière biphasique dépendant du système de partitionnement des chromosomes (Par). Je propose un modèle dans lequel le mouvement du réplisome et de l'anneau de division dépendent de Par, et détermine finalement le lieu de division.

La coordination de la croissance cellulaire et de la division est nécessaire pour l'homéostasie de la taille des cellules. Trois modèles du control de division ont été proposés : soit les cellules se divisent un fois une taille prédéterminée atteinte, soit elles se divisent après qu'un certain temps se soit écoulé après leur naissance, soit après qu'elles se soit allongées d'une certaine quantité, indépendamment de leur taille à la naissance. J'ai démontré que les cellules qui grandissent de manière bilinéaire sont capables d'atteindre une homéostasie de la taille des cellules. Je démontre finalement que les modèles de croissance de cellules individuelles (linéaire, exponentiel ou bilinéaire) ne sont pas tous compatibles avec tous les modèles de control de division et qu'il est donc fondamental de connaitre le modèle de croissance des cellules individuelles afin de déterminer le mécanisme permettant une homéostasie de la taille des cellules.

Mots clés

microscopie time-lapse, DnaA, DnaN, FtsZ, ParB, modèle de croissance cellulaire, progression du cycle cellulaire, division cellulaire, vitesse de croissance, homéostasie de la taille des cellules.

Table of Contents

| | |
|---|-----------|
| ACKNOWLEDGEMENTS..... | 1 |
| ABSTRACT | 3 |
| KEYWORDS..... | 4 |
| RÉSUMÉ | 5 |
| MOTS CLÉS | 6 |
| TABLE OF CONTENTS | 7 |
| CHAPTER 1 INTRODUCTION | 11 |
| 1.1 BACTERIAL CELL ELONGATION AND GROWTH | 12 |
| 1.1.1 <i>Bacterial growth models.....</i> | 12 |
| 1.1.2 <i>Mycobacteria growth model</i> | 14 |
| 1.2 BACTERIAL CELL CYCLE..... | 15 |
| 1.2.1 <i>Bacterial cell cycle.....</i> | 15 |
| 1.2.2 <i>Mycobacterium smegmatis cell cycle</i> | 15 |
| 1.2.3 <i>Initiation of DNA replication</i> | 16 |
| 1.2.4 <i>Chromosome organization during replication</i> | 18 |
| 1.2.5 <i>Multifork replication</i> | 19 |
| 1.3 BACTERIAL CELL DIVISION..... | 20 |
| 1.3.1 <i>Bacterial cell division</i> | 20 |
| 1.3.2 <i>Positioning of the FtsZ division ring</i> | 21 |
| 1.3.3 <i>Division site selection in Mycobacterium smegmatis</i> | 21 |
| 1.3.4 <i>Chromosome segregation and division site selection in Mycobacterium smegmatis.....</i> | 22 |
| 1.4 CELL SIZE HOMEOSTASIS..... | 22 |
| 1.4.1 <i>Models for cell division control</i> | 23 |
| 1.4.2 <i>Impact of growth rate on cell size homeostasis.....</i> | 24 |
| 1.5 SINGLE-CELL ANALYSIS | 25 |
| 1.5.1 <i>Florescence time-lapse microscopy</i> | 26 |
| 1.5.2 <i>Microfluidic devices</i> | 26 |
| 1.5.3 <i>Image analysis</i> | 27 |
| AIMS OF THE THESIS..... | 29 |
| CHAPTER 2 GROWTH-SPEED IS COUPLED TO POLE ELONGATION SPEED AND NETO TIMING IN MYCOBACTERIUM SMEGMATIS | 31 |
| 2.1 ABSTRACT | 32 |
| 2.2 INTRODUCTION | 32 |
| 2.3 RESULTS | 33 |
| 2.3.1 <i>Pole elongation is slower when cells are grown in nutrient-poor medium</i> | 33 |
| 2.3.2 <i>NETO is delayed when cells are grown in nutrient-poor medium.....</i> | 33 |
| 2.3.3 <i>The single-cell growth model depends on the timing of NETO.</i> | 34 |
| 2.3.4 <i>Overexpression of DnaA causes increased cell growth speed due to earlier NETO without affecting pole growth speed.....</i> | 35 |

| | | |
|---|--|----|
| 2.3.5 | <i>Cells optimize the pole growth speed and NETO timing to maximize the cell growth speed</i> | 35 |
| 2.4 | DISCUSSION..... | 36 |
| 2.5 | METHODS | 37 |
| 2.5.1 | <i>Data selection</i> | 37 |
| 2.5.2 | <i>NETO detection</i> | 38 |
| 2.5.3 | <i>Bilinear and trilinear fit</i> | 38 |
| 2.5.4 | <i>Bacterial strains and culture conditions</i> | 38 |
| 2.5.5 | <i>Bacterial culture conditions</i> | 39 |
| 2.5.6 | <i>Pulse chase labelling of the old cell wall</i> | 39 |
| 2.5.7 | <i>Time-lapse fluorescence microscopy</i> | 39 |
| 2.5.8 | <i>Simulation of cell growth speed in function of NETO and pole growth speed</i> | 40 |
| 2.6 | FIGURES..... | 41 |
| 2.7 | SUPPLEMENTARY FIGURE | 47 |
| 2.8 | ACKNOWLEDGEMENTS | 47 |
| 2.9 | AUTHOR CONTRIBUTIONS | 48 |
| 2.10 | REFERENCES | 48 |
| CHAPTER 3 CELL-CYCLE PROGRESSION AND MULTIFORK REPLICATION IN MYCOBACTERIUM SMEGMATIS AT DIFFERENT GROWTH SPEEDS..... 51 | | |
| 3.1 | ABSTRACT | 52 |
| 3.2 | INTRODUCTION | 52 |
| 3.3 | RESULTS | 53 |
| 3.3.1 | <i>Cell size responds to carbon availability but not temperature</i> | 53 |
| 3.3.2 | <i>Initiation of DNA replication is delayed in carbon-limited cells, resulting in shrinkage of the C_{init} period and expansion of the B period</i> | 54 |
| 3.3.3 | <i>Temperature-limited growth exacerbates the delayed initiation of DNA replication in response to carbon limitation</i> | 55 |
| 3.3.4 | <i>Cell-cycle progression is different in cells growing at different speeds under the same culture conditions</i> | 55 |
| 3.3.5 | <i>Cell-cycle progression is similar in cells growing at the same speed under different growth conditions</i> | 56 |
| 3.3.6 | <i>Overexpression of DnaA causes earlier initiation of DNA replication, faster growth, shorter interdivision time, and increased cell size</i> | 56 |
| 3.3.7 | <i>Multifork replication is not determined by interdivision time at the single-cell level</i> | 57 |
| 3.3.8 | <i>Decreasing the inter-initiation time or increasing the C-period duration increases the frequency of multifork replication independent of the interdivision time</i> | 58 |
| 3.4 | DISCUSSION..... | 59 |
| 3.5 | METHODS | 61 |
| 3.5.1 | <i>Cell cycle reporter strain of M. smegmatis</i> | 61 |
| 3.5.2 | <i>DnaA-overexpressing strain of M. smegmatis</i> | 61 |
| 3.5.3 | <i>Bacterial culture conditions</i> | 62 |
| 3.5.4 | <i>Time-lapse fluorescence microscopy</i> | 62 |
| 3.5.5 | <i>Data selection for cell length and cell cycle measurements</i> | 62 |
| 3.5.6 | <i>Cell length measurements</i> | 62 |

| | | |
|---|--|-----------|
| 3.5.7 | <i>Measurement of cell cycle periods.....</i> | 63 |
| 3.5.8 | <i>Selection of cells with overlapping growth speeds</i> | 63 |
| 3.5.9 | <i>Statistical analysis</i> | 63 |
| 3.6 | FIGURES..... | 65 |
| 3.7 | SUPPLEMENTARY FIGURES | 72 |
| 3.8 | AUTHOR CONTRIBUTIONS | 75 |
| 3.9 | REFERENCES | 75 |
| CHAPTER 4 COLOCALIZATION AND BIPHASIC MOVEMENT OF THE DNA REPLISOME AND FTSZ | | |
| DIVISION RING DETERMINE THE SITE OF CELL DIVISION IN <i>MYCOBACTERIUM SMEGMATIS</i>..... | | 79 |
| 4.1 | ABSTRACT | 80 |
| 4.2 | INTRODUCTION | 80 |
| 4.3 | RESULTS | 81 |
| 4.3.1 | <i>The DNA replisome and cell division ring colocalize in space and time</i> | 81 |
| 4.3.2 | <i>Coupled movement of the DNA replisome and cell division ring towards the future division site</i> | 82 |
| 4.3.3 | <i>The DNA replisome and cell division ring switch between tracking first the old pole (phase I) and then the new pole (phase II).....</i> | 82 |
| 4.3.4 | <i>ParB is not required for colocalization of the DNA replisome and cell division ring</i> | 83 |
| 4.3.5 | <i>ParB is not required for coupled movement of the DNA replisome and cell division ring towards the future division site</i> | 83 |
| 4.3.6 | <i>ParB is required for the DNA replisome and cell division ring to track the old cell pole during phase I</i> | 84 |
| 4.4 | DISCUSSION..... | 84 |
| 4.5 | METHODS | 87 |
| 4.5.1 | <i>Bacterial strains</i> | 87 |
| 4.5.2 | <i>Bacterial culture conditions</i> | 87 |
| 4.5.3 | <i>Time-lapse fluorescence microscopy</i> | 87 |
| 4.5.4 | <i>Image analysis</i> | 87 |
| 4.5.5 | <i>Selection of mCherry-DnaN foci and FtsZ-GFP rings for trajectory analysis</i> | 88 |
| 4.5.6 | <i>Breaking point and kymograph</i> | 88 |
| 4.6 | FIGURES..... | 89 |
| 4.7 | AUTHOR CONTRIBUTIONS | 96 |
| 4.8 | REFERENCES | 96 |
| CHAPTER 5 COMPUTATIONAL ANALYSIS OF THE MUTUAL CONSTRAINTS BETWEEN SINGLE-CELL GROWTH AND DIVISION CONTROL MODELS..... | | |
| 99 | | 99 |
| 5.1 | ABSTRACT | 100 |
| 5.2 | INTRODUCTION | 100 |
| 5.3 | RESULTS | 102 |
| 5.3.1 | <i>Boundary conditions for computational simulations of single-cell growth</i> | 102 |
| 5.3.2 | <i>Single-cell growth models can be distinguished by residual analysis with Akaike and Bayesian information criteria</i> | 102 |
| 5.3.3 | <i>Correct identification of the division control model relies on accurate knowledge of the single-cell growth model.....</i> | 103 |

| | | |
|-------------------------------|--|------------|
| 5.3.4 | <i>The speed at which outliers return to a steady-state birth size is characteristic of each combination of single-cell growth and division models.....</i> | <i>105</i> |
| 5.3.5 | <i>The correlation between birth size and added size depends on the division control and single-cell growth models.....</i> | <i>106</i> |
| 5.3.6 | <i>Single-cell growth models and division control models can be distinguished by the speed of convergence of outlier cells in vector fields of birth size versus added size.....</i> | <i>107</i> |
| 5.4 | CONCLUSION | 108 |
| 5.5 | FIGURES..... | 110 |
| 5.6 | SUPPORTING INFORMATION | 116 |
| 5.7 | ACKNOWLEDGEMENTS | 117 |
| 5.8 | AUTHOR CONTRIBUTIONS..... | 117 |
| 5.9 | CONFLICT OF INTEREST | 117 |
| 5.10 | REFERENCES | 118 |
| CONCLUSION..... | | 121 |
| REFERENCES | | 127 |
| REFERENCES | | 128 |
| CURRICULUM VITAE | | 139 |

Chapter 1 Introduction

Cell growth, duplication and segregation of genetic material, and cell division are the three fundamental pillars of life propagation. However, how cells grow, duplicate and segregate their genetic material, or divide is dependent on each cell type. Cells are remarkably diverse in size; For example, prokaryotic cells that are on average 10 times smaller than eukaryotic cells can have sizes ranging from a few hundred nanometers for the smallest bacteria to a few hundred micrometers for the largest bacteria (Young, 2006). Cells are also remarkably diverse in shape. They can be round or rod-shaped but also crescent-shaped, star-shaped, or helical to cite only a few (Young, 2006; Levin and Angert, 2015). Probably arising from this diversity, cells have developed different strategies to grow and divide. For example, spherical bacteria of the genus *Streptococcus* grow by elongation from the division site solely, while the rod-shaped bacteria *Escherichia coli* and *Bacillus subtilis* elongate by addition of new cell wall material to the lateral cell wall (Daniel and Errington, 2003). Nevertheless, bacterial shape does not determine how cells grow since other strategies, such as polar elongation, may be adopted by rod-shaped bacteria (Daniel and Errington, 2003). Such extreme variation between cell types is also observed in the duplication of the genetic material. Usually, cells initiate DNA replication sometime after their birth and terminate DNA replication before division occurs. However, some fast-growing bacteria such as *E. coli* have an interdivision time shorter than the time needed to replicate DNA. In order to successfully duplicate their DNA before division, they evolved a strategy where they initiate a second cycle of DNA replication before the termination of the first cycle occurs, resulting in “multifork replication” (Cooper and Helmstetter, 1968).

No matter their size or shape, and no matter how they grow or duplicate their genetic material, cells need to approximately double in size before division to create two daughter cells of roughly equal sizes. If cell division consistently occurs too early or too late, cells will either become too small or too large and outside of the size window where they can survive or function optimally. Also, to ensure a correct ploidy, cells need to duplicate their genetic information and equally partition the chromosomes between the two future daughter cells in synchrony with division event. If cell division occurs too early or too late, DNA replication might not be finished or a new round of replication might have started, creating daughter cells with too few or too much genetic material. Thus, cell growth, chromosome replication and segregation, and cell division need to be coordinated.

Cells are constantly facing new challenges that push them out of equilibrium. For example, cell growth can be slowed down due to poor nutrient availability or DNA replication can be delayed due to unexpected DNA damage that needs repair. However, cells are most of the time able to adapt and keep cell growth, DNA replication/segregation, and cell division coordinated in order to survive, further demonstrating the importance of these three processes as well as their coordination.

Impairment of any of these processes has dramatic consequences on cells viability and on their capacity to proliferate. During an infection, the main “goals” of pathogenic bacteria are to survive and multiply in the host organism and spread to new hosts. Therefore, drugs targeting cell growth, DNA replication, and cell division are generally effective in treating infections. Penicillin, which was discovered in 1928, is a good example, as it inhibits bacterial cell wall synthesis. Soon after penicillin followed the discovery of antibiotics targeting specific proteins involved in DNA synthesis, such as fluoroquinolones. Promising new drugs targeting cell division such as ridinilazole are emerging, making cell division an exciting new area of drug discovery (Lock and Harry, 2008; Hutchings et al., 2019). However, declining commitment of the pharmaceutical industry to antibiotic discovery, coupled to an increase in bacterial antibiotic resistance, is creating an urgent need for drugs with new targets (Lock and Harry, 2008; Hutchings et al., 2019). The identification of new proteins and pathways involved in bacterial cell growth, DNA replication, and cell division is therefore of great interest.

Cell growth, DNA replication, and cell division are intensively studied in model organisms such as *Escherichia coli*, *Caulobacter crescentus*, and *Bacillus subtilis*, belonging to the Proteobacteria and Firmicutes phyla, respectively. Relatively fewer studies have focused on the phylum Actinobacteria, which is nonetheless a medically important phylum. Two Actinobacteria pathogens of the genus *Mycobacterium* are responsible for two of the most important plagues of humanity: tuberculosis (caused by *Mycobacterium tuberculosis*) and leprosy (caused by *Mycobacterium leprae*). The need for new drugs specifically targeting tuberculosis is urgent because multi-drug-resistant strains of *M. tuberculosis* are spreading and making the global epidemic more intractable to treatment. Mycobacteria have a unique cell wall composition differing from Gram-positive and Gram-negative bacteria that may hinder entry of antibacterial drugs into the cell. With this complexity of the cell wall comes the need for specialized mechanisms for cell growth and division (Hett and Rubin, 2008).

My doctoral thesis research has focused on the non-pathogenic and relatively fast-growing model organism *Mycobacterium smegmatis*. Although *M. smegmatis* is not a good model to study pathogenesis, it can be used to study basic cell processes such as cell growth, DNA replication/segregation, and cell division in mycobacteria (Hett and Rubin, 2008; Reytrat and Kahn, 2001).

This thesis aims to better understand mycobacterial cell growth, cell cycle progression, and cell division, in order to add to the foundation of knowledge that might, someday, be useful for the discovery of new drug targets.

1.1 Bacterial cell elongation and growth

1.1.1 Bacterial growth models

As mentioned above, bacteria are remarkably diverse in size and shape (Levin and Angert, 2015; Young, 2006). In most bacteria, cell shape is maintained by a peptidoglycan cell wall, a

meshwork composed of glycan strands crosslinked by peptides. When cells are growing, they need to insert new peptidoglycan into the preexisting meshwork and different strategies may be adopted. For example, the spherical bacteria *Streptococcus* grows solely by elongation from the division site (Daniel and Errington, 2003). On the other hand, in rod-shaped bacteria such as *E. coli* and *B. subtilis*, cell elongation occurs by insertion of new cell wall material into the lateral cell walls (Daniel and Errington, 2003; de Pedro et al., 1997; Kuru et al., 2012). In such cases, insertion of new cell wall material is driven by MreB, a bacterial actin homologue that assembles into helical cables and localizes early cell wall synthetic enzyme at regions with positive curvature (Daniel and Errington, 2003). In contrast, other rod-shaped bacteria such as Actinobacteria do not possess an MreB system and grow by polar extension by inserting new cell wall material at or near the cell poles (Botella et al., 2017; Eswara and Ramamurthi, 2017).

It has been speculated that different elongation patterns could result in different single-cell growth models (Daniel and Errington, 2003). According to this view, cells growing by extension of the lateral cell walls are more likely to exhibit exponential growth (i.e., the speed of growth increases proportionally to cell size) since the size of the growth zone increases as cells elongate. Conversely, cells growing by polar extension are more likely to exhibit linear growth (i.e., the speed of growth remains constant as the cell size increases) since the size of the polar growth zone remains constant as cells elongate (Sargent, 1975). Growth models other than these simple exponential or linear models have also been postulated. For example, the rod-shaped fission yeast *Schizosaccharomyces pombe* grows by polar extension with the newly formed pole initiating growth later than the old pole (Mitchison and Nurse, 1985). The asymmetry between the new-pole and old-pole growth results in bilinear growth (Horvath et al., 2013). Initiation of new-pole growth, known as “new end take-off” (NETO) is believed to be dependent on cell size and to be regulated by the cell cycle (Mitchison and Nurse, 1985).

Determining the correct single-cell growth model is challenging, and results and interpretations from different studies on the same organism are often contradictory. For example, single-cell growth of a single organism (*E. coli*) has variously been described as exponential, linear, or bilinear (Kubitschek, 1968, 1981; Mir et al., 2011). With the development of new technologies, such as time-lapse microscopy, identifying the correct growth model at the single-cell level has become easier. However, single-cell measurements of cell size or mass often remain too noisy for precise interpretation, and cell-to-cell phenotypic variations further challenge the correct assignment of single-cell growth models (Godin et al., 2010; Vuaridel-Thurre et al., 2020). Despite these difficulties, identification of the true single-cell growth model is of crucial importance since different models imply different mechanisms to maintain cell size homeostasis (Cooper, 2006; Vuaridel-Thurre et al., 2020).

1.1.2 Mycobacteria growth model

Mycobacteria are known to grow exclusively by polar extension and preferentially from the old pole (Thanky et al., 2007; Kieser and Rubin, 2014; Meniche et al., 2014; Botella et al., 2017). Addition of new cell wall material at the poles is thought to be directed by Wag31, a homologue of the DivIVA protein in *B. subtilis* (Kang et al., 2008; Jani et al., 2010; Meniche et al., 2014). Wag31 localizes at the poles and has been shown to play a major role in the recruitment of early cell wall biosynthetic enzymes in an annular subpolar region where the new peptidoglycan is deposited (Meniche et al., 2014).

Despite a general agreement that mycobacteria grow by addition of new material at the cell poles, the exact pattern of single-cell growth has been controversial. It has been argued that *M. smegmatis* growth is *unipolar*, with growth occurring exclusively at the old pole (Aldridge et al., 2012), or *bipolar*, with both poles growing at the same speed from birth to division (Santi et al., 2013). By combining time-lapse optical and atomic force microscopy, Hannebelle et al., 2020 recently proposed a unifying model in which mycobacteria grow in a biphasic manner that resembles the “new end take-off” (NETO) dynamics of fission yeast. According to this model, newborn cells grow exclusively from the old pole, while initiation of new-pole growth usually occurs at about 80% of the interdivision time in cells growing in rich medium. Although NETO usually occurs before cell division, in some cases it occurs after division, indicating that these events (NETO and division) are not causally linked.

Why the new cell pole does not start to grow immediately after birth remains unknown. It has been speculated that there is a lag phase in order for the new pole to mature (Botella et al., 2017). The lag phase could be due to the time needed to recruit the cell wall synthetic enzymes to the new pole. For example, it has been shown that the new pole initiates growth once a certain threshold of Wag31 is reached after its accumulation at the new pole, which occurs partially by relocalization of Wag31 from the old pole to the new pole (Hannebelle et al., 2020). However, maturation of the new pole might not be an absolute requirement for NETO, as suggested by the finding that one (morphologically abnormal) strain of *M. smegmatis* preferentially grows from the new pole immediately after cell division (Meniche et al., 2014).

The timing of NETO differs between fast-growing and slow-growing mycobacterial species. As a fraction of the interdivision time, slow-growing species exhibit NETO much earlier during the cell cycle compared to fast-growing species, and the timing of NETO at the single-cell level is highly variable within a species (Hannebelle et al., 2020). The reason for this variability is not yet understood but might reflect for example, that the timing of NETO is dependent on cell size and regulated by the cell cycle, similar to what has been observed in *S. pombe* (Mitchison and Nurse, 1985).

1.2 Bacterial Cell cycle

1.2.1 Bacterial cell cycle

Bacterial chromosome replication and segregation must be coordinated with cell growth and division to maintain the right ploidy. Most bacteria have a single circular chromosome and DNA replication starts at a unique origin of replication (*oriC*). Replication forks proceed bidirectionally from *oriC* and terminate DNA replication in the opposite region of the chromosome, about 180° from *oriC* (Hendrickson and Lawrence, 2007; Wang and Levin, 2009). The bacterial cell cycle has been subdivided into three periods: a B period from birth to initiation of DNA replication, C period from initiation to termination of DNA replication, and D period from termination to cell division (Figure 1a) (reviewed in Wang and Levin, 2009; Dewachter et al., 2018).

1.2.2 *Mycobacterium smegmatis* cell cycle

M. smegmatis is a relatively slow-growing bacterium with a generation time of about three hours in rich medium, and the cell cycle periods are usually well defined. However, under optimal growth conditions in rich medium, cells often initiate a second cycle of DNA replication after termination of the previous replication cycle but prior to division; in these cases, the C period spans the division event and the daughter cells inherit a partially replicated chromosome (Figure 1b) (Santi et al., 2013; Logsdon et al., 2017). For clarity in such cases, we may subdivide the C period into two parts, comprising the time from replication *initiation* to division in the mother cell (C_{init}), which has also been referred to as the “D period” (Logsdon et al., 2017), and the time from birth to replication *termination* in the daughter cell (C_{term}) (Figure 1b).

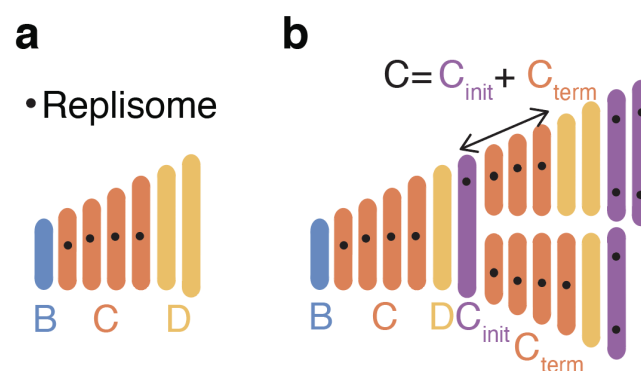


Figure 1. Cell cycle of *M. smegmatis*

(a) The canonical cell cycle in bacteria comprises a B period from birth to initiation of DNA replication, a C period from initiation to termination of DNA replication, and a D period from termination to cell division. (b) In *M. smegmatis*, initiation of the next cycle of DNA replication may occur after completion of the preceding cycle but prior to division. In such cases, one or both daughter cells inherit a partially replicated chromosome and there is no B period. Because the C period spans the division event, the first part of the C period takes place in the mother cell (C_{init}) while the second part takes

place in the daughter cell (C_{term}).

1.2.3 Initiation of DNA replication

Most of the current knowledge on initiation of DNA replication comes from studies in *E. coli*. Replication requires the assembly of the replisome at the chromosomal origin of replication (*oriC*) (Figure 2). Briefly, *oriC* contains binding sites for the initiator protein DnaA (Messer, 2002). Once enough ATP-DnaA are bound, DnaA promotes unwinding of the nearby AT-rich DNA region and the loading of the helicase DnaB and the helicase loader DnaC (Messer, 2002). The DNA primase DnaG then enters the complex and synthesizes the replication primer, onto which the sliding clamp DnaN (beta subunit of DNA polymerase III) will load. DnaN is a DNA binding protein that maintains the interaction between DNA polymerase III and DNA by encircling the DNA (Katayama et al., 2010). On the lagging strand, DnaN associates with

primers and DNA polymerase III jumps from DnaN to DnaN, i.e., from primer to primer (Su'etsugu and Errington, 2011).

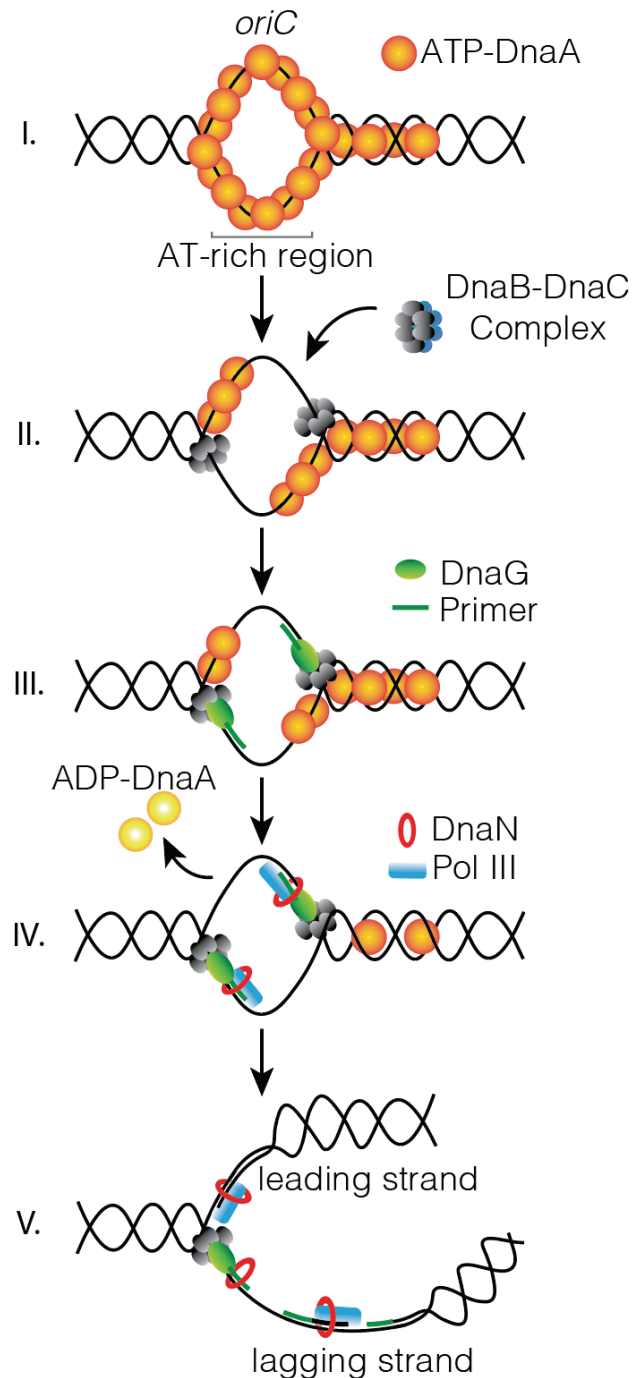


Figure 2. Initiation of DNA replication in *E. coli*

I. Binding of DnaA to DnaA binding sites near *oriC* and unwinding of the AT-rich region. **II.** Loading of the helicase DnaB by the helicase loader DnaC. **III.** Entry and primer synthesis of the DNA primase DnaG. **IV.** Loading of the sliding clamp DnaN and DNA Polymerase III (Pol III). **V.** Schematic of a single replication fork progressing along the DNA. Adapted from Messer, 2002 and Katayama et al., 2010.

Among the proteins involved in initiation of DNA replication, we are particularly interested in DnaA and DnaN. First, DnaA, because it is central in regulating initiation of DNA replication. Overexpression of DnaA triggers premature initiation of DNA replication (Xu and Bremer, 1988; Løbner-Olesen et al., 1989); conversely, blocking synthesis of DnaA prevents new initiation events (Schaus et al., 1981). Second, DnaN, because fluorescently tagged DnaN can be used as a subcellular marker for the DNA replisome that can be tracked using time-lapse microscopy; a fluorescent focus appears at the time of initiation of DNA replication and disappears once DNA replication is finished (Su’etsugu and Errington, 2011; Santi et al., 2013; Trojanowski et al., 2015). Manipulation of DnaA expression coupled to cell cycle tracking using fluorescently tagged DnaN is a powerful tool to study the cell cycle of *M. smegmatis*, as demonstrated in this thesis.

1.2.4 Chromosome organization during replication

Different species of bacteria follow different models for DNA replication. For example, in *Bacillus subtilis*, DNA replication takes place in a spatially fixed “replication factory”. In this model, the replisomes from the two replication forks (replicating the leading and lagging DNA strands) stay together near midcell and the chromosome is passed through this factory during replication (Lemon and Grossman, 2000). In contrast, in *E. coli*, the replisomes assemble near midcell and instead of remaining there, they split and independently follow the chromosome track during DNA replication (Reyes-Lamothe et al., 2008). A third model for DNA replication is observed in *C. crescentus*, where the replisomes assemble near the old pole and then move together toward midcell (Jensen et al., 2001).

M. smegmatis seems to follow a “replication factory” model, in which the two replisomes stay together and are relatively stationary within the cytoplasm, and DNA spools through the replisome as it is replicated (Santi and McKinney, 2015). During replication and spooling of DNA through the replication factory, the chromosomes display the following choreography: the recently duplicated *oriC* loci move rapidly toward opposite cell poles while the *attB* chromosomal locus (245° from *oriC*, roughly approximating the termination site) stays close to the new pole before moving rapidly to the replication factory prior to its duplication (Santi and McKinney, 2015; Ginda et al., 2017).

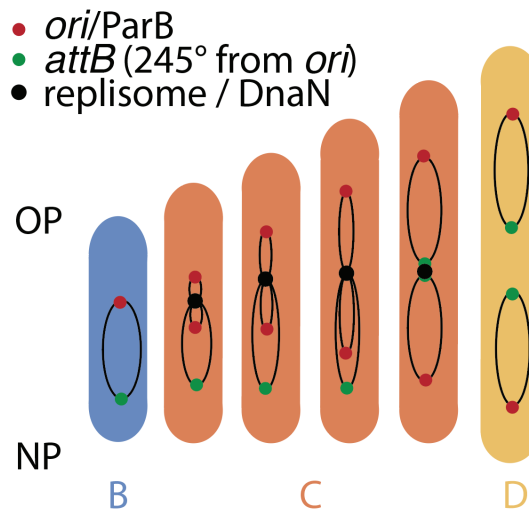


Figure 3. Chromosome organization during replication in *M. smegmatis*

Example of an *M. smegmatis* cell which cell cycle comprises a B period from birth to initiation of DNA replication, a C period from initiation to termination of DNA replication, and a D period from termination to cell division. Before replication, the terminus is located near the new pole and the origin is located near midcell. Replication starts near midcell and DNA spools through the replication factory that remains relatively stationary within the cytoplasm. The *attB* site moves then rapidly to the replication factory prior to its duplication.

1.2.5 Multifork replication

In fast-growing bacteria, when the time to replicate the genome is longer than the interdivision time, a new cycle of DNA replication may initiate before termination of the previous cycle, resulting in “multifork replication” (Cooper and Helmstetter, 1968; Wang and Levin, 2009). Remarkably, cells can adapt to varying growth rates by initiating new rounds of replication more or less frequently, and at very fast growth rates, cells may display up to eight simultaneous rounds of replication (Wang and Levin, 2009). It has long been known that multifork replication may occur in fast-growing bacteria such as *E. coli* under optimal culture conditions (Cooper and Helmstetter, 1968). However, a recent study identified multifork replication events in *M. smegmatis*, which has, on average, an interdivision time longer than the time required for DNA replication (Figure 4) (Trojanowski et al., 2017). Remarkably, multifork replication events in *M. smegmatis* were also observed in cells growing slowly at a suboptimal temperature. These discoveries pose a challenge to the presumed link between fast growth and multifork replication.

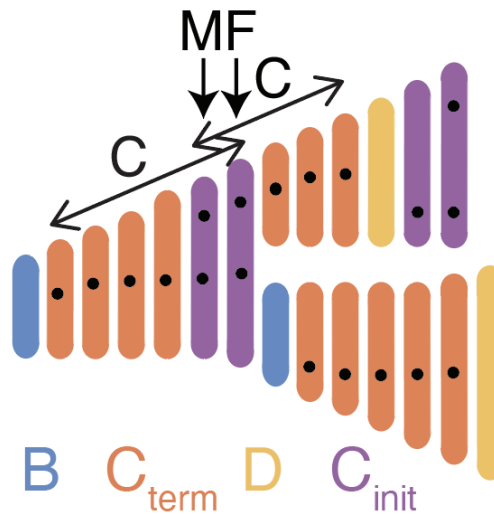


Figure 4. Multifork replication in *M. smegmatis*

In rare cases, multifork (MF) replication occurs because initiation of the next cycle of DNA replication precedes termination of the preceding cycle of replication, resulting in overlapping C periods.

1.3 Bacterial cell Division

1.3.1 Bacterial cell division

Cell division needs to be spatially and temporally regulated to ensure the formation of two approximately equal-sized daughters, both containing a full copy of the genetic information. Therefore, prior to division, cells must ensure a proper segregation of the chromosomes. The majority of bacteria have a chromosome partitioning system (the ParABS system) that initiates chromosome segregation at the same time as DNA replication is started. Other bacteria, such as *E. coli*, do not seem to have a specific system responsible for chromosome segregation, and in such cases it has been proposed that entropy is the principal driver of self-segregation of the chromosomes (Jun and Wright, 2010). To prepare for division as well as to ensure a proper partitioning of the chromosomes, cells form a septum at the future division site. In order to do so, the tubulin-like GTPase FtsZ forms a ring at the future division site. FtsZ is central to the division process. Once it is placed at the future division site, it recruits the division machinery, including the enzymes responsible for cell wall synthesis (Adams and Errington, 2009; Mahone and Goley, 2020). FtsZ polymerizes into dynamic filaments that treadmill around the division plane, forming a so-called “Z ring”. It has been shown in *E. coli* that the treadmilling of FtsZ into progressively smaller rings guides the insertion of new cell wall material, leading to progressive closure of the septum (Bisson-Filho et al., 2017). Septum closure results in cytokinesis, which divides the cytosol of the mother cell into two daughter cytosols that are no longer connected. Following cytokinesis, the full physical separation of

the two daughter cells is performed by membrane fusion and cell wall hydrolysis (Mahone and Goley, 2020).

1.3.2 Positioning of the FtsZ division ring

Spatial positioning of the FtsZ division ring is crucial to the formation of two equally sized daughters. Most of the findings on division site selection come from studies in *E. coli* and *B. subtilis*. Two main systems have been described and are based on the negative regulation of FtsZ ring formation. First, the nucleoid occlusion (Noc) system, prevents chromosome guillotining by inhibiting division in a region that contains DNA (Wu and Errington, 2012) and second, the canonical Minicell (Min) system that inhibits division near the cell poles (Rowlett and Margolin, 2015). Briefly, the Noc system is based on Noc (*B. subtilis*) or SlmA (*E. coli*) proteins that bind to specific DNA sequences distributed throughout the chromosome and inhibit FtsZ polymerization over regions containing DNA (Wu and Errington, 2012). The Min system is composed of three main proteins – MinC, MinD, and MinE – that act together to depolymerize FtsZ at the poles, where their time-averaged concentration is the highest (Rothfield et al., 2005). Most of the findings on division site selection come from studies in *E. coli* and *B. subtilis*. However, it is becoming evident that the Noc and Min system are not used by all bacteria (Monahan et al., 2014; Hajduk et al., 2016). For example, *C. crescentus* lacks both of those systems but uses a similar strategy based on a protein (MipZ) that is functionally analogous to the Min proteins (Thanbichler and Shapiro, 2006).

1.3.3 Division site selection in *Mycobacterium smegmatis*

In *M. smegmatis*, the Noc and Min systems seem to be absent and no mechanism for division site placement has yet been identified (Hett and Rubin, 2008). It has been reported that, in most cases, *M. smegmatis* divides slightly asymmetrically with a skew towards the new cell pole (Aldridge et al., 2012). Subsequently, Joyce et al., 2012 proposed that the nascent division septum is initially positioned precisely at midcell and subsequently shifts towards the new pole due to asymmetric (old-pole-dominant) growth (Aldridge et al., 2012). Alternatively, Singh et al., 2013 proposed that the division site might be positioned more or less randomly along the cell length, and chromosome segregation might be mediated by a pump (FtsK) that moves DNA across the division septum. None of these studies, however, identified a mechanism for division-site selection in mycobacteria. More recently, Eskandarian et al., 2017 demonstrated that the surface of *M. smegmatis* cells is “wavy” and division occurs predominantly within wave-troughs. Although these observations suggest that cell-surface morphological markers might play a role in division site selection, the underlying molecular mechanisms remain unknown.

1.3.4 Chromosome segregation and division site selection in *Mycobacterium smegmatis*

Accumulating evidence suggests that division site selection in bacteria might be linked to DNA replication and chromosome segregation (Moriya et al., 2010; Donovan et al., 2013; Hajduk et al., 2016; van Raaphorst et al., 2017). The chromosome partitioning (ParABS) system is responsible for segregation of newly replicated chromosomes in many bacteria, including *M. smegmatis* (reviewed in Kawalek et al., 2020). Although different models have been proposed for the Par-mediated mechanism of chromosome segregation, there is a consensus that the ParA motor protein mediates segregation by simultaneously interacting with polar proteins as well as ParB bound to *parS* sequences near the chromosomal origin of replication (reviewed in Badrinarayanan et al., 2015; Kawalek et al., 2020). In *M. smegmatis*, ParA bridges the pole-localized protein Wag31 and ParB-*parS* complexes bound next to the chromosomal replication origin (Jakimowicz et al., 2007; Kang et al., 2008; Ginda et al., 2013) (Figure 5). Mutants lacking ParA or ParB display defects in replisome positioning, chromosome segregation, and division site placement (Ginda et al., 2013; Santi and McKinney, 2015; Trojanowski et al., 2015; Eskandarian et al., 2017; Ginda et al., 2017), suggesting that replisome positioning and/or chromosome segregation might play a role in division site selection in *M. smegmatis*.

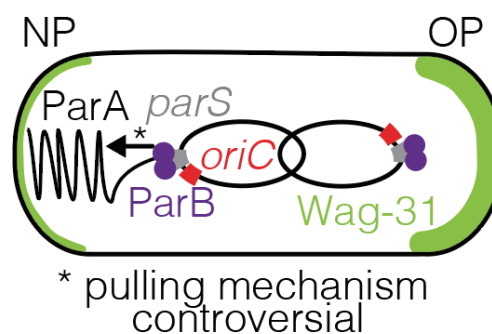


Figure 5. Chromosome segregation by the ParABS system in *M. smegmatis*

In *M. smegmatis*, ParA interacts with Wag31 located at the new pole (NP) and pulls the chromosome through ParB proteins bound to *parS* sequences located near the origin of replication (*oriC*).

1.4 Cell size homeostasis

Cell size homeostasis has been described as “one of the last big unsolved problems in cell biology” by Doug Kellogg (Weitzman, 2003). Although this statement was made almost twenty years ago, only parts of the answer have been uncovered in the intervening years. Prokaryotic cells are remarkably variable in size (less than a micron to more than half a centimeter) and shapes (from bean to triangular or helical, to cite only a few) (Young, 2006; Levin and Angert, 2015). It has been argued that cell size and shape are important selectable traits, since bacterial morphology has to be adapted to the environment in order to maximize

inter alia access to nutrients, motility, or adaptation to physical forces (Young, 2006). It has been shown through experimental evolution, after growing *E. coli* for over 50'000 generations, that *E. coli* cells alter their morphology in response to environmental conditions (in this case, limiting glucose) (Grant et al., 2021). However, it has also been argued that cell morphology could be a “byproduct” resulting from selection acting on other traits (Amir, 2017).

No matter their morphology, cells maintain a stable and narrow distribution of sizes over many generations (Levin and Angert, 2015). How cells achieve size homeostasis is not well understood but it is a common opinion that coordination between cell growth, cell cycle progression, and cell division is involved.

1.4.1 Models for cell division control

Three main models of division control have been proposed to achieve cell size homeostasis: sizer, timer, and adder (Jun and Taheri-Araghi, 2015; Sauls et al., 2016; Willis and Huang, 2017). According to the sizer model, cells divide after reaching a certain size. According to the timer model, cells divide after a certain amount of time has elapsed since their birth, following an internal clock. According to the adder model, cells must increase their size by a fixed amount before they divide, independent of their size at birth (Figure 6).

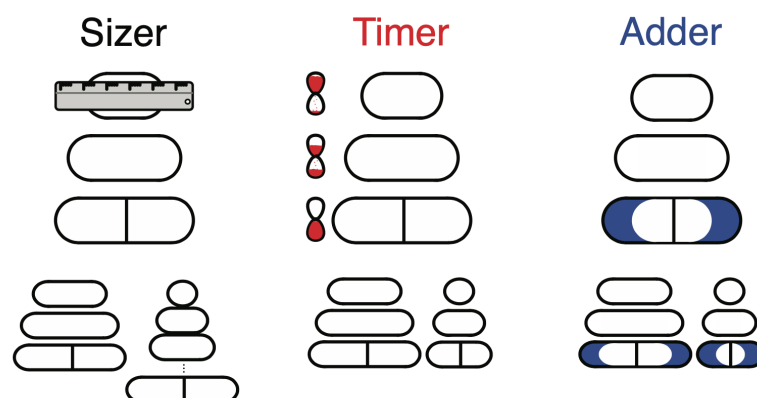


Figure 6. Schematic of three competing cell division control models.

According to the sizer model, cells divide after reaching a predetermined size (ruler). In the timer model, cells divide after a certain amount of time has elapsed since their birth, following an internal clock (hourglass). In the adder model, cells must add a certain fixed amount of volume (blue area) before they divide, independent of their birth size. The contrasting behaviors of a large cell and a small cell are depicted for each scenario. No specific single-cell growth model is assumed. Reproduced from Vuaridel-Thurre et al., 2020.

The adder model seems to be supported by single-cell data for a large variety of organisms (Campos et al., 2014; Taheri-Araghi et al., 2015; Deforet et al., 2015; Soifer et al., 2016; Chandler-Brown et al., 2017; Cadart et al., 2018). These models for division control, however, are not mutually exclusive, as some studies have reported that combinations of the different

mechanisms may operate in a single organism (Sveiczet al., 1996; Delarue et al., 2017). It is also worth noting that these models (sizer, timer, adder) could be invoked to explain how other cell cycle transitions are controlled, for example, initiation of DNA replication.

In *M. smegmatis* it has been proposed that cell division is governed by time since cell division appears to be synchronized in a microcolony (Aldridge et al., 2012). A later publication proposed a parallel adder as a model to coordinate cell cycle and cell division: a constant length is added between initiations of DNA replication and between initiation of DNA replication and division (Logsdon et al., 2017). However, the feasibility of those models for cell division needs to be put in perspective with the true single-cell growth model of *M. smegmatis* (e.g., exponential, linear, bilinear), which remains unknown.

1.4.2 Impact of growth rate on cell size homeostasis

Adaptation of bacteria to different environments is often accompanied by changes in growth speed, interdivision time, cell size, and cell cycle progression (reviewed in Young, 2006; Jonas, 2014; Westfall and Levin, 2017; Jun et al., 2018). Common environmental factors that may influence these cellular parameters include the abundance of nutrients and the ambient temperature. Changes in growth speed could potentially change the coordination between the DNA replication and cell division cycles at the single-cell level, as these cycles are not strictly coupled in bacteria and may respond differently to changes in growth speed (Dewachter et al., 2018).

1.4.2.1 Impact on cell size

In a classic study, Schaechter et al., 1958 found that growth speed, but not temperature, determines bacterial cell composition and cell size (Schaechter et al., 1958). The authors found a linear relationship between size and growth rate: cells growing more slowly due to poor nutrient availability are smaller than cells growing rapidly in rich media. Remarkably, they found that cell size correlates with growth rate rather than with nutrient availability, since different media providing the same growth speed produce cells with identical physiological states (same averaged size, DNA and RNA content). These conclusions, derived from experiments with the Gram-negative organism *Salmonella typhimurium*, became codified as the bacterial “growth law”. However, more recent studies discuss whether it is nutrient availability rather than growth rate *per se* that determines cell size (Ehrenberg et al., 2013; Vadia and Levin, 2015)

The growth law has also been challenged by more recent studies in *E. coli* showing that cells growing at a lower (suboptimal) temperature are smaller than cells growing at a higher (optimal) temperature (Trueba et al., 1982). The underlying reasons for this discrepancy are unclear, although the use of different organisms by different investigators might play a role.

Some molecular mechanisms that couple growth rate and cell size have been proposed, including potential size sensors coupling carbon metabolism to cell division: UgtP in *B. subtilis*

(Weart et al., 2007) and OpgH, an UgtP analogue, in *E. coli* (Hill et al., 2013). By using nutritional information, specifically by sensing the flux through the glycolipid biosynthesis pathway, UgtP can inhibit FtsZ ring formation and delay division under nutrient-rich conditions where cells grow rapidly. Other metabolic genes potentially involved in cell size control and cell cycle progression in *E. coli* and *B. subtilis* have also been proposed (Vadia and Levin, 2015).

Emerging evidence suggests that cell-to-cell variation in growth rate may also have an impact on cell size at the single-cell level. For example, in *M. smegmatis*, fast-growing individuals are larger and have shorter interdivision times compared to slow-growing individuals within the same population (Santi et al., 2013). Similar results have been obtained in *E. coli* (Wallden et al., 2016).

1.4.2.2 Impact on cell cycle progression

Consistent with changes observed in cell size upon variation of growth rates, adaptation of the cell cycle has also been observed in response to varying the growth rate. Fast-growing individuals initiate DNA replication earlier, resulting in a shorter-than-average B period, and divide sooner after termination of DNA replication, resulting in a shorter-than-average D period (Adiciptaningrum et al., 2015). Likewise, *M. smegmatis* cells that are larger than average at birth elongate faster and initiate DNA replication earlier in the cell cycle compared to cells that are smaller than average and elongate more slowly (Santi et al., 2013; Logsdon et al., 2017; Logsdon and Aldridge, 2018).

In the search for mechanisms that coordinate cell growth and DNA replication, Murray and Koh 2014 found that it is not only initiation of DNA replication that is involved in adaptation of the cell cycle but that multiple and diverse regulatory systems are involved in coordinating DNA replication with growth rate (Murray and Koh, 2014).

1.5 Single-cell analysis

Traditional population-based studies only grasp the average behavior of cells within a population. Clonal populations are nonetheless composed of individual cells that display very different traits or behaviors and population studies might lead to misinterpretation of the observed phenomena (Avery, 2006). For example, it would be complicated to infer a bilinear growth model with NETO events from population studies, since the timing of NETO varies between individuals. Population studies would only detect that growth is size-dependent and possibly misinterpret the single-cell growth model as exponential growth. (See Mitchison, 2005 and Cooper, 2006 for an interesting debate on the use of single-cell versus population data during the search for the true growth model in *S. pombe*). In recognition of this problem, single-cell analysis is gradually becoming the norm, and is more accessible thanks to the development of tools for single-cell analysis, such as fluorescence time-lapse microscopy.

1.5.1 Florescence time-lapse microscopy

Optical microscopy has long been one of the most important tools allowing the visualization of the microscopic world. Its popularization among microbiologists began in the late 17th century (Lane, 2015) and remains, today, one of the major tools used by microbiologists. The development of time-lapse microscopy, fluorescent reporters, and tools for quantitative image analysis allows the tracking of live individual cells and cellular processes over time (Locke and Elowitz, 2009). More recently, it became possible to precisely track proteins over time, thereby allowing the detection of phenomena (e.g., pulsatile protein expression, protein movements, or transient co-localization of proteins) that would be missed otherwise (for example, Bennett and Hasty, 2009; Wakamoto et al., 2013; Santi and McKinney, 2015). Interestingly, fluorescence time-lapse microscopy allows the study of cellular processes in unsynchronized populations, which is of particular interest for cell cycle studies. Moreover, it allows the tracking of cells over multiple generations, which is very valuable in studies on homeostasis.

Despite these technical advances, fluorescence time-lapse imaging of live single cells remains challenging. The environment, such as the medium composition and the temperature, must be tightly controlled in order to keep cells alive and unstressed for extended periods of time. In addition, with sequential image acquisition comes the potential problem of phototoxicity and trade-offs often have to be made between spatial resolution and temporal resolution.

1.5.2 Microfluidic devices

Microfluidic devices are useful to sustain cell growth and prevent cells from moving out of the field of view during long-term fluorescence time-lapse imaging. In biological applications, microfluidic devices are often made of polydimethylsiloxane (PDMS), a soft, transparent, biocompatible polymer that is permeable to gas and thus well suited for live-cell imaging (Duffy et al., 1998). In this thesis, I use a microfluidic device that was developed for long-term time-lapse imaging of mycobacteria (Santi et al., 2013; Wakamoto et al., 2013; Santi and McKinney, 2015). The device consists of a PDMS chip with a micro-patterned serpentine channel. Medium is flowed through the serpentine channel and reaches bacteria placed on top of a glass coverslip through a semi-permeable nitrocellulose membrane (Figure 7).

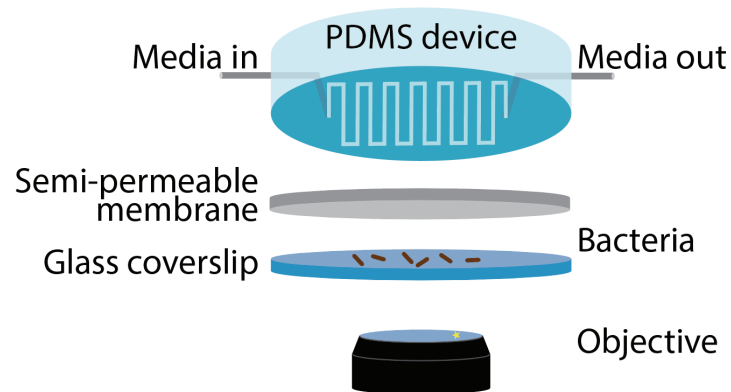


Figure 7. Microfluidic device for time-lapse imaging of mycobacteria

Adapted from [Delincé et al., 2016](#).

1.5.3 Image analysis

Following the automation of microscopic image acquisition, time-lapse experiments generate huge datasets, which pose a challenge for data analysis. Many software tools providing automated ways to segment and track cells over time have been developed ([Ducret et al., 2016](#); [Kaiser et al., 2018](#); [Fazeli et al., 2020](#)). However, due to the variety of cell morphology and spatial behavior, these software tools are usually adapted to specific cell types and image analysis remains difficult for *M. smegmatis*, which forms tightly packed clusters of cells in which detection of cell division is not trivial. In this thesis, I use a plugin for ImageJ (“Bisquit”) that tracks *M. smegmatis* cells in a semi-automated way over many generations; this tool was developed by a former master student (Olivia Mariani) in a joint collaboration between the McKinney and Unser labs at EPFL.

Aims of the thesis

Cell growth, cell cycle progression, and cell division are three fundamental processes that need to be coordinated in order to maintain cell size homeostasis. These processes are also high-priority targets for antibiotic development. For this reason, these processes are intensively studied in medically relevant organisms, including model organisms such as *M. smegmatis*. However, exactly how those three processes work, how they are coordinated, and how they adapt following environmental changes remain not well understood.

The goal of this thesis is to better understand cell growth, cell cycle progression, and cell division as well as their coordination to maintain cell size homeostasis in *M. smegmatis*, an experimentally tractable organism that is often used as a proxy for the important human pathogen *M. tuberculosis*. To pursue this goal, I used time-lapse microscopy to study single-cell behavior under different growth conditions, along with fluorescent reporter strains to observe DNA replication, chromosome segregation, and cell division dynamics at the single-cell level.

In the first chapter of this thesis, I report on studies of *M. smegmatis* cell growth. *M. smegmatis* grows by polar extension in a biphasic manner (Hannebelle et al., 2020). During the first phase, newborn cells grow in an asymmetric fashion, inasmuch as the old pole elongates rapidly while the new pole elongates slowly or not at all. During the second phase, cells grow symmetrically following an event that we call “new end take-off” (NETO) based on similar observations in the fission yeast *S. pombe* (Mitchison and Nurse, 1985). Why the new cell pole does not start to grow immediately after division remains unknown and the timing of NETO appears to be highly variable from cell to cell (Hannebelle et al., 2020). By analyzing the timing of NETO under different growth conditions, we aim to find how growth speed modulates the timing of NETO at the single-cell level.

In the second chapter, I present studies on cell-cycle progression in *M. smegmatis*. Although the impact of the environment on growth speed and cell-cycle progression has been well documented at the population level, there have been few attempts to quantify these parameters at the single-cell level in any organism and no previous studies, as far as we are aware, in *M. smegmatis*. Thus, in this chapter, I aim to describe the relationship between growth speed and cell-cycle progression under different growth conditions, specifically, carbon-limiting and temperature-limiting growth conditions. Unexpectedly, multifork replication events were recently discovered in *M. smegmatis*, a relatively slow-growing bacterium. Trying to reconcile this observation with the presumed link between fast growth and multifork replication, as observed in population studies of other bacteria, I aim to find parameters that account for multifork replication at the single-cell level.

In the third chapter, I present studies on *M. smegmatis* cell division. *M. smegmatis* lacks the two main mechanisms for division site placement present in *E. coli* and *B. subtilis*, namely the

nucleotide occlusion (Noc) and Minicell (Min) systems, and has no known mechanisms for division site placement. Published studies from several groups suggest that there may be a link between chromosome replication/segregation and division site selection in *M. smegmatis*, since depletion of components of the chromosome partitioning (Par) system results in highly asymmetric divisions along with mis-positioning of the DNA replication machinery. In this chapter, I aim to identify the link between replisome positioning and placement of the cell division site.

In the fourth chapter, I use computational simulations to assess the importance of determining the true dynamics of single-cell growth in order to distinguish between alternative division control models operating in the context of cell size homeostasis. This analysis was prompted by the discovery that *M. smegmatis* cells grow in a biphasic manner, which differs from the simple exponential growth model that has been experimentally validated in other well-studied bacteria, such as *E. coli*.

Chapter 2 Growth-speed is coupled to pole elongation speed and NETO timing in *Mycobacterium smegmatis*

Gaëlle Vuaridel-Thurre, Neeraj Dhar, John D. McKinney

¹School of Life Sciences, Swiss Federal Institute of Technology in Lausanne (EPFL), CH-1015 Lausanne, Switzerland

Keywords: growth speed, NETO, single-cell time-lapse microscopy, DnaA

*Address correspondence to: john.mckinney@epfl.ch

2.1 Abstract

Bacteria are remarkably diverse in sizes and shapes and exhibit different strategies to grow at the single cell level. *Mycobacterium smegmatis* is rod-shaped and grows by tip elongation in a biphasic manner with a “new end take off” (NETO) similar to fission yeasts. Although the timing of NETO has been reported to be very variable, why some cells initiate NETO earlier than others remains unknown. Here, we use time-lapse microscopy to measure NETO timing along with pole growth speed under different growth conditions. We show that *M. smegmatis* grown at different growth speed modulates the timing of NETO along with the pole growth speed. Using simulations, we show that both are co-varied and propose a model in which cells initiate pole growth at a timing that optimises the cell growth speed. As a consequence of different timings of NETO, the pole growth dynamics changes and the single cell growth model appears different.

2.2 Introduction

Cells are very heterogeneous in shape and size. Even among cells that are similar in shape, there is a big difference in how they grow. For example, *Escherichia coli*, a rod shaped bacteria grows by adding new material to the side walls (Eswara and Ramamurthi, 2017; Kuru et al., 2012) which is believed to be responsible for an exponential growth at the single cell level (Daniel and Errington, 2003). Another rod shaped bacteria, *Mycobacterium smegmatis*, grows by tip elongation (Aldridge et al., 2012; Eswara and Ramamurthi, 2017; Meniche et al., 2014; Santi et al., 2013) and it has recently been shown that they grow in a biphasic manner resembling the new end take off (NETO) of *Schizosaccharomyces pombe* (Hannebelle et al., 2020). The transition from slow-growth to fast-growth of the new pole has been shown to be highly variable, changing the degree of growth asymmetry in a range between unipolar to bipolar growth. How the transition from slow-growth to fast-growth of the new pole is regulated in *M. smegmatis* is unknown. We hypothesise that in order to regulate its growth speed, *M. smegmatis* could change its pole elongation speed (Figure 1a) or the timing of NETO (Figure 1b) or both (Figure 1c).

Using time-lapse microscopy, we analysed growth (pole elongation speed and timing of NETO) of single cells grown in different mediums providing a large range of growth speeds. We decreased the growth speed of *M. smegmatis* cells by limiting the glycolytic flux using different ratios (10:1, 20:1, 40:1) of α -methylglucoside (α MG) to glucose in M9 medium (carbon-limited growth). α MG is a non-metabolizable analogue of glucose that competes with glucose for transportation into the cell (Hansen et al., 1975). By varying the ratio of α MG to glucose, the growth speed can be varied without causing the pleiotropic effects on gene expression or changes to metabolic pathways that usually occur upon switching between different carbon sources (Hansen et al., 1975). In order to increase the growth speed of cells grown within the same medium, we analysed growth (pole elongation speed and timing of NETO) in a strain overexpressing DnaA. DnaA is a highly conserved bacterial protein that

triggers the formation of replication forks by binding to specific sites adjacent to the chromosomal origin of replication (reviewed in [Katayama et al., 2010](#); [Skarstad and Katayama, 2013](#)). DnaA overexpression in *M. smegmatis* has been shown to result in premature initiation of DNA replication and increase in growth speed ([Vuaridel-Thurre et al. in prep](#); see chapter 2).

We found that cells modulate their growth speed using both, pole elongation speed and the timing of NETO. Through simulations, we show that cell growth speed is optimally increased by co-variation of the poles growth speed and the timing of NETO. Cells modulate NETO in such extreme ways that NETO can occur even after several generations when the new pole already became an old pole. The timing of NETO changes the pole growth dynamics and results in apparent different single cell growth models.

2.3 Results

2.3.1 Pole elongation is slower when cells are grown in nutrient-poor medium

We asked whether nutrient deprivation affects the pole elongation speed, as diagrammed in [Figure 1a](#), by using time-lapse microscopy of cells that were surface-labelled with the fluorescent dye Alexa-488, as described previously ([Aldridge et al., 2012](#)). We followed the elongation of single poles in rich medium (7H9) and poor medium (M9 medium containing 20 times more α MG than glucose (20:1 α MG)). We used time-lapse images after pulse chase labelling the old cell wall allowing us to precisely measure the pole elongation by measuring the distance between the old, stained, cell wall and the new, unstained, growing pole after a division event ([Figure 2a](#)). We were able to track the pole elongation through two to three generations and we show in [Figure 2b](#) one representative pole elongation curve for growth in 7H9 (green) and in 20:1 α MG (purple). We observed in both growth conditions that pole growth is first slow (pre-NETO) and then faster (post-NETO). We performed a bilinear fit and compared the elongation speed between 7H9 and 20:1 α MG, both pre- and post-NETO ([Figure 2c](#)). This comparison showed that the pole elongation speed is different between the two media, both pre-NETO and post-NETO, and that post NETO it is two times faster in 7H9 ([Figure 2c](#)). For detection of NETO events, we found that the results obtained using Alexa-488 pulse-labelling vs. phase-contrast images alone were similar ([Figure 2d](#)). Since Alexa-488 pulse-labelling is useful for detection of NETO events over only one or two generations, due to dilution of the dye over time, hereafter we use phase-contrast images to detect NETO in order to increase the throughput of our experiments.

2.3.2 NETO is delayed when cells are grown in nutrient-poor medium

We asked whether nutrient deprivation delays NETO, as diagrammed in [Figure 1b](#), by using time-lapse microscopy of cells and detection of NETO in phase-contrast images ([Figure 3a](#)). NETO detection on phase-contrast time-lapse images was possible using cell features such as kinks, small differences in cell width or in phase darkness as references for pole elongation

(Figure 3a). We decreased the growth speed of *M. smegmatis* cells by growing them in 10:1 α MG, 20:1 α MG and 40:1 α MG. We found that as the medium gets poorer and growth speed decreases, NETO occurs later which is represented by a timing of NETO getting constantly bigger than the interdivision time (Figure 3b). Our data for 7H9 are consistent with the averaged data found by AFM measurements in Hannebelle et al., 2020 (Figure 3b). Since the timing of NETO is very variable from cell to cell, we investigated the dynamic of pole growth at the single cell level. For each growth condition, we detailed for 100 cells which pole was growing slowly (pre-NETO) and fast (post-NETO) and the duration of those periods in proportion to the cell cycle (Figure 3c). In agreement with (Hannebelle et al., 2020), we found that in 7H9, the majority of cells were born with the old pole already growing fast, followed by the new end take off later in the cell cycle. We show that as the medium gets poorer, NETO occurs later in the cell cycle, resulting in fewer cells with both poles growing fast during their cell cycle. Moreover, as the medium gets poorer, an increasing number of cells display no fast growth for both of their poles during a fraction of the cell cycle. It is also remarkable that in the two poorest conditions (20:1 α MG and 40:1 α MG), when none of the poles are growing fast, it is more often the new pole that starts growing fast before the old pole (Figure 3c). The timing of NETO thus changes the dynamic of pole growth. We show in Figure 3d an example drawn from a time lapse in 40:1 α MG where a new end take off occurs before an old end take off (NETO-before-OETO). The division of the first cell (green) creates two new poles. By following the growth of one of the two daughter cell (purple), we observe the old pole which is growing fast, moving away from the “kink” present on the cell while the new pole is almost non-growing. The purple cell divides after 8 hours of the time lapse and the previously new pole becomes the old pole of the pink daughter cell. This now old pole remains non-growing while the new pole of this pink cell transitions quickly to fast growth (NETO-before-OETO). The pink cell divides after 14h of the time-lapse and the non-growing old pole is inherited by the blue daughter cell and becomes three generations old. Both poles remain almost non-growing until 16 hours of the time lapse, when finally, the pole formed by the division of the green cell starts growing at a faster speed.

2.3.3 The single-cell growth model depends on the timing of NETO.

The timing of NETO changes the dynamic of pole growth which potentially impacts the apparent single cell growth model. We illustrate in Figure 4 all possible scenarios derived from the timing of NETO along with the corresponding single cell growth curves obtained from our experiments. The typical situation, is when the old pole is growing from the start and the new pole starts growing toward the end of the cell cycle. This gives rise to a fast-biphasic cell growth (Figure 4a). The reverse situation where the new pole is growing first and the old pole grows later in the cell cycle is equivalent but is almost never observed. As an example of biphasic fast growth, we show a typical growth curve from 7H9. A bilinear model was selected as the best fit among linear, trilinear and exponential models (the selection was performed using the method described in Vuaridel-Thurre et al., 2020, Supplementary Figure 1). In some cases, especially in M9, 10:1 α MG and 20:1 α MG, cell growth is unipolar, resulting in a

monophasic cell growth pattern (Figure 4b). Unipolar growth is almost always from the old pole. As an example of monophasic growth, we show a growth curve from 10:1 α MG. A linear model was selected as the best model for this growth curve (Supplementary Figure 1). However, half of the cells following a monophasic growth fitted best a linear growth and the other half fitted best an exponential growth (data not shown) and we were unable to distinguish between exponential and linear pole elongation. In some cases, we observed cells with both, a NETO and an OETO happening during the cell cycle. In such case, cell growth is triphasic (Figure 4c) and a trilinear model was indeed selected as the best model for the growth curve shown here (Supplementary Figure 1). Finally, in the poorest mediums (20:1 α MG and 40:1 α MG), a large percentage of cells have no poles growing at the beginning of their cell cycle with one of the pole (usually the new pole) taking off later in the cell cycle. Those cells also display a biphasic growth (Figure 4d), albeit a slower biphasic growth than the biphasic growth observed in Figure 4a. A bilinear model was selected as the best model for the representative growth curve (Supplementary Figure 1).

2.3.4 Overexpression of DnaA causes increased cell growth speed due to earlier NETO without affecting pole growth speed

By decreasing the growth speed using different mediums, we showed that the pole elongation speed was decreased, and that NETO was delayed. We then aimed to verify that upon an increase in growth speed occurring within the same medium, pole elongation speed was increased and NETO occurred earlier. To this end, we used DnaA overexpressing cells that were shown to grow faster than wild type (WT) cells (Vuaridel-Thurre et al. in prep; see chapter 2). We first confirmed that the cell growth speed was increased upon DnaA overexpression in 7H9 (Figure 5a). Then, by analysing phase-contrast images, we measured the pole growth speed post-NETO and unexpectedly found out that it was not increased upon DnaA overexpression (Figure 5b). Only NETO was occurring earlier and explained the increase in growth speed (Figure 5c).

2.3.5 Cells optimize the pole growth speed and NETO timing to maximize the cell growth speed

In order to understand the impact that pole elongation speed and the timing of NETO have on the cell growth speed, we simulated cell growth speed in function of both. We implemented growth in fast growing mediums, assuming that the old pole is already growing fast at the cell's birth. We fixed a pre-NETO growth speed of the new pole of 0.15 $\mu\text{m}/\text{h}$ as it was the median value in 7H9 found in Figure 2c. We then varied the post-NETO growth speed from 0.15 to 1.1 $\mu\text{m}/\text{h}$ while also varying the NETO timing from 0% of the cell cycle (both poles are growing fast during the whole cell cycle) to 100% of the cell cycle (the new pole never takes off). The cell growth speed resulting from this simulation is shown in Figure 6, with the highest cell growth speed occurring at the highest pole growth speed and the earliest NETO. Starting from any pole growth speed or NETO timing, an optimal increase in cell growth

speed is obtained by varying both, NETO and pole elongation speed, following the cell growth speed gradient (Figure 6a). The cell growth speed gradient is not symmetric for shifts in pole growth speed and shifts in NETO timing. For example, if NETO happens at 0% of the cell cycle, the pole growth speed must be increased but no change in the NETO timing is needed in order to increase cell growth speed. If the pole growth speed is around 1 $\mu\text{m}/\text{h}$ and NETO quite late (90% of the cell cycle for example), cell growth speed is best increased by shifting NETO to an earlier time than by increasing pole elongation speed. We overlapped to Figure 6a data of the WT and DnaA inducible strains from the growth conditions where most of the cells follow a biphasic fast growth, similar to the parameters of the simulation. This overlap allows us to follow two interesting individual trajectories. First, we observe that the WT strain has an increased pole elongation speed and an earlier NETO when grown in 7H9 compared to M9, and the shift of the NETO timing and pole elongation speed from M9 to 7H9 follows well the cell growth speed gradient. The second trajectory is the shift observed in the DnaA inducible strain. Upon overexpression of DnaA, the DnaA inducible strain shifts NETO to an earlier time but has no changes in pole growth speed (not significant, see Figure 5b). Although an increase in pole growth speed should have happened for an optimal increase in cell growth speed, a bigger shift in NETO than in growth speed was predicted by the simulation.

2.4 Discussion

We report a co-variation of pole elongation speed and timing of NETO during changes in cell growth speed as illustrated in Figure 1c. Through simulations we show that such a covariation optimizes the cell growth speed. This suggests that it is energetically favourable for the cell to optimise the two parameters in function of each other. For example, it might not be worth for a cell to invest energy to have both poles growing (through an early NETO) when increasing the speed of the growing pole results in a better increase in cell growth speed. Similarly, when pole growth speed is already high, the benefit of having both poles growing might be higher than increasing further pole elongation speed. However, we saw that upon DnaA overexpression leading to an increase in growth speed, the DnaA inducible strain only decreased the timing of NETO and did not increase pole growth speed even-though it does not perfectly optimize the increase in cell growth speed. One possible explanation could be that there is a limit to the maximal growth speed that can be reached by the poles (around 0.9 $\mu\text{m}/\text{h}$?). However, if there is truly such a limit to the pole elongation growth speed, it seems to be only reached in exceptional cases of fast growing mutants.

We saw that the timing of NETO results in different dynamics of pole elongation. In the poorest mediums, NETO often occurs after the next division. Resulting from such a late NETO, there is a period of time during which none of the poles of the newborn cell have transitioned to fast growth. Interestingly, in such cases it is rather the new pole that starts to grow first rather than the old pole ("NETO-before-OETO"). The same behaviour can be observed upon antibiotics treatments (unpublished observations), with some poles that seem inactive. It

could indicate that cells grown under stressful conditions are able to “inactivate” one pole and favour growth of the most recent and healthy pole to optimise cell growth.

Resulting from different timings of NETO, the single cell growth model may *seem* to vary while show mono, bi or even tri-phasic growth pattern. This has a potential impact on the study of cell size homeostasis since it has been shown that growth at the single cell level is of crucial importance when studying the controls of cell division (Vuaridel-Thurre et al., 2020; see chapter 4). Since the timing of NETO, and therefore the single cell growth pattern, is different under different growth conditions, it might be possible that the control of cell division needs to be different for each growth condition in order to maintain cell size homeostasis. This speculation is supported by (Wallden et al., 2016) who reported different controls for cell division for *Escherichia coli* cells grown at different growth rates.

Even though it is now clear that single cell growth can be mono, bi or tri-phasic, the long-standing problem to distinguish between linear or exponential growth persists since we were unable to distinguish between linear and exponential pole growth. The implications of linear or exponential (cell) growth are very different and well described in (Sveiczzer et al., 2014). One of the challenge for linear growth is to allow daughter cells to have the same growth speed as their mother with only half of the mother’s cell content (Mitchison, 2003). Pole growth could be linear if the zone of insertion of the new cell wall material is limiting or exponential if it can expand (Daniel and Errington, 2003) Even though linear cell growth seems more unlikely, the context of phasic growth with changes in growth speed that can happen throughout generations provides the opportunity for a subpopulation of cells to grow linearly while bypassing some of the limitations that are described for a purely linear growing population. For example, a linearly growing cell that has only one pole growing, can produce at division three non-growing poles and only one growing pole. This allows a majority of the population (see Figure 3c, 10:1 α MG) to grow linearly without a doubling of cell growth speed after division.

In the future, it would be interesting to determine whether the pole growth dynamic is the same in different mediums providing the same growth speeds or to perform the same study on *Mycobacterium Tuberculosis* that has a much slower pole growth speed and a relatively early NETO (Hannebelle et al., 2020). Co-variation of pole elongation speed and NETO timing in order to optimize cell growth speed might be a general rule for pole-growing organisms and it would be interesting to verify if it is conserved across phyla.

2.5 Methods

2.5.1 Data selection

For the growing poles of the 100 cells in Figure 3c, 100 cells were randomly selected using the *randperm()* function of MATLAB.

2.5.2 NETO detection

From the time lapses with the old cell wall stained, the timing of NETO was found using a bilinear fit (see next section). In phase-contrast time-lapse images, we used a Fiji plugin (Bisquit) developed specifically for *M. smegmatis* by O. Mariani to track cell length, poles and poles ages through lineage tracking. Poles were then followed over several generations using a custom made Matlab GUI allowing us to manually mark the NETO when we detected it using cell irregularities as visual markers for cell elongation. The program then automatically marked the poles as non-growing for each time point before NETO and as growing for each time point after NETO.

2.5.3 Bilinear and trilinear fit

The fit was performed in Matlab. After smoothing of the pole growth curve using the *smooth()* function, the best timing for NETO was found using the functions *lsqnonlin()* and *fitnlm()* for a bilinear model with four coefficients (the slope before NETO, the slope after NETO, the timing of NETO and an offset). For the trilinear model, we used the *lsqcurvefit()* function with six coefficients (the slope before the first rate change, the slope between the two rate changes, the slope after the second rate change and the two timings of the rate changes, and an offset). Different starting point were tried for the *lsqnonlin()* and *lsqcurvefit()* functions and the model providing the smallest sum of squares error when compared to the data was kept.

2.5.4 Bacterial strains and culture conditions

M. smegmatis mc²155 wild type strain expressing mCherry-DnaN (Santi et al., 2013) was used when measuring the pole elongation speed when the old cell wall was stained (Figure 2). *M. smegmatis* mc²155 wild type strain expressing mCherry-DnaN and Wag31-GFP (Santi et al., 2013) was used for the detection of the NETO timing in the different growth mediums (Figure 3 & 4). *M. smegmatis* mc²155 wild type expressing mCherry-DnaN with inducible *dnaA* was used to study the effect of *dnaA* overexpression on pole elongation speed and NETO timing (Figure 5). The WT control was the same, but uninduced strain. For the DnaA-overexpressing strain of *M. smegmatis*, the *dnaA* locus was amplified from *M. smegmatis* using forward (GGTTAATTAA ACGAGG TATCTCC ATG ACT GCT GAC CCC GAC CCA CCG TTC G) and reverse (GGTTAATTAA GC TCA GC GTT TGG CGC GCT GGC GGA TGC G) primers and *M. smegmatis* genomic DNA as the template. The primers were designed to contain PacI restriction sites and an optimized Shine-Dalgarno sequence upstream of the translational start site (Woong Park et al., 2011). The amplified sequence was confirmed by DNA sequencing and cloned into the PacI site of pND255, downstream of a tetracycline (Tet)-inducible promoter (Ehrt et al., 2005). pND255 is a mycobacterial plasmid containing sequences for single-copy integration at the chromosomal *attB* site, the gene encoding the Tet repressor, and the hygromycin resistance marker. The resulting plasmid, pND285, was transformed into an *M. smegmatis* mCherry-DnaN reporter strain and transformants were selected on LB plates containing 50 µg/ml

hygromycin. For experiments involving DnaA overexpression, anhydrotetracycline (Takara) was added to the bacterial culture at 200 ng/ml (7H9 medium) or 50 ng/ml (20:1 α MG medium) starting 4 hours before the cells were transferred from batch culture to microfluidic culture.

2.5.5 Bacterial culture conditions

Bacteria were grown in Middlebrook 7H9 liquid medium (Difco) supplemented with 0.5% albumin, 0.2% glucose, 0.085% NaCl, 0.5% glycerol, and 0.02% Tyloxapol, or in minimal M9 medium supplemented with 0.2% glucose and a 10:1, 20:1, or 40:1 excess of α -methylglucoside (α MG) to glucose. Cultures were grown with aeration at 30°C and 37°C to mid-log phase, corresponding to an optical density at 600 nm (OD_{600}) of 0.2 to 0.5 and stored at -80°C with (7H9 medium) or without (M9 medium) addition of glycerol to 15%. Frozen aliquots were thawed, used once, and discarded. Cells frozen in M9 medium were used for experiments with α MG. For experiments involving DnaA overexpression, anhydrotetracycline (Takara) was added to the bacterial culture at 200 ng/ml (7H9 medium) or 50 ng/ml (20:1 α MG medium) starting 4 hours before the cells were transferred from batch culture to microfluidic culture.

2.5.6 Pulse chase labelling of the old cell wall

The same protocol that was previously described by (Santi et al., 2013) and (Aldridge et al., 2012) was used. Briefly, cells were either grown in 7H9 or in 20:1 α MG to an OD_{600} of 0.5. 1ml of the cell suspension was centrifuged during 5 minutes at 2'500g and then washed with PBST (0.2% Tween 20). The pellet was then re-suspended in 1/10th of the original volume of PBST. Alexa Fluor 488 carboxylic acid succinimidyl ester (Invitrogen) was then added at a final concentration of 0.05mg/ml, gently mixed to the cell suspension and washed immediately after. The washing was again performed by 5 minutes centrifugation at 2500g and using PBST. The cells were re-suspended either in 2 ml of 7H9 or 20:1 α MG and put in the microfluidic device for immediate imaging.

2.5.7 Time-lapse fluorescence microscopy

Time-lapse microscopy was performed as described (Santi et al., 2013) Briefly, bacterial cultures were grown to OD_{600} 0.2 to 0.5 and agitated to separate single cells from clumps. A 3 μ l aliquot was spread on a semipermeable membrane, assembled in a custom-made microfluidic device, and imaged through a glass coverslip. Medium was flowed through the serpentine channels of the device at a speed of 18 μ l/min. Temperature around the microscope stage was maintained at 37°C. Cells were imaged on phase-contrast and fluorescence channels every 10 minutes (7H9), 15 or 17 minutes (M9), 15 minutes (10:1 α MG and 20:1 α MG) and 30 minutes (40:1 α MG). Transmitted polarized light exposure was set at 0.08 or 0.1 seconds and 32% or 50% of LED power. mCherry LED exposure was set at 0.08 or 0.15 seconds and 5% of LED power. GFP LED exposure was set at 0.1 or 0.2 seconds and 5%

LED exposure. Images were acquired using a CoolSnap HQ2 camera with 2x2 binning.

2.5.8 Simulation of cell growth speed in function of NETO and pole growth speed

The simulation was performed in Matlab. Growth in rich medium with the old pole already growing fast at the cell birth was simulated. pré-NETO speed of the new pole was set to 0.15 $\mu\text{m}/\text{h}$. Cell growth was simulated through two loops, one varying the NETO timing and one varying the post-NETO pole elongation speed. The whole cell elongation speed was calculated as the total elongation divided by the time during which the cell grew.

2.6 Figures

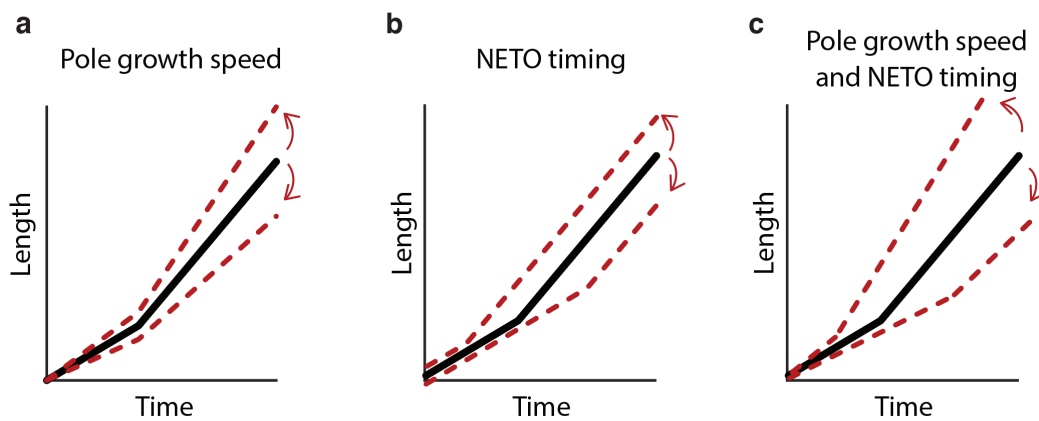


Figure 1. Two possible models to vary single-cell growth speed.

Cell growth speed could be varied by **(a)** changing the pole elongation speed, or **(b)** changing the timing of “new end take-off” (NETO), or **(c)** with a combination of both.

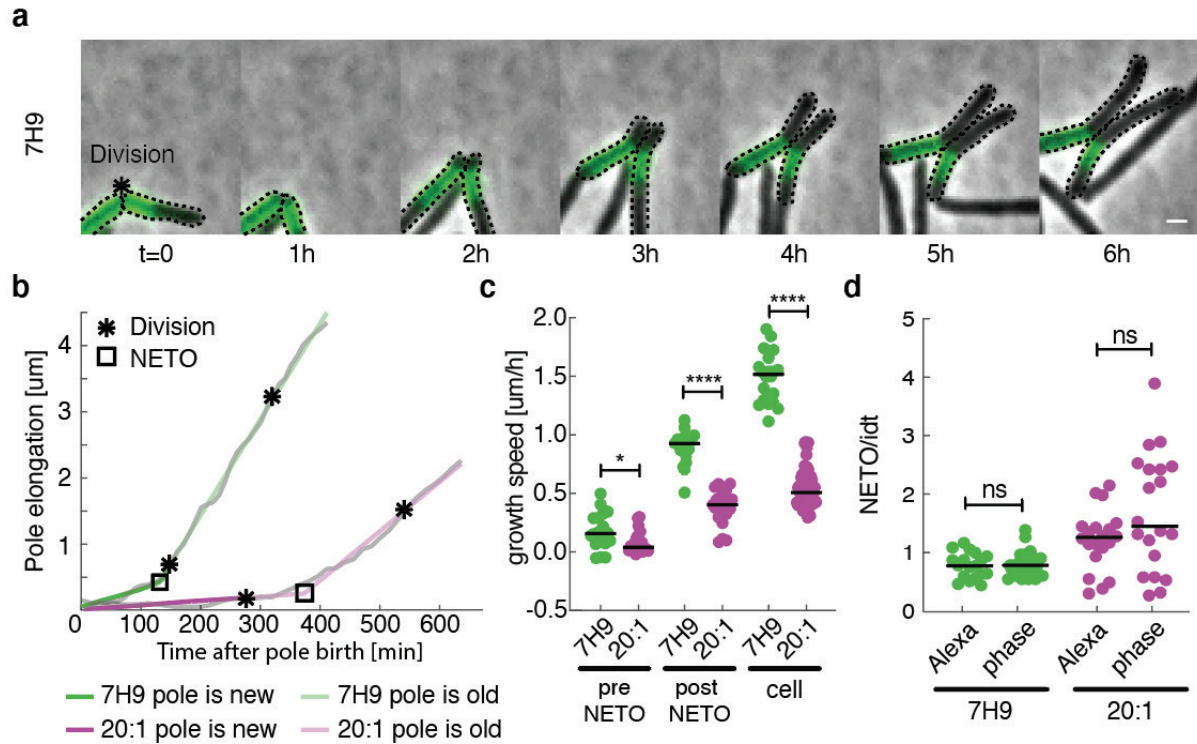


Figure 2. Pole elongation is slower when cells are grown in nutrient-poor medium.

Bacteria were pre-stained with Alexa-488, which labels the cell surface, then grown in a microfluidic device with a constant flow of 7H9 or 20:1 α MG medium (without Alexa-488). Images were taken every 10 (7H9) or 15 (20:1 α MG) minutes. **(a)** Measurement of pole elongation in Alexa-488-pulse-labeled daughter cells after cell division. Scale bar, 1 μ m. **(b)** Representative pole elongation curves spanning three generations in 7H9 (green) or 20:1 α MG (purple) medium. See Methods for bilinear fitting. **(c)** Pre-NETO and post-NETO pole elongation speeds and growth speed of the entire cell (cell) between birth and division. Pre- and post-NETO poles: $n = 18$ in 7H9 and $n = 20$ in 20:1 α MG. Cells: $n = 22$ in 7H9 and $n = 58$ in 20:1 α MG. **(d)** NETO timing in 7H9 or 20:1 α MG medium, as measured using bilinear fits of pole elongation obtained by pulse-chase labelling of the old cell wall (Alexa: $n = 18$ in 7H9; $n = 20$ in 20:1 α MG) or phase images (phase: $n = 27$ in 7H9 and 18 in 20:1 α MG).

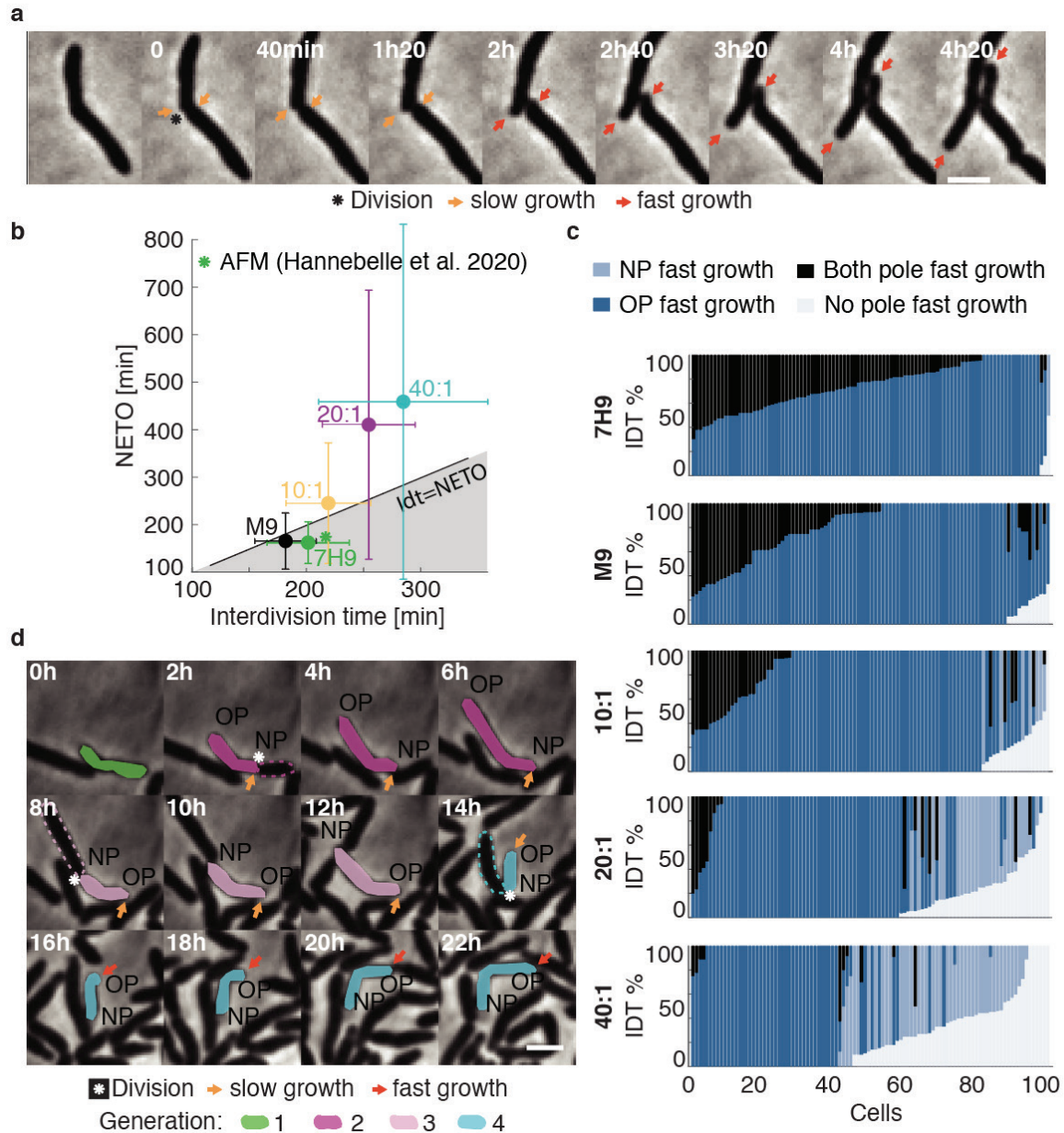


Figure 3. NETO is delayed when cells are grown in nutrient-poor medium.

Bacteria were grown in a microfluidic device with a constant flow of 7H9, M9, 10:1 α MG, 20:1 α MG, or 40:1 α MG medium. Images were taken at intervals specified in the Methods. **(a)** Detection of NETO using time-lapse phase-contrast microscopy for cells grown in 7H9 medium. **(b)** Timing of NETO in *M. smegmatis* grown in 7H9 (59 poles), M9 (67 poles), 10:1 α MG (59 poles), 20:1 α MG (74 poles), or 40:1 α MG (43 poles) vs. interdivision time for each growth condition (100 cells per growth condition). Symbols represent means; lines represent standard deviations. **(c)** Single-cell dynamics of pole elongation normalized to the interdivision time (IDT). Each bar represents one cell (100 cells per growth condition) **(d)** Representative example of a cell grown in 40:1 α MG in which NETO precedes “old end take-off” (OETO). Scale bar, 2 μ m. NP, new pole. OP, old pole.

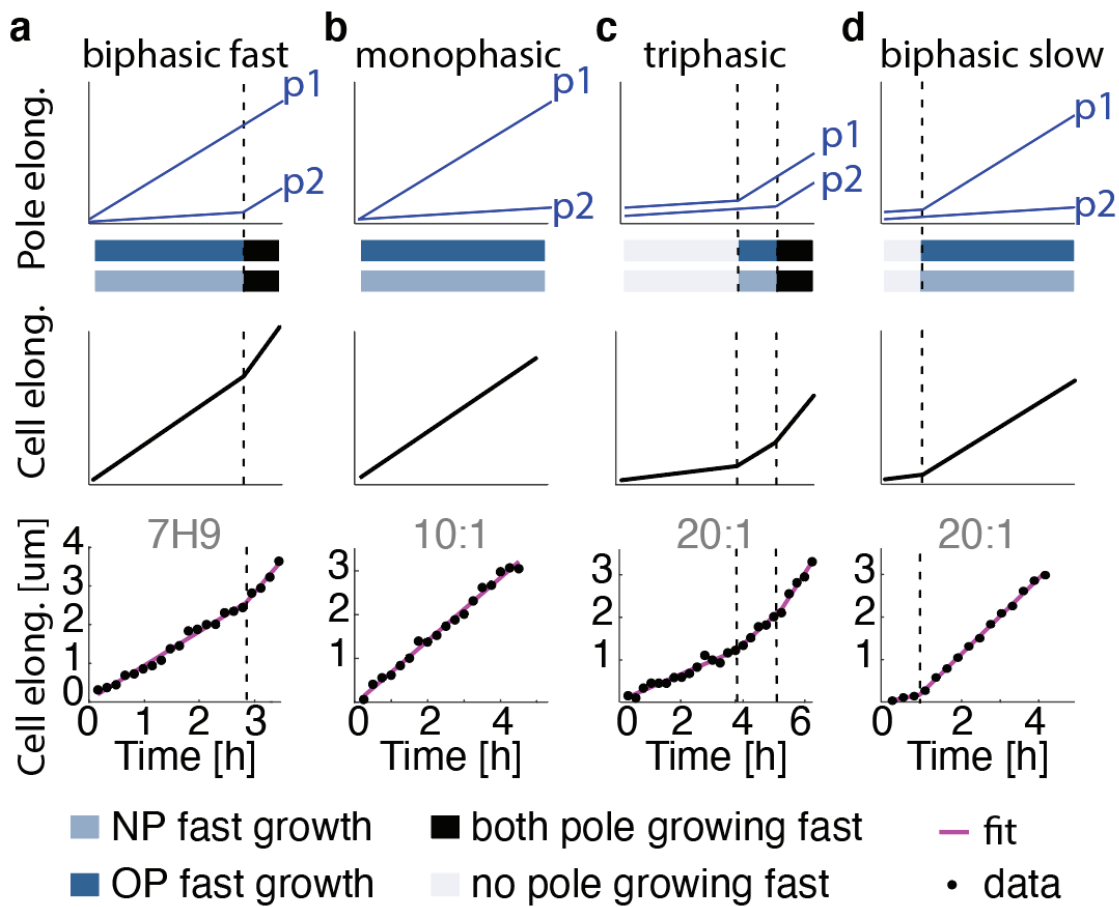


Figure 4. The single-cell growth model depends on the timing of NETO.

(a) Biphasic fast growth model. One pole (p1) is already growing fast at cell birth, as it took off during a previous generation. The second pole (p2) takes off (fast growth) later but before division. Bottom panel: representative cell growth curve from 7H9 medium. **(b) Monophasic growth model.** p1 is already growing fast at cell birth. p2 never takes off before division. Bottom panel: representative cell growth curve from 10:1 α MG medium. **(c) Triphasic growth model.** Both poles are growing slowly at cell birth. p1 takes off first. p2 takes off after p1 but before cell division. Bottom panel: representative cell growth curve from 20:1 α MG medium. **(d) Biphasic slow growth model.** p1 and p2 are both growing slowly at cell birth. Only p1 takes off before cell division. Bottom panel: representative cell growth curve from 20:1 α MG medium. See [Supplementary Figure 1](#) for the procedure for model selection based on fitting to the experimental data.

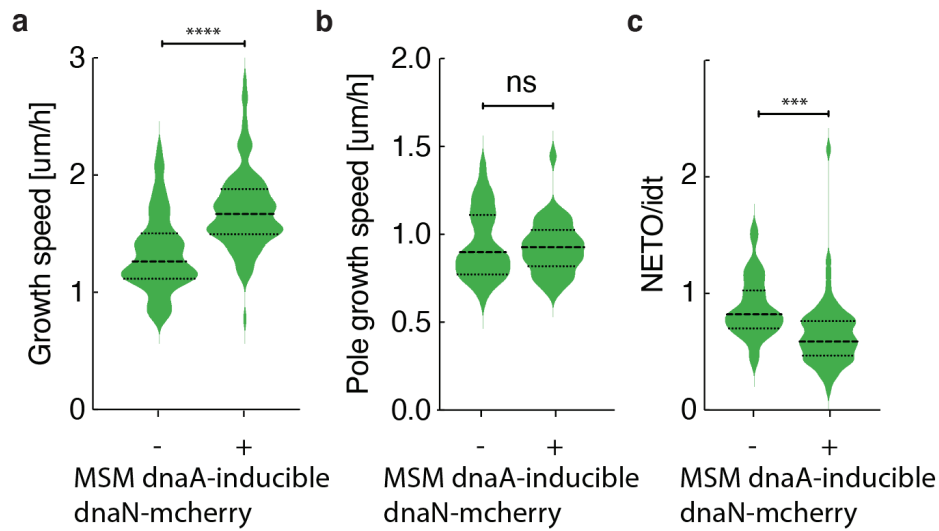


Figure 5. Overexpression of DnaA causes increased cell growth speed due to earlier NETO without affecting pole growth speed.

Bacteria expressing a second copy of *dnaA* from a Tet-inducible promoter were grown in a microfluidic device with a constant flow of 7H9 medium with (+) or without (–) inducer. Images were taken at 10-minute intervals. **(a)** Cell growth speed is faster in induced cells compared to uninduced cells ($n = 100$ cells for both conditions). **(b)** Pole growth speed is similar in induced cells ($n = 25$ poles) and uninduced cells ($n = 33$ poles). **(c)** NETO occurs earlier in induced cells ($n = 55$ poles) compared to uninduced cells ($n = 34$ poles).

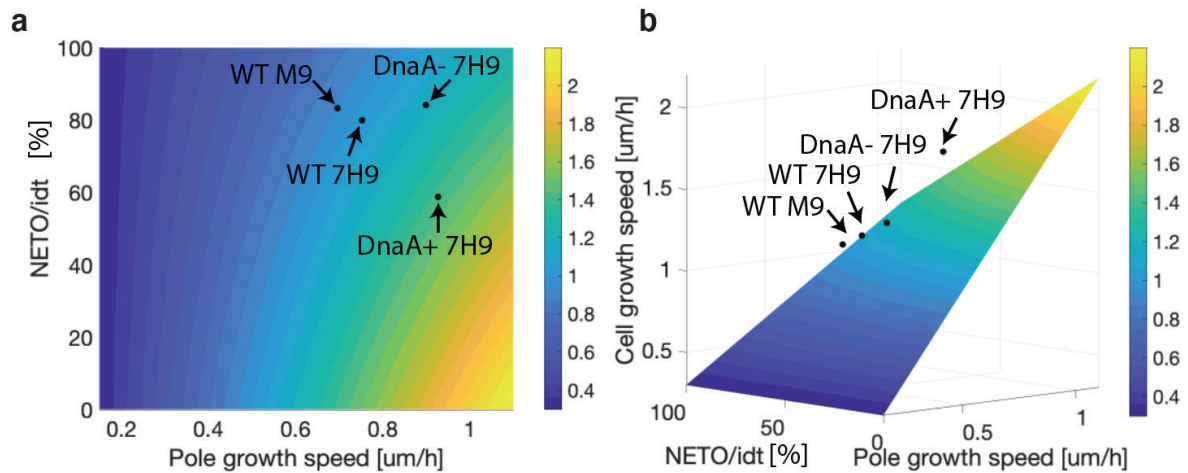
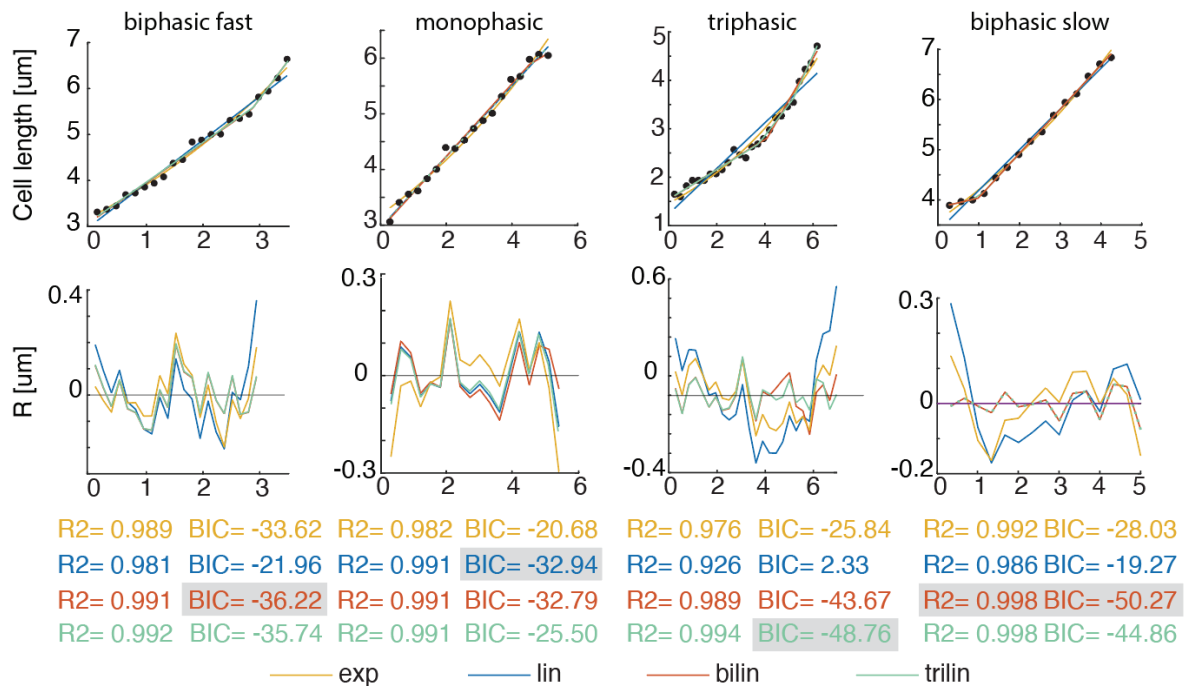


Figure 6. Cells optimize the pole growth speed and NETO timing to maximize the cell growth speed.

(a) Cell growth speed as a function of pole growth speed (post-NETO) and the timing of NETO normalized to the interdivision time (NETO/IDT). Symbols indicate data from the median values of wild-type bacteria grown in 7H9 medium (WT 7H9) or M9 medium (WT M9), and from the DnaA-inducible strain grown in 7H9 medium with inducer (DnaA+) or without inducer (DnaA-). Median values of pole growth speeds were calculated for wild-type cells grown in 7H9 medium ($n = 23$) or M9 medium ($n = 10$), and for DnaA-inducible cells grown in 7H9 medium with inducer ($n = 33$) or without inducer ($n = 25$). Median values of NETO timing were calculated for wild-type cells grown in 7H9 medium ($n = 59$) or M9 medium ($n = 67$), and for DnaA-inducible cells grown in 7H9 medium with inducer ($n = 55$) or without inducer ($n = 33$). **(b)** 3D plot to show the experimentally measured cell growth speeds for each strain and growth condition (symbols) relative to the simulation.

2.7 Supplementary Figure



Supplementary Figure 1. Selection of growth models based on experimentally measured cell growth curves.

Model selection of the growth curves depicted in Figure 4 was performed following the method described in (Vuaridel-Thurre et al., 2020). Single-cell growth models can be distinguished by analysis of residuals and BIC criteria. Each growth curve was fitted with a linear, bilinear, trilinear and exponential function. For each fit, R square (R2), residuals (R), and BIC criterion were evaluated in order to select the best fit (highlighted in grey) among the models tested. A good fit shows a high r square value, no pattern in the distribution of residuals and a low BIC criterion.

2.8 Acknowledgements

The authors are grateful to Aimie DuLac who participated in the acquisition of one of the 20:1 α MG movie in the context of her bachelor project and to Ambroise R. Vuaridel for his help with the Matlab script to track NETO on phase images. This work was funded in part by a grant to J.D.M. from the Swiss National Science Foundation (310030B_176397).

2.9 Author Contributions

G.V-T., N.D. and J.D.M. conceived the project. G.V-T. performed the experiments and simulations, wrote the Matlab script to analyze the data, analyzed the data and interpreted the results. N.D. constructed the DnaA strain. G.V-T., and J.D.M. wrote the paper. N.D. and J.D.M. supervised the project.

2.10 References

Aldridge, B.B., Fernandez-Suarez, M., Heller, D., Ambravaneswaran, V., Irimia, D., Toner, M., and Fortune, S.M. (2012). Asymmetry and aging of mycobacterial cells lead to variable growth and antibiotic susceptibility. *Science* 335, 100–104.

Daniel, R.A., and Errington, J. (2003). Control of cell morphogenesis in bacteria. *Cell* 113, 767–776.

Ehrt, S., Guo, X.V., Hickey, C.M., Ryou, M., Monteleone, M., Riley, L.W., and Schnappinger, D. (2005). Controlling gene expression in mycobacteria with anhydrotetracycline and Tet repressor. *Nucleic Acids Research* 33, e21–e21.

Eswara, P.J., and Ramamurthi, K.S. (2017). Bacterial cell division: Non-models poised to take the spotlight. *Annu Rev Microbiol* 71, 393–411.

Hannebelle, M.T.M., Ven, J.X.Y., Toniolo, C., Eskandarian, H.A., Vuaridel-Thurre, G., McKinney, J.D., and Fantner, G.E. (2020). A biphasic growth model for cell pole elongation in mycobacteria. *Nature Communications* 11, 452.

Hansen, M.T., Pato, M.L., Molin, S., Fill, N.P., and von Meyenburg, K. (1975). Simple downshift and resulting lack of correlation between ppGpp pool size and ribonucleic acid accumulation. *J. Bacteriol.* 122, 585–591.

Katayama, T., Ozaki, S., Keyamura, K., and Fujimitsu, K. (2010). Regulation of the replication cycle: conserved and diverse regulatory systems for DnaA and *oriC*. *Nature Reviews Microbiology* 8, 163–170.

Kuru, E., Velocity Hughes, H., Brown, P.J., Hall, E., Tekkam, S., Cava, F., de Pedro, M.A., Brun, Y.V., and VanNieuwenhze, M.S. (2012). In situ probing of newly synthesized peptidoglycan in live bacteria with fluorescent D-amino acids. *Angew Chem Int Ed Engl* 51, 12519–12523.

Meniche, X., Otten, R., Siegrist, M.S., Baer, C.E., Murphy, K.C., Bertozzi, C.R., and Sassetti, C.M. (2014). Subpolar addition of new cell wall is directed by DivIVA in mycobacteria. *Proc Natl Acad Sci U S A* 111, E3243–E3251.

Mitchison, J.M. (2003). Growth during the cell cycle. *Int. Rev. Cytol.* 226, 165–258.

Santi, I., Dhar, N., Bousbaine, D., Wakamoto, Y., and McKinney, J.D. (2013). Single-cell dynamics of the chromosome replication and cell division cycles in mycobacteria. *Nature Communications* 4, 2470.

Skarstad, K., and Katayama, T. (2013). Regulating DNA replication in bacteria. *Cold Spring Harb Perspect Biol* 5.

Sveicz, Á., Horváth, A., and Buchwald, P. (2014). Is there a universal rule for cellular growth? – Problems in studying and interpreting this phenomenon. *FEMS Yeast Research* 14, 679–682.

Vuaridel-Thurre, G., Vuaridel, A.R., Dhar, N., and McKinney, J.D. (2020). Computational analysis of the mutual constraints between single-cell growth and division control models. *Advanced Biosystems* 4, 1900103.

Wallden, M., Fange, D., Lundius, E.G., Baltekin, Ö., and Elf, J. (2016). The synchronization of replication and division cycles in individual *E. coli* cells. *Cell* 166, 729–739.

Woong Park, S., Klotzsche, M., Wilson, D.J., Boshoff, H.I., Eoh, H., Manjunatha, U., Blumenthal, A., Rhee, K., Barry, C.E., Aldrich, C.C., et al. (2011). Evaluating the sensitivity of *Mycobacterium tuberculosis* to Biotin Deprivation Using Regulated Gene Expression. *PLoS Pathog* 7.

Chapter 3 Cell-cycle progression and multifork replication in *Mycobacterium smegmatis* at different growth speeds

Gaëlle Vuaridel-Thurre¹, Neeraj Dhar¹, Paul Murima¹, John D. McKinney^{1*}

¹School of Life Sciences, Swiss Federal Institute of Technology in Lausanne (EPFL), CH-1015 Lausanne, Switzerland

Keywords: growth speed, interdivision time, cell-cycle progression, DNA replication, multifork replication, single-cell time-lapse microscopy, DnaA, hydroxyurea

*Address correspondence to: john.mckinney@epfl.ch

3.1 Abstract

Bacteria are capable of adapting to a wide range of environmental conditions, such as fluctuations in nutrient availability and ambient temperature. Although the impact of the environment on growth speed, generation time, and cell-cycle progression has been well documented at the population level, there have been few attempts to quantify these parameters at the single-cell level. Here, we use microfluidic cultures and single-cell time-lapse microscopy to investigate the relationship between growth speed, interdivision time, and cell-cycle progression in *Mycobacterium smegmatis* under carbon-limiting and temperature-limiting growth conditions. We report that there is marked cell-to-cell variation in growth speed under all growth conditions, and single-cell growth speed is a better predictor of cell cycle progression than the environmental conditions *per se*. Thus, cell-cycle progression is similar when comparing cells growing at the same speed under different environmental conditions but different when comparing cells growing at different speeds under the same environmental conditions. Contrary to the prevailing view that multifork DNA replication occurs when the interdivision time is shorter than the time required to replicate the genome (the C period), we find that multifork replication occurs when the time between DNA replication initiation events is shorter than the C period, which may occur even in slowly growing cells with interdivision times exceeding the C period. We also find that multifork replication and interdivision time are linked between generations, inasmuch as cells that undergo multifork replication have normal or longer-than-average interdivision times but give rise to daughters with shorter-than-average interdivision times.

3.2 Introduction

Adaptation of bacteria to different environments is often accompanied by changes in growth speed, interdivision time, cell size, and cell cycle progression (Young, 2006; Jonas, 2014; Westfall and Levin, 2017; Jun et al., 2018). Common environmental factors that may influence these cellular parameters include the abundance of nutrients and the ambient temperature. Changes in growth speed could potentially change the coordination between the DNA replication and cell division cycles at the single-cell level, as these cycles are not strictly coupled in bacteria and may respond differently to changes in growth speed (Dewachter et al., 2018).

The bacterial cell cycle comprises a B period from birth to initiation of DNA replication, C period from initiation to termination of DNA replication, and D period from termination to cell division (Figure 1a) (reviewed in Wang and Levin, 2009; Dewachter et al., 2018). In *M. smegmatis*, cells often initiate a second cycle of DNA replication after termination of the previous replication cycle but prior to division; in these cases, the C period spans the division event and the daughter cells inherit a partially replicated chromosome (Figure 1b) (Santi et al., 2013; Logsdon et al., 2017). For clarity in such cases, we may subdivide the C period into two parts, comprising the time from replication *initiation* to division in the mother cell (C_{init})

and the time from birth to replication *termination* in the daughter cell (C_{term}) (Figure 1b).

In fast-growing bacteria, when the time to replicate the genome is longer than the interdivision time, a second cycle of DNA replication may initiate before termination of the first cycle, resulting in “multifork replication” (Figure 1c) (Wang and Levin, 2009). It has long been known that multifork replication may occur in fast-growing bacteria such as *Escherichia coli* under optimal culture conditions (Cooper and Helmstetter, 1968). However, a recent study identified multifork replication events in the relatively slow-growing organism *Mycobacterium smegmatis* (Trojanowski et al., 2017), which poses a challenge to the presumed link between fast growth and multifork replication.

Emerging evidence suggests that cell-to-cell variation in growth rate may also have an impact on cell-cycle progression at the single-cell level. In *E. coli*, fast-growing individuals are larger and have shorter inter-division times compared to slow-growing individuals (Wallden et al., 2016). Fast-growing individuals also initiate DNA replication earlier, resulting in a shorter-than-average B period, and divide sooner after termination of DNA replication, resulting in a shorter-than-average D period (Adiciptaningrum et al., 2015). In the relatively slow-growing organism *M. smegmatis*, cells that are larger than average at birth elongate faster and initiate DNA replication earlier in the cell cycle compared to cells that are smaller than average at birth (Santi et al., 2013; Logsdon et al., 2017; Logsdon and Aldridge, 2018). However, the link between growth speed, interdivision time, cell-cycle progression, and multifork replication has not been systematically explored at the single-cell level.

Here, we use time-lapse microscopy and single-cell analysis to determine how growth speed affects cell-cycle progression and multifork replication in *M. smegmatis* in three different ways: by comparing cells growing at different speeds due to progressive carbon limitation or temperature limitation; by comparing fast-growing and slow-growing individuals in the same environment; by comparing individuals growing at the same speed in different environments (Supplementary Figure S1). All three comparisons indicate that single-cell variation in cell-cycle progression is linked to single-cell variation in growth speed rather than the environmental conditions *per se*. We also find that multifork replication is linked to short interdivision time not in the cells undergoing multifork replication but in the daughters of these cells, a point that could be discovered only through single-cell lineage analysis.

3.3 Results

3.3.1 Cell size responds to carbon availability but not temperature

Mycobacterium smegmatis is rod-shaped and grows by tip elongation. We therefore assumed a constant cell width and used cell length as a proxy for cell size (Adiciptaningrum et al., 2015; Witz et al., 2019). We measured the growth speed of single cells over time by culturing the bacteria in a microfluidic device and imaging them by time-lapse microscopy (Figure 1d). In order to measure the duration of each cell-cycle period, we used a reporter strain expressing

a red-fluorescent fusion protein (mCherry-DnaN) to track the chromosome replication cycle (Santi et al., 2013). DnaN is the sliding clamp of the DNA polymerase and marks the DNA replisome, which assembles when DNA replication initiates and disassembles when DNA replication terminates (Katayama et al., 2010).

We controlled the single-cell growth speed in two ways: by reducing the ambient temperature from 37°C to 30°C (temperature-limited growth) or by limiting the glycolytic flux using different ratios (10:1, 20:1, 40:1) of α -methylglucoside (α MG) to glucose in M9 medium (carbon-limited growth). α MG is a non-metabolizable analogue of glucose that competes with glucose for transportation into the cell (Hansen et al., 1975). By varying the ratio of α MG to glucose, the growth speed can be varied without causing the pleiotropic effects on gene expression or changes to metabolic pathways that usually occur upon switching between different carbon sources (Hansen et al., 1975).

We confirmed that decreasing the rate of glucose uptake (by increasing the ratio of α MG to glucose) or the ambient temperature reduces growth speed at the single-cell level (Figure 1e) and population level (Supplementary Figure S2). We also found that cell length at division decreases with decreasing carbon availability but is not affected by decreasing the ambient temperature (Figure 1f).

3.3.2 Initiation of DNA replication is delayed in carbon-limited cells, resulting in shrinkage of the C_{init} period and expansion of the B period

We measured the duration of cell-cycle periods in two ways: as the *absolute* duration of each period (expressed in minutes), and as the *fractional* duration of each period relative to the interdivision time of the cell (expressed as 0 to 1). We measured the absolute and fractional durations of single cells grown at 37°C in M9 medium (median doubling time, 180 minutes) or M9 medium containing 10:1 α MG (225 minutes), 20:1 α MG (240 minutes), or 40:1 α MG (270 minutes). As the growth speed decreases, the absolute durations of the B and C_{term} periods expand whereas the C_{init} period shrinks (Figure 2a, upper panels; Figure 2b). Similar results were obtained for cells grown at 30°C, although the absolute duration of each cell-cycle period is longer at 30°C compared to 37°C (Figure 2a, lower panels; Figure 2b).

We also found that the *fractional* durations of cell-cycle periods respond differently to carbon-limited growth at 37°C (Figure 2c, upper panels; Figure 2d). The C_{term} period is maintained at about 0.72 despite progressive carbon limitation. However, the timing of initiation of DNA replication relative to cell division is progressively delayed in response to carbon-limited growth. Consequently, the fractional duration of the C_{init} period is highest in M9 medium (0.17) and shrinks in response to carbon limitation, becoming undetectable in most cells growing in 40:1 α MG medium. Conversely, the fractional duration of the B period is lowest in M9 medium (undetectable in most cells) and expands in response to progressive carbon limitation.

We conclude that as cells grow more and more slowly due to progressive carbon limitation, initiation of DNA replication is increasingly delayed, resulting in shrinkage of the C_{init} period and expansion of the B period.

3.3.3 Temperature-limited growth exacerbates the delayed initiation of DNA replication in response to carbon limitation

Comparing cells grown in M9 medium at 37°C (median doubling time, 180 minutes) or 30°C (240 minutes), we found that temperature-limited growth expands the *absolute* time duration of all cell-cycle periods roughly equally (Figure 2a, 2b), and thus has little effect on the *fractional* duration of each period (Figure 2c, 2d). This is in sharp contrast to the effect of carbon-limited growth at 37°C, which results in shrinkage of the C_{init} period and expansion of the B period, as shown in the previous section. However, when we combined the two growth-limiting conditions, we found that temperature limitation further exacerbates the effects of carbon limitation (Figure 2c, 2d). Comparing cells grown at 37°C or 30°C under severe carbon-limiting conditions (20:1 α MG and 40:1 α MG media), the *fractional* duration of the B period expands while *both* the C_{init} and C_{term} periods shrink, resulting in a shortened C period (Figure 2d, Supplementary Figure S3).

We conclude that the B period expands while the C_{init} period shrinks in response to carbon limitation, and reducing the temperature from 37°C to 30°C exacerbates these effects. The effect of temperature on the fractional duration of cell-cycle periods in carbon-limited cells is noteworthy, because cell length at division is not affected by temperature, even in carbon-limited cells. These observations suggest that cell size and cell cycle progression are not strictly coupled.

3.3.4 Cell-cycle progression is different in cells growing at different speeds under the same culture conditions

We asked whether the changes in the fractional durations of cell cycle periods that we observed in carbon-limited cells (Figure 2) were due to carbon limitation *per se* or to reduced growth speed. We addressed this point by comparing the fractional durations of cell-cycle periods in cells growing at different speeds under the same culture conditions; for example, the growth speed of single cells of *M. smegmatis* in M9 medium ranges from 0.67 μ m/h to 1.41 μ m/h (Figure 3). Comparing single cells growing at different speeds in M9 medium, we found that the fractional duration of the C_{init} period is longer in fast-growing individuals compared to slow-growing individuals, and very few cells exhibit a B period (Figure 3). Conversely, comparing cells growing at different speeds in 40:1 α MG medium, the fractional duration of the B period is longer in slow-growing cells compared to fast-growing cells, and very few cells exhibit a C_{init} period (Figure 3). Cells growing in 10:1 α MG or 20:1 α MG medium exhibit intermediate behaviors (Figure 3). A similar relationship between single-cell growth speeds and fractional duration of the B and C_{init} periods was observed in temperature-limited cells growing at 30°C (Supplementary Figure S4).

These observations suggest that the fractional duration of cell cycle periods is determined not by the culture conditions *per se* but rather by the single-cell growth speed, which may vary widely between individuals growing under the same culture conditions.

3.3.5 Cell-cycle progression is similar in cells growing at the same speed under different growth conditions

We further tested the idea that the fractional duration of cell-cycle periods is linked to single-cell growth speed rather than culture conditions *per se* by comparing the fractional duration of cell-cycle periods in cells growing at the same speed under different culture conditions (Figure 4). For this analysis, we exploited the overlap between single-cell growth speed distributions of cells grown under different culture conditions (indicated by the black-shaded regions of the distributions in Figure 4a-c). As expected, we found that the average fractional durations of cell-cycle periods were different in cells growing in M9 medium (Figure 4d-f, bar IV) compared to 10:1 α MG medium (Figure 4d, bar I), 20:1 α MG medium (Figure 4e, bar I), or 40:1 α MG medium (Figure 4f, bar I). However, focusing on the small number of cells growing at the same speed in the matched media, which comprise the fastest-growing individuals in the α MG-containing media and the slowest-growing individuals in M9 medium, we found that the fractional durations of cell-cycle periods were very similar (Figure 4d-f, bars II and III).

We conclude that the fractional distribution of cell-cycle periods is very similar in single cells growing at the same speed in different culture conditions. These observations confirm our conclusion that the fractional duration of cell cycle periods is determined not by the culture conditions *per se* but rather by the single-cell growth speed, which may vary widely between individuals growing under the same conditions.

3.3.6 Overexpression of DnaA causes earlier initiation of DNA replication, faster growth, shorter interdivision time, and increased cell size

Based on the observed link between growth speed and the timing of initiation of DNA replication at the single-cell level (fast-growing cells initiate earlier, expanding the C_{init} period; slow-growing cells initiate later, expanding the B period), we hypothesized that forcing premature initiation of DNA replication by overexpression of DnaA would result in increased growth speed. DnaA is a highly conserved bacterial protein that triggers the formation of replication forks by binding to specific sites adjacent to the chromosomal origin of replication (reviewed in Katayama et al., 2010; Skarstad and Katayama, 2013). Overexpression of DnaA has been shown to result in premature initiation and increased cell size in several bacterial species (Atlung et al., 1985; Greendyke et al., 2002; Løbner-Olesen et al., 1989).

We used time-lapse microscopy to track growth and cell-cycle progression in DnaA-overexpressing bacteria tagged with the mCherry-DnaN replisome marker. As expected, we found that DnaA overexpression causes earlier initiation of DNA replication, resulting in expansion of the fractional duration of the C_{init} period and a corresponding shrinkage of the

B period, in both rich 7H9 medium and carbon-limited 20:1 α MG medium (Figure 5a). In rare cases, DnaA-overexpressing mother cells complete a second round of DNA replication and then divide to give rise to two daughter cells, each containing two chromosomes. Even more rarely, some DnaA-overexpressing mother cells initiate a third round of replication before dividing, giving rise to two daughter cells, each containing two partially replicated chromosomes. We have never observed these phenomena in wild-type bacteria. In such cases, the cell cycle cannot be classified using the established nomenclature for cell-cycle periods; therefore, our analysis of cell-cycle periods excluded these cells, which comprise about 30% of the total for cells grown in 7H9 medium.

Consistent with the hypothesized link between initiation of DNA replication and growth speed, we found that DnaA-overexpressing cells elongate faster than wild-type cells: 50% faster in 7H9 medium and 20% faster in 20:1 α MG medium (Figure 5b). Likely as a consequence of faster cell elongation, DnaA overexpression also decreases the average interdivision time by 30 minutes in 7H9 medium or 19 minutes in 20:1 α MG medium (Figure 5c), and increases the average cell length at division by 1.7 μ m in 7H9 medium and by 1.0 μ m in 20:1 α MG medium (Figure 5d).

We further tested the idea that single-cell growth speed is linked to the timing of initiation of DNA replication by comparing the fractional duration of cell cycle periods in wild-type and DnaA-overexpressing cells growing at the same speed. For this analysis, we exploited the overlap between the single-cell growth speed distributions of wild-type and DnaA-overexpressing cells (selected areas of overlap are indicated by the black-shaded regions of the distributions in Figure 5e,f). As expected, we found that the average fractional durations of cell-cycle periods were strikingly different in wild-type cells (Figure 5g,h, bar I) compared to DnaA-overexpressing cells (Figure 5g,h, bar IV). However, focusing on the selected subpopulations of wild-type and DnaA-overexpressing cells growing at similar speeds, we found that the fractional duration of cell-cycle periods was very similar (Figure 5g, bars II and III; Figure 5h, bars II and III).

We conclude that there is a causal relationship between growth speed and the timing of DNA replication initiation works in both directions: not only does increased growth speed result in earlier initiation, but also, conversely, earlier initiation results in increased growth speed.

3.3.7 Multifork replication is not determined by interdivision time at the single-cell level

In fast-growing bacteria such as *E. coli*, the time required to replicate the chromosome may exceed the time required to double the cell mass and divide. In these situations, cells initiate a new round of DNA synthesis before the previous round has been completed, resulting in simultaneous replication from multiple replication forks, i.e., “multifork replication” (Cooper and Helmstetter, 1968). Recently, the presumed link between fast growth and multifork replication has been challenged by the discovery that slow-growing bacteria such as *M.*

smegmatis may exhibit multifork replication, even though the inter-division time is longer, on average, than the time required to complete a full round of DNA replication (Trojanowski et al., 2017).

We used time-lapse microscopy and strains of *M. smegmatis* expressing the mCherry-DnaN replisome marker to measure the frequency of multifork replication. In wild-type cells, the frequency of multifork replication is low (about 6%) in 7H9 medium (Figure 6a) and undetectable in 20:1 α MG medium (Figure 6b). Compared to wild-type cells, multifork replication is more common in DnaA-overexpressing cells: about 40% in 7H9 medium (Figure 6c) and about 10% in 20:1 α MG medium (Figure 6d). In both strains, multifork replication events occur more frequently in fast-growing cells (7H9 medium) compared to slow-growing cells (20:1 α MG medium), consistent with observations in fast-growing species such as *E. coli*. On average, the period of multifork replication lasts 32 ± 29 minutes in 7H9 medium ($n = 23$) and 39 ± 29 minutes in 20:1 α MG medium ($n = 10$).

At the population level, consistent with previous observations, we found that the faster the cells grow, the higher the frequency of multifork replication (Figure 6e). However, the average C period is shorter than the average interdivision time under all of the growth conditions that we tested (Figure 6f), which raises the question, why do some cells exhibit multifork replication? We hypothesized that some cells undergo multifork replication because their C period is longer than the interdivision time *at the single-cell level*. Against this hypothesis, in DnaA-overexpressing cells in 7H9 medium, we found that 7 out of 20 cells undergoing multifork replication had an interdivision time longer than the C period (Figure 6g). Conversely, in cases of non-multifork replication, 12 out of 30 cells had a C period exceeding the interdivision time (Figure 6g). These observations suggest that the conventional model of multifork replication, which holds that multifork replication occurs whenever the C period is longer than the interdivision time, is not correct at the single-cell level.

3.3.8 Decreasing the inter-initiation time or increasing the C-period duration increases the frequency of multifork replication independent of the interdivision time

Multifork replication occurs when the time between two successive DNA replication initiation events (IIT) is shorter than the C-period duration (Figure 7a). Previously, it was thought that this condition ($IIT < C$) would occur only if the interdivision time (IDT) is shorter than the C-period duration ($IDT < C$). Our finding that multifork replication is independent of the interdivision time at the single-cell level prompted us to ask whether the frequency of multifork replication could be altered by manipulating either the inter-initiation time or the C-period duration. We attempted to decrease the time between DNA replication initiation events by overexpressing the DnaA initiator protein (Grigorian et al., 2003; Riber et al., 2006). Conversely, we attempted to expand the C period by treating cells with hydroxyurea, which slows down progression of DNA replication forks by reducing the pool of deoxyribonucleotide

precursors (Koc et al., 2004; Winder and Barber, 1973).

We found that overexpression of DnaA decreases the inter-initiation time by about 30 minutes ($p < 0.0001$) (Figure 7b) while having little effect on the C-period duration (Figure 7c). Conversely, treatment of cells with hydroxyurea increases the C-period duration by about 20 minutes ($p < 0.0001$) (Figure 7c) while having little effect on the inter-initiation time (Figure 7b). Compared to the low frequency of multifork replication events in wild-type cells (about 6%; Figure 7d), we observed a marked increase in the frequency of multifork replication events in cells with a reduced inter-initiation time (about 40%; Figure 7e) and in cells with an expanded C period (about 38%; Figure 7f). We confirmed that multifork replication is not associated with shorter-than-average interdivision times in cells undergoing multifork replication; on the contrary, multifork replication is associated with *longer*-than-average interdivision times in hydroxyurea-treated cells (Figure 7g). These results seem to contradict the prevailing idea that multifork replication is associated with fast growth and short interdivision times. However, when we tracked single-cell lineages through multiple generations, we found that the daughters of multifork mother cells have shorter interdivision times, on average, than the daughters of non-multifork mother cells (Figure 7h).

We conclude that the association between short interdivision time and multifork replication is a property of cell lineages rather than individual cells, inasmuch as cells undergoing multifork replication have normal or longer-than-average interdivision times but give rise to daughter cells with shorter-than-average interdivision times.

3.4 Discussion

In a classic study, Schaechter et al., 1958 found that growth speed, rather than the specific composition of the growth medium, determines bacterial cell composition and cell size (Schaechter et al., 1958). These conclusions, derived from experiments with the Gram-negative organism *Salmonella typhimurium*, became codified as the bacterial “growth law”. More recently, however, this view has been challenged by experiments showing that nutrient availability rather than growth speed determines cell size in *Escherichia coli* (Gram-negative) and *Bacillus subtilis* (Gram-positive) (Ehrenberg et al., 2013; Vadia and Levin, 2015). Schaechter et al. 1958 also found that temperature has little effect on cell size in *S. typhimurium*, a view that has also been challenged more recently in studies on *E. coli* (Trueba et al., 1982). The underlying reasons for these discrepancies are unclear, although the use of different organisms by different investigators might play a role. The paucity of published studies that dissect the relative contributions of growth speed and environmental conditions to cell size control is noteworthy, given the fundamental nature of these questions. In our studies of *Mycobacterium smegmatis*, belonging to the ancient phylum Actinobacteria (Lewin et al., 2016), we observed that cell size is linked to nutrient availability rather than growth speed (unpublished observations) and is unaffected by temperature.

Here, we addressed the related question of whether cell-cycle progression in *M. smegmatis* is determined by the growth speed or by the environmental conditions (nutrient availability and temperature) *per se*. Contrary to our observations on cell size, we found that cell-cycle progression at the single-cell level depends on growth speed rather than nutrient availability. Thus, single cells growing at different speeds in the same nutrient environment display marked differences in cell-cycle progression; conversely, cell-cycle progression is very similar in cells growing at the same speed in different nutrient environments. Similar results were obtained in a previous study of budding yeast, which showed that cell-cycle progression depends on growth speed rather than the nutrient environment (Brauer et al., 2007). The impact of temperature on cell cycle progression in *M. smegmatis* is more complex: in nutrient-rich environments, cell-cycle progression is apparently not affected by temperature, whereas temperature has a substantial impact on cell-cycle progression in nutrient-poor environments.

Our finding that cell-cycle progression is linked to growth speed rather than the nutritional environment *per se* raised the question whether this link is bidirectional, i.e., whether accelerating cell cycle progression would also increase the single-cell growth speed. We achieved this goal by constructing a strain of *M. smegmatis* that overexpresses the initiator protein DnaA, whose DNA-binding activity is thought to be rate limiting for initiation of DNA replication in bacteria (Katamaya et al. 2010). As we predicted, overexpression of DnaA resulted in earlier initiation of DNA replication, resulting in expansion of the C_{init} period and shrinkage of the B period. Consistent with the idea that single-cell growth speed and cell-cycle progression are linked bidirectionally, we found that overexpression of DnaA resulted in a roughly 50% increase in growth speed (from 1.2 to 1.7 microns per hour) and a roughly 15% decrease in the interdivision time (from 200 to 168 minutes), on average, at the single-cell level. Although the mechanism linking DnaA overexpression and increased growth speed is currently unknown, we speculate that premature duplication of the ribosomal RNA locus, which is adjacent to the chromosomal origin of replication, may play a role, as ribosome production is thought to be the main determinant of the overall rate of cell growth (Belliveau et al., 2020). To the best of our knowledge, this is the first demonstration that overexpression of DnaA can result in faster growth and shorter interdivision time at the single-cell level. We note, however, that faster growth and shorter interdivision time come with a fitness cost, inasmuch as cell death occurs at a high rate (about 9%) in DnaA-overexpressing cells, whereas we have never observed a spontaneous cell-death event in wild-type cells (unpublished observations).

In a classic study, the authors demonstrated that multifork DNA replication occurs in fast-growing bacteria, such as *E. coli* cultured in rich medium (Cooper and Helmstetter, 1968). They proposed that multifork replication allows cells to achieve interdivision times shorter than the C period by initiating a new cycle of DNA synthesis prior to the completion of the previous replication cycle. This view has been challenged by a recent study demonstrating the occurrence of multifork replication in the relatively slow-growing organism *M. smegmatis*,

even when the average interdivision time exceeds the average C-period duration (Trojanowski et al., 2017). Here, we show that the link between multifork replication and short interdivision time is multigenerational, inasmuch as cells undergoing multifork replication have normal or longer-than-average interdivision times but give rise to daughters with shorter-than-average interdivision times. However, in some cases we found that the interdivision times of multifork mother cells as well as their daughters exceed the C-period duration; in these cases, there would seem to be no necessity for multifork replication. Our findings seem to conflict with one of the observations of Trojanowski et al., 2017, who reported that cells undergoing multifork replication have shorter-than-average interdivision times. The underlying reason for this discrepancy is currently unclear. However, consistent with our conclusion that the link between multifork replication and short interdivision time is a multigenerational phenomenon, we found that shrinking the inter-initiation time (by overexpression of DnaA) or expanding the C-period duration (by treatment of cells with hydroxyurea) resulted in a sharp increase in multifork replication without disrupting the link between multifork replication in the mother cell and shortened interdivision times in the daughter cells. The robustness of this link is particularly noteworthy because DnaA overexpression and hydroxyurea treatment have opposing effects by increasing or decreasing the interdivision time, respectively.

3.5 Methods

3.5.1 Cell cycle reporter strain of *M. smegmatis*

An *M. smegmatis* mc²155 strain expressing Wag31-GFP (which tags the cell division septum and cell poles) and mCherry-DnaN (which tags the DNA replisome machinery) was described previously (Santi et al., 2013).

3.5.2 DnaA-overexpressing strain of *M. smegmatis*

The *dnaA* locus was amplified from *M. smegmatis* using forward (GGTTAATTAA ACGAGG TATCTCC ATG ACT GCT GAC CCC GAC CCA CCG TTC G) and reverse (GGTTAATTAA GC TCA GC GTT TGG CGC GCT GGC GGA TGC G) primers and *M. smegmatis* genomic DNA as the template. The primers were designed to contain PacI restriction sites and an optimized Shine-Dalgarno sequence upstream of the translational start site (Woong Park et al., 2011). The amplified sequence was confirmed by DNA sequencing and cloned into the PacI site of pND255, downstream of a tetracycline (Tet)-inducible promoter (Ehrt et al., 2005). pND255 is a mycobacterial plasmid containing sequences for single-copy integration at the chromosomal *attB* site, the gene encoding the Tet repressor, and the hygromycin resistance marker. The resulting plasmid, pND285, was transformed into an *M. smegmatis* mCherry-DnaN reporter strain and transformants were selected on LB plates containing 50 µg/ml hygromycin. For experiments involving DnaA overexpression, anhydrotetracycline (Takara) was added to the bacterial culture at 200 ng/ml (7H9 medium) or 50 ng/ml (20:1 αMG medium) starting 4 hours before the cells were transferred from batch culture to microfluidic culture. For experiments

involving hydroxyurea (Sigma-Aldrich), hydroxyurea was added to the wild-type bacterial culture at 0.4 mg/ml (7H9 medium) when cells were transferred from batch culture to microfluidic culture.

3.5.3 Bacterial culture conditions

Bacteria were grown in Middlebrook 7H9 liquid medium (Difco) supplemented with 0.5% albumin, 0.2% glucose, 0.085% NaCl, 0.5% glycerol, and 0.02% Tyloxapol, or in minimal M9 medium supplemented with 0.2% glucose and a 10:1, 20:1, or 40:1 excess of α -methylglucoside (α MG) to glucose. Cultures were grown with aeration at 30°C and 37°C to mid-log phase, corresponding to an optical density at 600 nm (OD_{600}) of 0.2 to 0.5 and stored at -80°C with (7H9 medium) or without (M9 medium) addition of glycerol to 15%. Frozen aliquots were thawed, used once, and discarded. Cells frozen in M9 medium were used for experiments with α MG.

3.5.4 Time-lapse fluorescence microscopy

Time-lapse microscopy was performed as described ([Santi et al., 2013](#)). Briefly, bacterial cultures were grown to OD_{600} 0.2-0.5, diluted two- to four-fold in fresh medium, and agitated to separate single cells from clumps. A 3 μ l aliquot was spread on a semipermeable membrane, assembled in a custom-made microfluidic device, and imaged through a glass coverslip. Medium was flowed through the serpentine channels of the device at a speed of 18 μ l/min. Temperature around the microscope stage was maintained at 30°C or 37°C. Cells were imaged on phase-contrast and fluorescence channels at intervals of 10 minutes (7H9 medium at 37°C or 30°C), 15 minutes (M9, 10:1 α MG, or 20:1 α MG medium at 37°C), 20 minutes (M9, 10:1 α MG, or 20:1 α MG medium at 30°C), 30 minutes (40:1 α MG medium at 37°C), or 60 minutes (40:1 α MG medium at 30°C). Prior to imaging, cells were allowed to adapt to conditions in the microfluidic device for up to 23 hours, depending on the medium and temperature. Transmitted light (polarization) exposure was set at 32-50% LED power and 0.08-0.1 seconds. mCherry LED exposure was set at 5% LED power and 0.08-0.15 seconds. GFP LED exposure was set at 5% LED power and 0.1-0.2 seconds. Images were acquired using a CoolSnap HQ2 camera with 2x2 binning.

3.5.5 Data selection for cell length and cell cycle measurements

Only movies with more than 40 analyzable cells were used. One to three movies were analyzed for each growth condition. For each condition, movies were obtained from one or two experiments; two experiments were performed if the movies made in the first experiment did not span a sufficient number of generations.

3.5.6 Cell length measurements

Cell length measurements and lineage tracking were performed using a Fiji plugin (Bisquit) developed specifically for *M. smegmatis* by O. Mariani. A complementary Matlab script was

developed and used instead of updating the plugin. Cell division was detected by eye using the abrupt snapping movement of the sibling cells away from each other that occurs during cell division, which is visible in phase-contrast images (Hannebelle et al., 2020). Snapping usually occurs within a few frames before or after the first appearance of the Wag31-GFP marker at the division site. Cell length at division (L_d) was calculated as the sum of the lengths at birth (L_b) of the sibling cells. Interdivision time (I_t) was defined as the time between birth and division. Since individual cells of *M. smegmatis* grow in a biphasic rather than exponential manner (Hannebelle et al., 2020), the metric growth speed ($\mu\text{m/h}$) is more appropriate than the growth rate ($1/h$). Growth speed was calculated as $\frac{L_d - L_b}{I_t} [\mu\text{m/h}]$. Growth rate was calculated as $\frac{L_d/L_b}{I_t} [h^{-1}]$.

3.5.7 Measurement of cell cycle periods

Absolute and fractional durations of cell-cycle periods were measured and assigned to individual cells in a semi-automated manner. First, a Matlab script with an interactive graphical user interface was developed and used to detect mCherry-DnaN foci and assign them to cells using the cell positions outputted by the Fiji plugin Bisquit. Bacteria expressing the mCherry-DnaN replisome marker may, in some cases, exhibit fluorescent foci that split and remerge over time (Santi and McKinney, 2015; Trojanowski et al., 2015); for clarity, we focused on cells that exhibited few or no such events. In a second step, a classification script (Matlab) was developed and applied to find the duration of each period of the cell cycle for each cell. The classification did not perform equally well for each medium, ranging from 90% correct assignments for cells grown in 7H9 medium at 37°C to 77% correct assignments for cells grown in M9 medium at 37°C. Thus, the third step was to manually modify cells displaying incorrect assignments of cell-cycle periods (e.g., an aberrantly long or unexpected period in a defined medium). Some aberrant cell cycles (e.g., of multinucleoid cells) could not be classified, even manually. When multifork replication was detected, the cell was classified as entering the C_{init} period. Overall, 98% of cells were correctly classified in all growth conditions.

3.5.8 Selection of cells with overlapping growth speeds

Individual cells growing in different media but with similar growth speeds were selected from the overlapping high-end tail (low growth speed culture) and low-end tail (high growth speed culture) of the growth speed distributions. The window of overlapping growth speed was selected to be at the intersection between both Gaussian distributions, and to contain a similar number of cells in both conditions.

3.5.9 Statistical analysis

Figure 1

The standard deviation (σ) across all growth conditions was around 1 μm . Following the

observation that the median of the size at division could vary by 0.2 μm between two movies from the same experiment, we chose an effect size E of 0.2 μm . We then calculated the number of cells to analyze using a z of 1.96 (representing the 97.5th percentile of the normal distribution):

$$n = \left(\frac{z \times \sigma}{E} \right)^2 = 100$$

To analyze 100 cells for each growth condition and be completely unbiased regarding which cells were chosen, we wrote a Matlab script that merged all of the movies analyzed per condition and randomly picked 100 cells from the merge. Only 92 cells were available for cells grown in 40:1 αMG medium at 37°C; however, using the exact standard deviation of this experiment ($\sigma = 0.91$), we determined that only 80 cells were necessary in this case. We then used an unpaired parametric t-test (assuming a Gaussian distribution and equal standard deviations between the pairs tested) to test the equality of the mean division size between 30°C and 37°C in each growth medium. We kept the same sets of cells for all of the following analyses.

Figure 5

We used an unpaired parametric t-test (assuming a Gaussian distribution and equal standard deviations between the pairs tested) to test the equality of the mean growth speeds, interdivision times, and cell lengths at division between wild-type and DnaA-overexpressing cells grown in 7H9 medium or 20:1 αMG medium.

Figure 7

We used an unpaired parametric t-test (assuming a Gaussian distribution and equal standard deviations between the pairs tested) to test the equality of the duration of the inter-initiation times, C periods, and interdivision times of multifork vs. non-multifork cells.

3.6 Figures

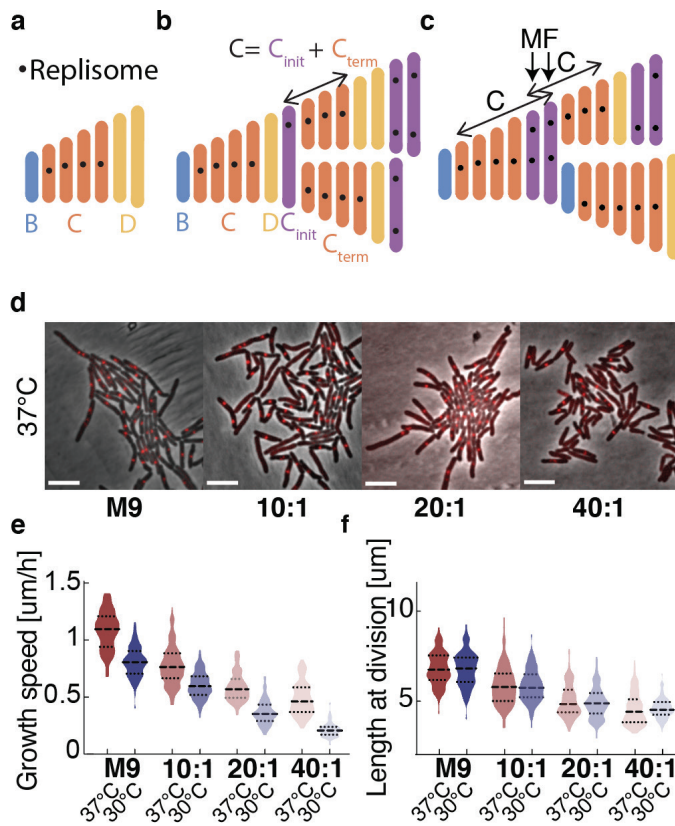


Figure 1. Cell size of *M. smegmatis* is affected by carbon limitation but not by temperature-limited growth.

(a) The canonical cell cycle in bacteria comprises a B period from birth to initiation of DNA replication, a C period from initiation to termination of DNA replication, and a D period from termination to cell division. **(b)** In *M. smegmatis*, initiation of the next cycle of DNA replication may occur after completion of the preceding cycle but prior to division. In such cases, one or both daughter cells inherit a partially replicated chromosome and there is no B period. Because the C period spans the division event, the first part of the C period takes place in the mother cell (C_{init}) while the second part takes place in the daughter cell (C_{term}). **(c)** In rare cases, multifork (MF) replication occurs because initiation of the next cycle of DNA replication precedes termination of the preceding cycle of replication, resulting in overlapping C periods. **(d-f)** Carbon availability was titrated by growing cells in M9 medium or M9 medium containing a 10:1, 20:1, or 40:1 excess of α MG relative to glucose, thereby limiting the glucose influx into the cell. **(d)** Microscopic snapshots of *M. smegmatis* expressing mCherry-DnaN (a marker of the DNA replisome) grown in different culture media at 37°C. Cells were grown in a microfluidic device and imaged by time-lapse microscopy. Scale bar, 5 μm . **(e)** The single-cell growth speed of *M. smegmatis* decreases with decreasing carbon availability or decreasing temperature from 37°C to 30°C. **(f)** Bacterial cell length at division decreases with reduced carbon availability but is not affected by reduced temperature. **(e,f)** $n = 100$ for all growth conditions except in 40:1 α MG at 37°C where $n = 92$.

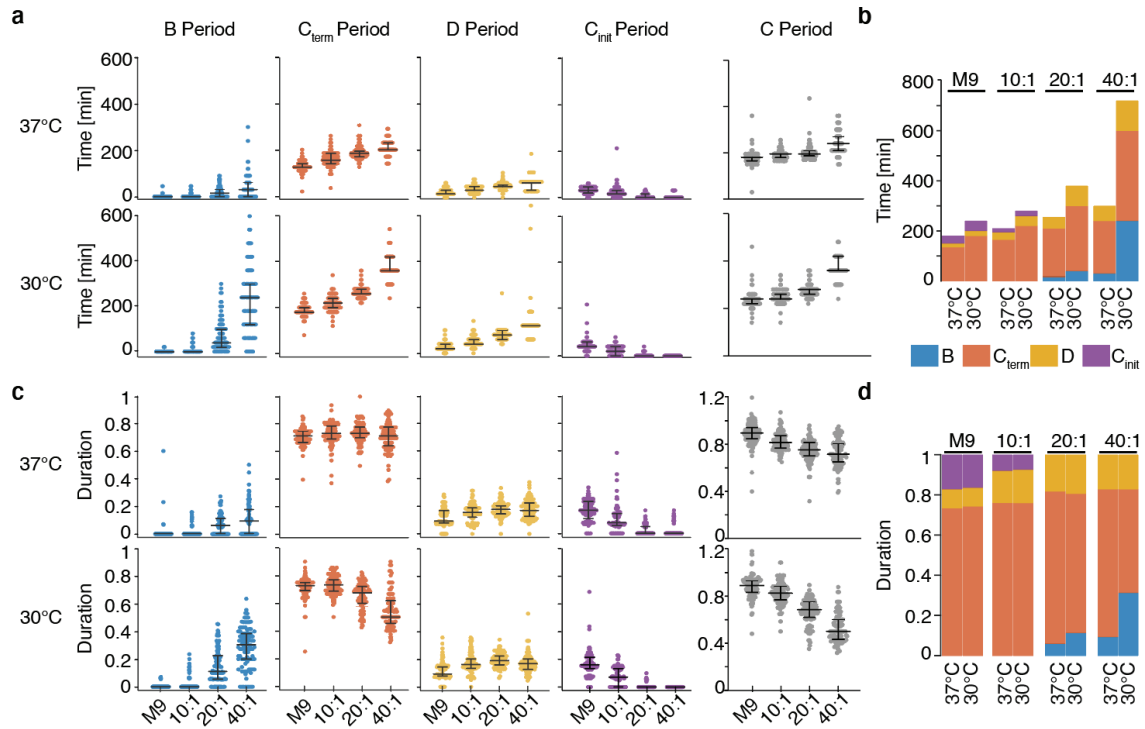


Figure 2. Initiation of DNA replication is delayed by carbon limitation and by temperature in carbon-limited cells.

(a-d) Bacteria expressing the mCherry-DnaN replisome marker were grown in a microfluidic device with a constant flow of M9 medium or M9 medium containing a 10:1, 20:1, or 40:1 excess of α MG to glucose at 37°C or 30°C and images were acquired by time-lapse microscopy. $n = 100$ cells for each condition except 40:1 α MG medium at 37°C ($n = 92$ cells). **(a)** Absolute duration of cell-cycle periods. Each symbol represents one cell. Horizontal lines represent median value and interquartile range. **(b)** Data from panel (a) presented as bar plots to summarize the impact of carbon limitation and temperature on the absolute duration of cell-cycle periods. **(c)** Fractional duration of cell-cycle periods. Each symbol represents one cell. Horizontal lines represent median value and interquartile range. **(d)** Data from panel (c) presented as bar plots to summarize the impact of carbon limitation and temperature on the fractional duration of cell-cycle periods.

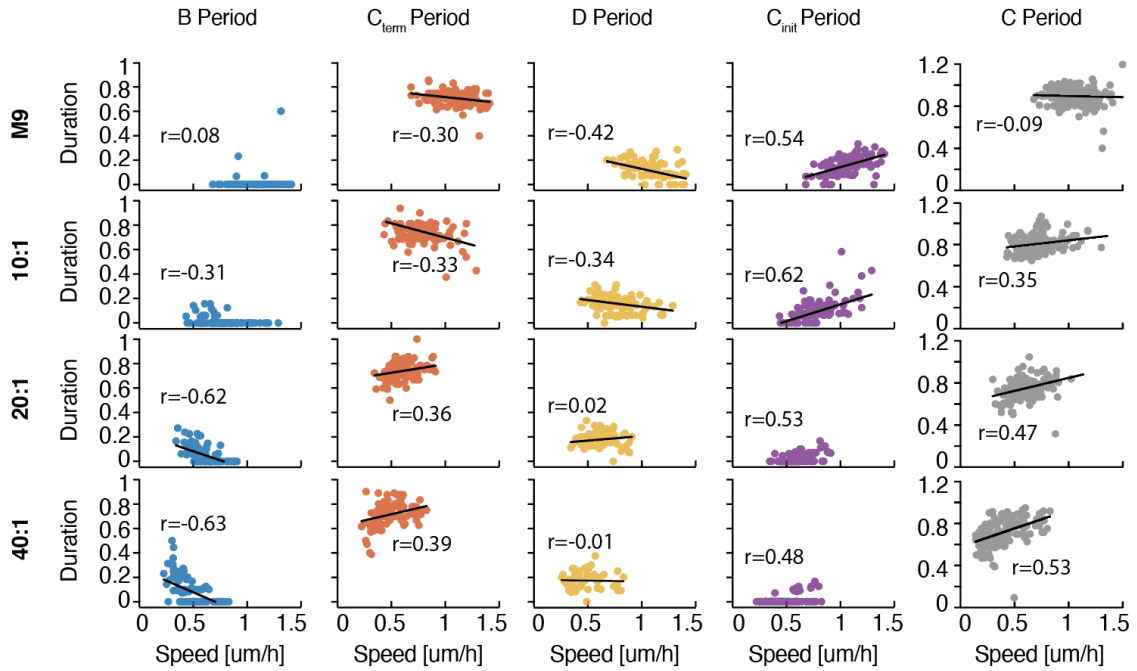


Figure 3. The timing of initiation of DNA replication is linked to variation in single-cell growth speed under all growth conditions.

Bacteria expressing the mCherry-DnaN replisome marker were grown in a microfluidic device with a constant flow of M9 medium or M9 medium containing a 10:1, 20:1, or 40:1 excess of α MG to glucose at 37°C and images were acquired by time-lapse microscopy. $n = 100$ cells for each condition except 40:1 α MG medium ($n = 92$ cells). In M9 and 10:1 α MG media, the C_{init} period is longer in fast-growing cells compared to slow-growing cells, and few cells exhibit a B period. In 20:1 α MG and 40:1 α MG media, the B period is shorter in fast-growing cells compared to slow-growing cells, and few cells exhibit a C_{init} period. r values, Pearson's correlation coefficient. Lines, robust linear regressions. Corresponding data for cells grown at 30°C can be found in [Supplementary Figure S4](#).

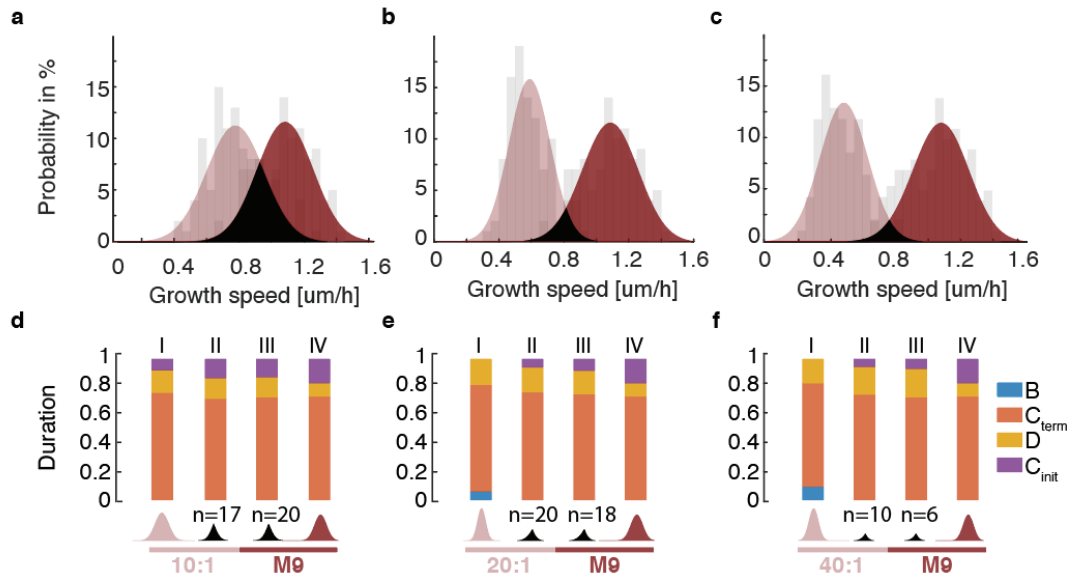


Figure 4. At the single-cell level the fractional duration of cell-cycle periods is linked to growth speed rather than growth conditions.

Bacteria expressing the mCherry-DnaN replisome marker were grown in a microfluidic device with a constant flow of M9 medium or M9 medium containing a 10:1, 20:1, or 40:1 excess of α MG to glucose at 37°C. Images were acquired by time-lapse microscopy. $n = 100$ cells for each condition except 40:1 α MG medium ($n = 92$ cells). **(a-c)** Single-cell growth-speed histograms fitted with normal distributions. The regions of overlap between the distributions are shown in black. The indicated number of cells with similar growth speeds were selected for comparison. Bacteria were grown in M9 medium (dark red) or 10:1 α MG (a), 20:1 α MG (b), or 40:1 α MG (c) medium (light red). **(d-f)** Bars represent the median fractional duration of each cell-cycle period corresponding to panels a-c, respectively. Bars I and IV represent median values for each distribution. Bars II and III represent median values for areas of overlap between the distributions.

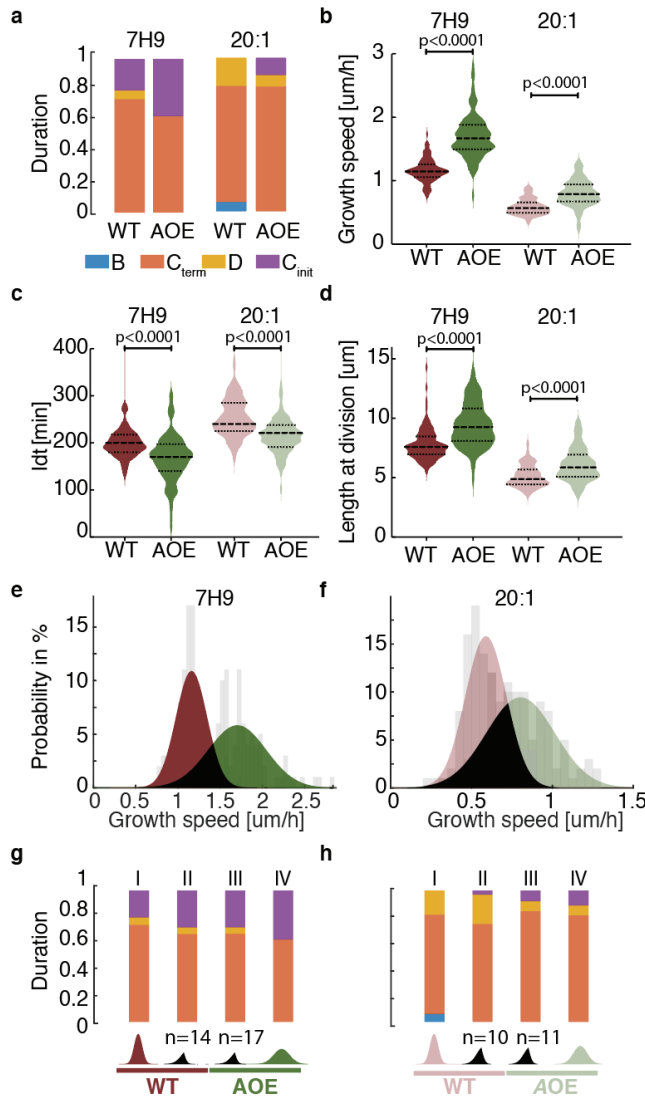


Figure 5. Overexpression of DnaA results in earlier initiation of DNA replication, faster growth, shorter interdivision time and larger cell size.

(a-f) Wild-type (WT) or DnaA-overexpressing (AOE) bacteria expressing the mCherry-DnaN

replisome marker were grown in a microfluidic device with a constant flow of 7H9 medium or 20:1 α MG medium at 37°C. Images were acquired by time-lapse microscopy. $n = 100$ cells for each condition. **(a)** Bars represent the median fractional duration of each cell-cycle period. **(b)** Growth speed. **(c)** Interdivision time. **(d)** Cell length at division. **(e,f)** Single-cell growth-speed histograms fitted with normal distributions. The regions of overlap between the distributions are shown in black. The indicated number of cells with similar growth speeds were selected for comparison. **(e)** WT (dark red) and AOE (dark green) cells in 7H9 medium. **(f)** WT (light red) and AOE (light green) cells in 20:1 α MG medium. **(g,h)** Bars represent the median fractional duration of each cell-cycle period corresponding to panels e and f, respectively. Bars I and IV represent median values for each distribution. Bars II and III represent median values for selected areas of overlap between the distributions.

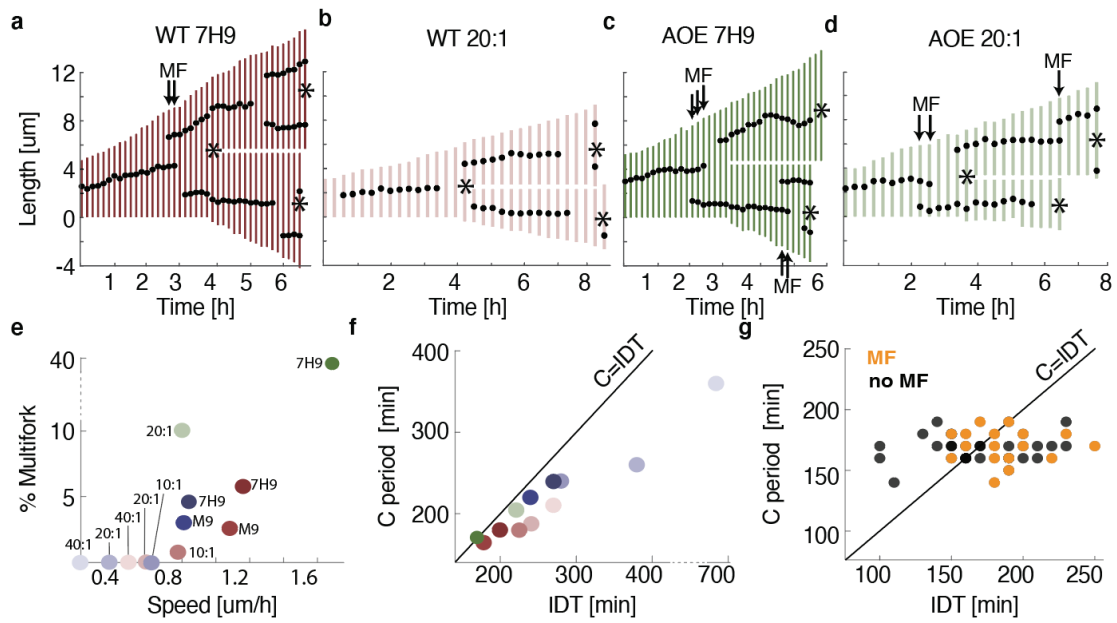


Figure 6. Multifork replication occurs even when the inter-division time is longer than the C period at the single-cell level.

(a-d) Wild-type cells (WT) or DnaA-overexpressing cells (AOE) expressing the mCherry-DnaN replisome marker were grown in a microfluidic device with a constant flow of 7H9 medium or 20:1 α MG medium. Images were acquired by time-lapse microscopy. Cell length tracked from birth to division of two generations of cells along with the position of mCherry-DnaN foci in wild-type and DnaA-overexpressing cells grown in 7H9 medium **(a,c)** or 20:1 α MG medium **(b,d)**. Overlap of the replication periods (arrows), corresponding to a brief period of multifork replication, is observed in WT (7H9) or DnaA-overexpressing cells (7H9 medium and 20:1 α MG medium). **(e)** Correlation between the growth speed and the percentage of cells exhibiting multifork replication. For each growth condition, the median growth speed is plotted against the percentage of multifork cells ($n = 100$ cells except for 40:1 α MG medium at 37°C, where $n = 92$). Blue symbols, wild-type cells at 30°C. Red symbols, wild-type cells at 37°C. Green symbols, DnaA-overexpressing cells at 37°C. **(f)** Correlation between the duration of the C period and the interdivision time. For each growth condition, the median interdivision time is plotted against the median duration of the C period ($n = 100$ cells except for 40:1 α MG medium at 37°C, where $n = 92$). **(g)** C period duration vs. interdivision time of DnaA-overexpressing cells in 7H9 medium at 37°C. Orange symbols, cells that exhibit multifork replication ($n = 20$). Black symbols, cells that do not exhibit multifork replication ($n = 30$).

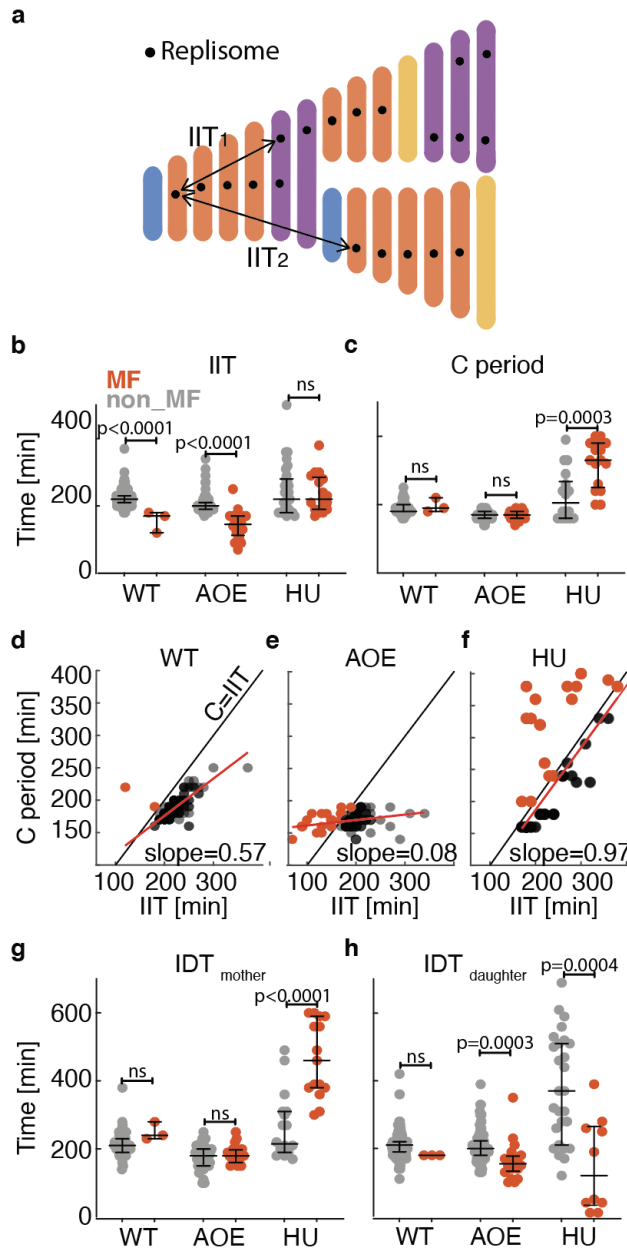
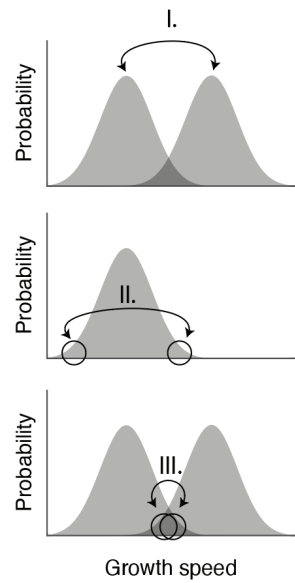


Figure 7. Multifork replication occurs when the inter-initiation time is shorter than the C period at the single-cell level.

(a) Inter-initiation time (IIT) is the time between two DNA replication initiation events. In each chromosome replication cycle, two IIT values can be measured (IIT₁ and IIT₂), corresponding to the time between the first initiation event for the mother chromosome and the subsequent initiation events for the two daughter chromosomes. **(b-h)** Wild-type cells (WT), DnaA-overexpressing cells (AOE), and

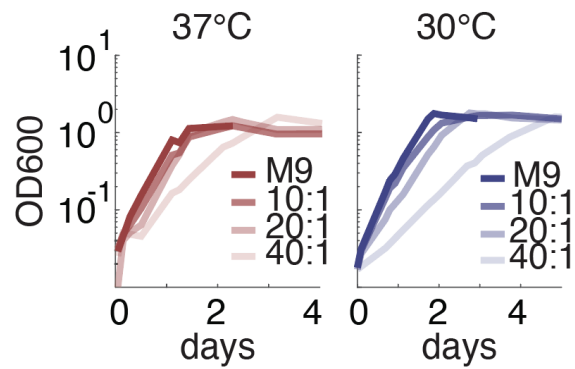
hydroxyurea-treated wild-type cells (HU) expressing the mCherry-DnaN replisome marker were grown in a microfluidic device with a constant flow of 7H9 medium. Images were acquired by time-lapse microscopy. **(b)** Inter-initiation time (n = 100). Orange symbols, multifork chromosomes. **(c)** C-period duration (n = 50). Orange symbols, multifork cells. **(d-f)** Inter-initiation time vs. C-period duration in wild-type cells **(d)**, DnaA-overexpressing cells **(e)**, and hydroxyurea-treated wild-type cells **(f)**. Orange symbols, multifork chromosomes (IIT) or cells (C period). **(g)** Interdivision time of mother cells (n = 50). Orange symbols, multifork mother cells. **(h)** Interdivision time of daughter cells (n = 100). Orange symbols, daughters of multifork mother cells.

3.7 Supplementary Figures



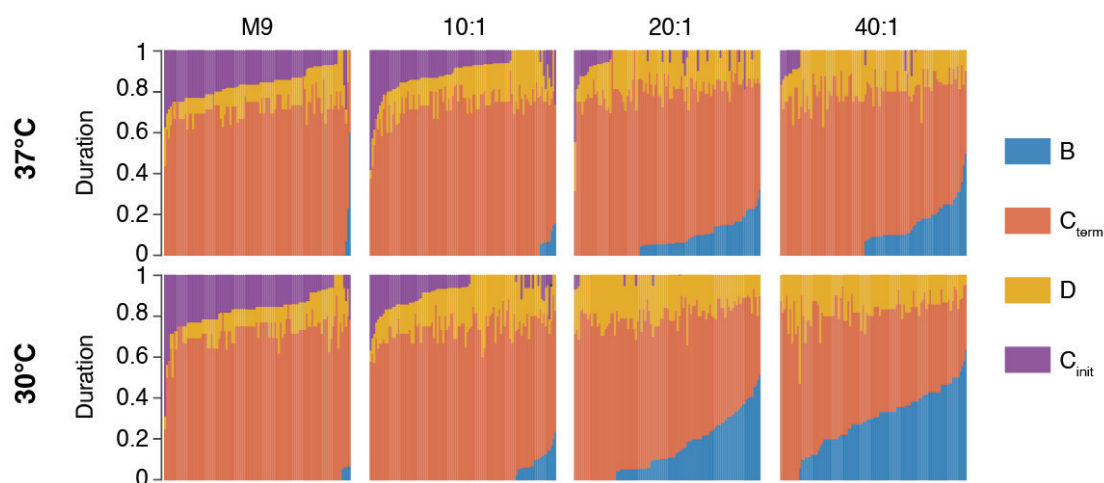
Supplementary Figure S1. Schematic of three comparisons made to determine how growth speed affects cell-cycle progression at the single-cell level.

(I.) Comparison between the mean values of two cell populations growing at different speeds due to progressive carbon limitation. **(II.)** Comparison between fast-growing and slow-growing individuals in the same environment. **(III.)** Comparison between individuals growing at the same speed in different environments.



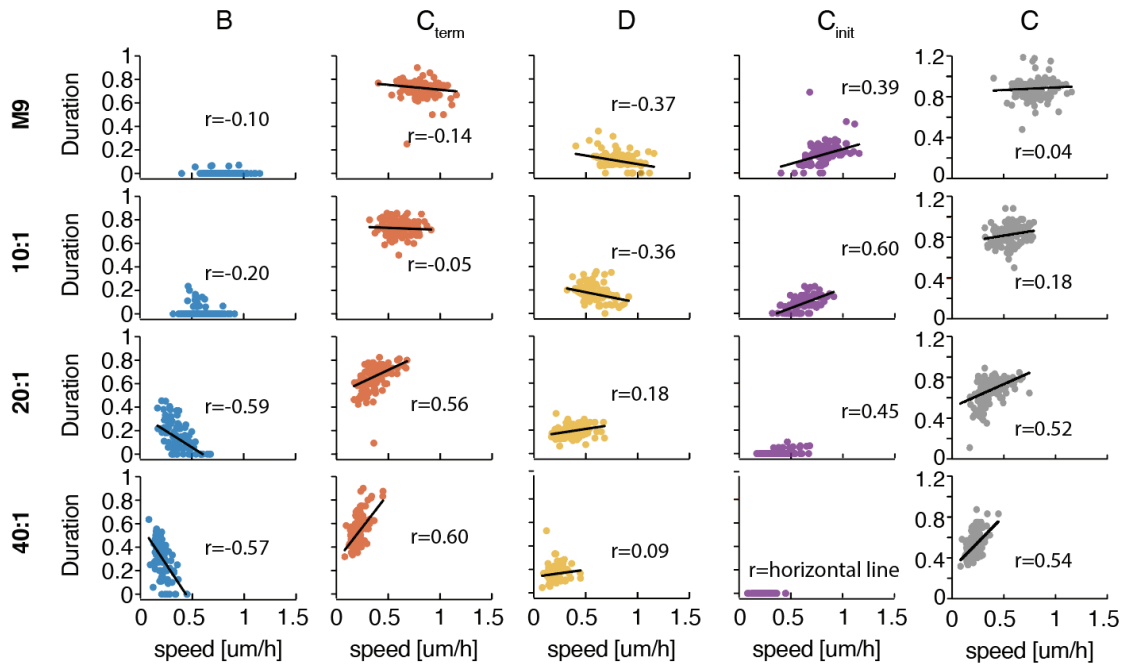
Supplementary Figure S2. Impact of carbon limitation and temperature on bacterial growth speed at the population level.

Bacteria expressing the mCherry-DnaN replisome marker were grown in batch cultures with aeration in M9 medium or M9 medium containing a 10:1, 20:1, or 40:1 excess of α MG to glucose at 37°C or 30°C. The optical density of each culture at 600 nm (OD₆₀₀) was measured repeatedly over time.



Supplementary Figure S3. Fractional duration of each cell-cycle period for single cells.

Bacteria expressing the mCherry-DnaN replisome marker were grown in a microfluidic device with a constant flow of M9 medium or M9 medium containing a 10:1, 20:1, or 40:1 excess of α MG to glucose at 37°C or 30°C and images were acquired by time-lapse microscopy. $n = 100$ cells for each condition except 40:1 α MG medium at 37°C ($n = 92$ cells). The corresponding lumped single-cell data can be found in [Figure 2d](#).



Supplementary Figure S4. The timing of initiation of DNA replication is linked to variation in single-cell growth speed under all growth conditions at 30°C.

Bacteria expressing the mCherry-DnaN replisome marker were grown in a microfluidic device with a constant flow of M9 medium or M9 medium containing a 10:1, 20:1, or 40:1 excess of α MG to glucose at 30°C and images were acquired by time-lapse microscopy. $n = 100$ cells for each condition except 40:1 α MG medium ($n = 92$ cells). In M9 and 10:1 α MG media, the C_{init} period is longer in fast-growing cells compared to slow-growing cells, and few cells exhibit a B period. In 20:1 α MG and 40:1 α MG media, the B period is shorter in fast-growing cells compared to slow-growing cells, and few cells exhibit a C_{init} period. r values, Pearson's correlation coefficient. Lines, robust linear regressions. Corresponding data for cells grown at 37°C can be found in [Figure 3](#).

3.8 Author Contributions

G.V-T., N.D. and J.D.M. conceived the project. G.V-T. performed the experiments and simulations, wrote the Matlab script to analyze the data, analyzed the data and interpreted the results. N.D. constructed the DnaA strain. G. V-T., N.D. and J.D.M. wrote the paper. N.D. and J.D.M. supervised the project.

3.9 References

Adiciptaningrum, A., Osella, M., Moolman, M.C., Lagomarsino, M.C., and Tans, S.J. (2015). Stochasticity and homeostasis in the *E. coli* replication and division cycle. *Sci. Rep.* 5, 18261.

- Atlung, T., Clausen, E.S., and Hansen, F.G. (1985). Autoregulation of the *dnaA* gene of *Escherichia coli* K12. *Mol. Gen. Genet.* *MGG* *200*, 442–450.
- Belliveau, N.M., Chure, G., Hueschen, C.L., Garcia, H.G., Kondev, J., Fisher, D.S., Theriot, J.A., and Phillips, R. (2020). Fundamental limits on the rate of bacterial growth. *BioRxiv* 2020.10.18.344382.
- Brauer, M.J., Huttenhower, C., Airoidi, E.M., Rosenstein, R., Matese, J.C., Gresham, D., Boer, V.M., Troyanskaya, O.G., and Botstein, D. (2007). Coordination of growth rate, cell cycle, stress response, and metabolic activity in yeast. *Mol. Biol. Cell* *19*, 352–367.
- Cooper, S., and Helmstetter, C.E. (1968). Chromosome replication and the division cycle of *Escherichia coli* B/r. *J. Mol. Biol.* *31*, 519–540.
- Dewachter, L., Verstraeten, N., Fauvart, M., and Michiels, J. (2018). An integrative view of cell cycle control in *Escherichia coli*. *FEMS Microbiol. Rev.* *42*, 116–136.
- Ehrenberg, M., Bremer, H., and Dennis, P.P. (2013). Medium-dependent control of the bacterial growth rate. *Biochimie* *95*, 643–658.
- Ehrt, S., Guo, X.V., Hickey, C.M., Ryou, M., Monteleone, M., Riley, L.W., and Schnappinger, D. (2005). Controlling gene expression in mycobacteria with anhydrotetracycline and Tet repressor. *Nucleic Acids Res.* *33*, e21–e21.
- Greendyke, R., Rajagopalan, M., Parish, T., and Madiraju, M.V.V.S. (2002). Conditional expression of *Mycobacterium smegmatis dnaA*, an essential DNA replication gene. *Microbiology*, *148*, 3887–3900.
- Grigorian, A.V., Lustig, R.B., Guzmán, E.C., Mahaffy, J.M., and Zyskind, J.W. (2003). *Escherichia coli* Cells with increased levels of DnaA and deficient in recombinational repair have decreased viability. *J. Bacteriol.* *185*, 630–644.
- Hannebelle, M.T.M., Ven, J.X.Y., Toniolo, C., Eskandarian, H.A., Vuaridel-Thurre, G., McKinney, J.D., and Fantner, G.E. (2020). A biphasic growth model for cell pole elongation in mycobacteria. *Nat. Commun.* *11*, 452.
- Hansen, M.T., Pato, M.L., Molin, S., Fill, N.P., and von Meyenburg, K. (1975). Simple downshift and resulting lack of correlation between ppGpp pool size and ribonucleic acid accumulation. *J. Bacteriol.* *122*, 585–591.
- Jonas, K. (2014). To divide or not to divide: control of the bacterial cell cycle by environmental cues. *Curr. Opin. Microbiol.* *18*, 54–60.
- Jun, S., Si, F., Pugatch, R., and Scott, M. (2018). Fundamental principles in bacterial physiology—history, recent progress, and the future with focus on cell size control: a review. *Rep. Prog. Phys.* *81*, 056601.
- Katayama, T., Ozaki, S., Keyamura, K., and Fujimitsu, K. (2010). Regulation of the replication cycle: conserved and diverse regulatory systems for DnaA and *oriC*. *Nat. Rev. Microbiol.* *8*, 163–170.
- Koc, A., Wheeler, L.J., Mathews, C.K., and Merrill, G.F. (2004). Hydroxyurea arrests DNA replication by a mechanism that preserves basal dNTP pools. *J. Biol. Chem.* *279*, 223–230.

- Lewin, G.R., Carlos, C., Chevrette, M.G., Horn, H.A., McDonald, B.R., Stankey, R.J., Fox, B.G., and Currie, C.R. (2016). Evolution and ecology of *Actinobacteria* and their bioenergy applications. *Annu. Rev. Microbiol.* 70, 235–254.
- Løbner-Olesen, A., Skarstad, K., Hansen, F.G., von Meyenburg, K., and Boye, E. (1989). The DnaA protein determines the initiation mass of *Escherichia coli* K-12. *Cell* 57, 881–889.
- Logsdon, M.M., and Aldridge, B.B. (2018). Stable regulation of cell cycle events in mycobacteria: insights from inherently heterogeneous bacterial populations. *Front. Microbiol.* 9.
- Logsdon, M.M., Ho, P.-Y., Papavinasasundaram, K., Richardson, K., Cokol, M., Sassetti, C.M., Amir, A., and Aldridge, B.B. (2017). A parallel adder coordinates mycobacterial cell-cycle progression and cell-size homeostasis in the context of asymmetric growth and organization. *Curr. Biol. CB* 27, 3367–3374.e7.
- Riber, L., Olsson, J.A., Jensen, R.B., Skovgaard, O., Dasgupta, S., Marinus, M.G., and Løbner-Olesen, A. (2006). Hda-mediated inactivation of the DnaA protein and *dnaA* gene autoregulation act in concert to ensure homeostatic maintenance of the *Escherichia coli* chromosome. *Genes Dev.* 20, 2121–2134.
- Santi, I., and McKinney, J.D. (2015). Chromosome organization and replisome dynamics in *Mycobacterium smegmatis*. *MBio* 6, e01999-14.
- Santi, I., Dhar, N., Bousbaine, D., Wakamoto, Y., and McKinney, J.D. (2013). Single-cell dynamics of the chromosome replication and cell division cycles in mycobacteria. *Nat Commun* 4, 2470.
- Schaechter, M., MaalOe, O., and Kjeldgaard, N.O. (1958). Dependency on medium and temperature of cell size and chemical composition during balanced growth of *Salmonella typhimurium*. *J. Gen. Microbiol.* 19, 592–606.
- Skarstad, K., and Katayama, T. (2013). Regulating DNA replication in bacteria. *Cold Spring Harb. Perspect. Biol.* 5.
- Trojanowski, D., Ginda, K., Pióro, M., Hołowka, J., Skut, P., Jakimowicz, D., and Zakrzewska-Czerwińska, J. (2015). Choreography of the Mycobacterium replication machinery during the cell cycle. *MBio* 6, e02125-14.
- Trojanowski, D., Hołowka, J., Ginda, K., Jakimowicz, D., and Zakrzewska-Czerwińska, J. (2017). Multifork chromosome replication in slow-growing bacteria. *Sci. Rep.* 7, 43836.
- Trueba, F.J., van Spronsen, E.A., Traas, J., and Woldringh, C.L. (1982). Effects of temperature on the size and shape of *Escherichia coli* cells. *Arch. Microbiol.* 131, 235–240.
- Vadia, S., and Levin, P.A. (2015). Growth rate and cell size: a re-examination of the growth law. *Curr. Opin. Microbiol.* 24, 96–103.
- Wallden, M., Fange, D., Lundius, E.G., Baltekin, Ö., and Elf, J. (2016). The synchronization of replication and division cycles in individual *E. coli* cells. *Cell* 166, 729–739.
- Wang, J.D., and Levin, P.A. (2009). Metabolism, cell growth and the bacterial cell cycle. *Nat. Rev. Microbiol.* 7, 822–827.

Westfall, C.S., and Levin, P.A. (2017). Bacterial cell size: multifactorial and multifaceted. *Annu. Rev. Microbiol.* 71, 499–517.

Winder, F.G., and Barber, D.S. (1973). Effects of hydroxyurea, nalidixic acid and zinc limitation on DNA polymerase and ATP-dependent deoxyribonuclease activities of *Mycobacterium smegmatis*. *J. Gen. Microbiol.* 76, 189–196.

Witz, G., van Nimwegen, E., and Julou, T. (2019). Initiation of chromosome replication controls both division and replication cycles in *E. coli* through a double-adder mechanism. *ELife* 8, e48063.

Woong Park, S., Klotzsche, M., Wilson, D.J., Boshoff, H.I., Eoh, H., Manjunatha, U., Blumenthal, A., Rhee, K., Barry, C.E., Aldrich, C.C., et al. (2011). Evaluating the sensitivity of *Mycobacterium tuberculosis* to biotin deprivation using regulated gene expression. *PLoS Pathog.* 7.

Young, K.D. (2006). The selective value of bacterial shape. *Microbiol. Mol. Biol. Rev.* 70, 660–703.

Chapter 4 Colocalization and biphasic movement of the DNA replisome and FtsZ division ring determine the site of cell division in *Mycobacterium smegmatis*

Gaëlle Vuaridel-Thurre¹, Neeraj Dhar¹, John D. McKinney^{1*}

¹School of Life Sciences, Swiss Federal Institute of Technology in Lausanne (EPFL), CH-1015 Lausanne, Switzerland

Keywords: DnaN, FtsZ, ParB, ParA, cell division

*Address correspondence to: john.mckinney@epfl.ch

4.1 Abstract

Division site selection in bacteria is governed by the nucleoid occlusion (Noc) and minicell (Min) systems. However, mycobacteria do not encode known homologs of the Noc or Min proteins, which implies the existence of an alternative mechanism(s) for division site selection in these organisms. Although genetic ablation of the chromosome partitioning (Par) system has been shown to result in defective division site selection, suggesting a link between chromosome replication/segregation and cell division, the mechanistic basis of this link is unknown. Here, we use time-lapse fluorescence microscopy to track the DNA replisome and FtsZ cell division ring in space and time in *Mycobacterium smegmatis*. We show that the replisome and division ring colocalize and move together in a biphasic trajectory: in phase I, they move towards the old cell pole at a speed that matches the pole's elongation speed; in phase II, they stop moving and remain stationary until cell division. Their coordinated movement (but not their colocalization) is Par-dependent, which explains why disruption of Par results in aberrant division site selection. We propose a model in which Par-dependent movement of the replisome and division ring ultimately determines the site of cell division.

4.2 Introduction

Cell division needs to be spatially regulated to ensure a proper distribution of chromosomes to the daughter cells while avoiding their guillotining by the cell division septum. How spatial regulation of cell division takes place is a question that has been well studied although a lot remains to be understood. Rod-shaped bacteria use two main systems to divide at midcell. There is the nucleoid occlusion (Noc) system, which prevents chromosome guillotining by inhibiting division in a region that contains DNA (Wu and Errington, 2012) and the canonical Minicell (Min) system that inhibits division near the cell poles (Rowlett and Margolin, 2015). However, some species of bacteria do not encode obvious homologues of either the Noc or Min systems, suggesting that these species have evolved different mechanisms to determine the division site (Monahan et al. 2014; Hajduk et al. 2016).

In *M. smegmatis*, the Noc and Min systems seem to be absent and no mechanism for division site placement has yet been identified (Hett and Rubin, 2008). It has been reported that, in most cases, *M. smegmatis* divides slightly asymmetrically with a skew towards the new cell pole (Aldridge et al., 2012). Subsequently, Joyce et al., 2012 proposed that the nascent division septum is initially positioned precisely at midcell and subsequently shifts towards the new pole due to asymmetric (old-pole-dominant) growth (Aldridge et al., 2012). Alternatively, Singh et al., 2013 proposed that the division site might be positioned more or less randomly along the cell length, and chromosome segregation might be mediated by a pump that moves DNA across the division septum. None of these studies, however, identified a mechanism for division-site selection. More recently, Eskandarian et al., 2017 demonstrated that the surface of *M. smegmatis* cells is “wavy” and division occurs predominantly within wave-troughs.

Although these observations suggest that cell-surface morphological markers might play a role in division site selection, the underlying molecular mechanisms remain unknown.

Accumulating evidence suggests that division site selection in bacteria might be linked to DNA replication and chromosome segregation (Donovan et al., 2013; Hajduk et al., 2016; Moriya et al., 2010; van Raaphorst et al., 2017). DNA replication in *M. smegmatis* seems to follow a “replication factory” model, in which the replisome is stationary within the cytoplasm and DNA spools through the replisome as it is replicated; concurrent with chromosome replication, the two nascent daughter chromosomes move towards opposite cell poles (Santi and McKinney, 2015). The chromosome partitioning (ParABS) system is responsible for segregation of newly replicated chromosomes in many bacteria, including *M. smegmatis* (reviewed in Kawalek et al., 2020). Although different models have been proposed for the Par-mediated mechanism of chromosome segregation, there is a consensus that the ParA motor protein mediates segregation by interacting with polar proteins as well as ParB bound to *parS* sequences near the chromosomal origin of replication (reviewed in Kawalek et al., 2020). In *M. smegmatis*, ParA bridges the pole-localized protein Wag31 and ParB-*parS* complexes bound next to the chromosomal replication origin (Ginda et al., 2013; Jakimowicz et al., 2007; Kang et al., 2008). Mutants lacking ParA or ParB display defects in replisome positioning, chromosome segregation, and division site placement (Ginda et al., 2013; Santi and McKinney, 2015; Trojanowski et al., 2015; Eskandarian et al., 2017; Ginda et al., 2017), suggesting that replisome positioning and/or chromosome segregation might play a role in division site selection in *M. smegmatis*.

Here, we show that the replisome and FtsZ division ring colocalize and move together along the cell length in a biphasic fashion. In phase I, the replisome and division ring move in the direction of the (growing) old pole, thus maintaining a constant distance from the old pole while moving away from the (non-growing) new pole. In phase II, movement of the replisome and division ring ceases and thereafter they maintain a constant distance from the new pole while seeming to move away from the old pole due to old-pole elongation. Old-pole-directed movement of the replisome and division ring in phase I requires ParB, and the position of the replisome and division ring at the breakpoint between phases I and II coincides with the future division site. These results clarify why aberrant chromosome segregation results in mislocalized cell division in Par-deficient cells, and suggest a new model for division site selection in mycobacteria.

4.3 Results

4.3.1 The DNA replisome and cell division ring colocalize in space and time

We tracked the positions of the DNA replisome and cell division ring along the cell length using cells expressing the sliding clamp of the DNA polymerase (DnaN) tagged with mCherry (red) and FtsZ tagged with GFP (green), respectively (Figure 1a). Time-lapse microscopy of cells grown in a microfluidic device revealed that the division ring assembles in close proximity

to the replisome at around 30 minutes on average after replisome assembly (Figure 1b). The replisome and division ring remain colocalized for about 135 minutes on average, until completion of DNA replication and replisome disassembly (Figure 1c). After termination of DNA replication, the division ring persists for around 75 minutes on average and disassembles after the completion of cell division (Figure 1b). In agreement with previous reports (Santi et al., 2013; Trojanowski et al., 2015), we observed that the replisome occasionally undergoes splitting (Figure 1d), which may reflect dissociation of the replisomes replicating the left and right arms of the chromosome. In the majority of cases, when the replisome splits, a second cell division ring also appears and colocalizes with the second replisome (Figure 1d). However, appearance of the second replisome and its associated cell division ring is usually transient.

4.3.2 Coupled movement of the DNA replisome and cell division ring towards the future division site

Colocalization of the replisome and division ring throughout the cell cycle could be due to their independent assembly and persistence at a location near mid-cell. Alternatively, colocalization could be due to concerted assembly and movement of the replisome and division ring. We addressed this question by asking whether DnaN/FtsZ are stationary or move together along the cell length over time. Consistent with the idea that colocalization may reflect coupling between the replisome and division ring, we found that DnaN and FtsZ move together along the cell length relative to the new pole (Figure 2a) or old pole (Figure 2b). The single-cell DnaN/FtsZ trajectories appear to be biphasic, with a breakpoint between the two phases. Despite large cell-to-cell variation in the timing of the breakpoint, which occurs at about 60 ± 30 minutes after first appearance of the division ring (Figure 2c,d), kymographs show that the DnaN/FtsZ trajectories in individual cells are similar after alignment to the breakpoint (Figure 2e,f). We conclude that colocalization and coordinated movement of the replisome and division ring towards the future division site is likely to reflect coupling between these macromolecular assemblies.

4.3.3 The DNA replisome and cell division ring switch between tracking first the old pole (phase I) and then the new pole (phase II)

We used time-lapse microscopy to measure the speed of movement of DnaN/FtsZ relative to the new and old cell poles (Figure 3). We found that DnaN/FtsZ initially maintain a relatively constant distance (median speed close to zero) relative to the old pole while moving away from the new pole at a speed that matches the old-pole elongation speed (Figure 3a,b). This pattern of movement, which we define as “phase I”, was unexpected because in *M. smegmatis* cells initially grow mainly by old-pole extension, whereas the new pole does not initiate fast growth until very late in the cell division cycle (Hannebelle et al., 2020). Thus, in order to track with the old pole, DnaN/FtsZ must move in the old-pole direction at a speed that matches the old-pole elongation speed. Subsequently, following a breakpoint, DnaN/FtsZ maintain a relatively constant distance (median speed close to zero) relative to the new pole while moving away from the old pole at a speed that matches the old-pole elongation speed

(Figure 3a,b). This pattern of movement, which we define as “phase II”, suggests that DnaN/FtsZ track with the new pole because they are stationary and the new pole is not growing.

We conclude that movement of DnaN/FtsZ follows a biphasic trajectory: during phase I, DnaN/FtsZ move in the old-pole direction at a speed matching the old-pole elongation speed; during phase II, DnaN/FtsZ move away from the old pole at a speed matching the old-pole elongation speed (Figure 3c). These observations suggest that DnaN/FtsZ switches from active movement in the old-pole direction during phase I to stationary persistence during phase II.

4.3.4 ParB is not required for colocalization of the DNA replisome and cell division ring

We asked whether colocalization of the replisome and division ring persists when the replisome is mislocalized, as occurs in $\Delta parB$ mutant cells lacking the ParB chromosome partitioning protein (Santi and McKinney, 2015). To answer this question, we used time-lapse microscopy to track the positions of mCherry-DnaN and FtsZ-GFP along the cell length in $\Delta parB$ cells (Figure 4a). These studies revealed that, similar to wild-type cells, the division ring assembles in close proximity to the replisome around 30 minutes after replisome assembly in $\Delta parB$ cells (Figure 4b). Although DnaN/FtsZ colocalization is noisier in $\Delta parB$ cells compared to wild-type cells, colocalization of the replisome and division ring persists throughout the period of DNA replication (about 120 minutes) (Figure 4c). After termination of DNA replication, signalled by disappearance of the mCherry-DnaN focus, the division ring persists for about 75 minutes, until division occurs (Figure 4b). We conclude that colocalization of the replisome and division ring is not strictly dependent on correct positioning of the replisome within the cell, which suggests that changing the position of the replisome results in repositioning of the division ring as well.

4.3.5 ParB is not required for coupled movement of the DNA replisome and cell division ring towards the future division site

We found that the trajectories of DnaN/FtsZ toward the future cell division site are more variable in $\Delta parB$ cells compared to wild-type cells (Figure 5). In wild-type cells, DnaN/FtsZ track with the old pole in phase I and with the new pole in phase II. In sharp contrast, movement of DnaN/FtsZ does not track with the old pole in either phase I or phase II in $\Delta parB$ cells (Figure 5a,b). Rather, on average, movement of DnaN/FtsZ in $\Delta parB$ cells appears to track with the new pole (Figure 5c,e) rather than the old pole (Figure 5d,f) in both phase I and phase II. Although movement of DnaN/FtsZ appears to be random in both phases in $\Delta parB$ cells, nonetheless, their movement is coordinated, suggesting that ParB is not required for coupled movement of DnaN and FtsZ towards the future cell division site.

4.3.6 ParB is required for the DNA replisome and cell division ring to track the old cell pole during phase I

In wild-type cells, on average, movement of DnaN/FtsZ away from the old pole is close to zero in phase I and roughly equal to the speed of old-pole elongation in phase II (Figure 3a,b). These results suggest that movement of DnaN/FtsZ in the old-pole direction is coupled to elongation of the old pole during phase I but uncoupled from old-pole elongation during phase II (Figure 3c). In sharp contrast, on average, the speed of movement of DnaN/FtsZ away from the old pole is roughly equal to the speed of old-pole elongation in both phases I and II in $\Delta parB$ cells, and the speed of movement of DnaN/FtsZ relative to the non-growing new pole is close to zero (Figure 6a,b). These results suggest that movement of DnaN/FtsZ is uncoupled from old-pole elongation during both phases I and II in $\Delta parB$ cells (Figure 6c).

4.4 Discussion

We found that the replisome and cell division ring not only colocalize, they also move together in time and space, suggesting the existence of a coupling mechanism between them. Their coupling is independent of ParB but it might not represent a direct physical interaction between the replisome and division ring because they occasionally move apart (and later rejoin) in the course of time-lapse experiments. This behavior may suggest that their interaction is mediated by a flexible linker, although it is also possible that separation and rejoining occur due to direct but reversible binding and rebinding between them. We also found that occasional splitting of the replisome (Santi et al., 2013; Trojanowski et al., 2015) is usually accompanied by duplication of the division ring, which suggests the intriguing possibility that the replisome might function as a scaffold for assembly of the division ring. In future, it would be interesting to determine whether cells engineered to contain multiple replication origins in the chromosome (Dimude et al., 2018) would also assemble multiple replisomes and, if so, whether each replisome would be accompanied by a division ring.

Colocalization of the replisome and division ring might be important to ensure that each daughter cell receives a complete chromosome. During ongoing DNA replication, the replisome serves as the locus of segregation of the nascent daughter chromosomes, one chromosome moving towards the old cell pole and one chromosome moving towards the new cell pole. Thus, the locus of chromosome segregation (the replisome) might also be the optimal site for cell division to occur. Linking these two macromolecular machines would provide a simple mechanism to ensure that the cell division septum is placed between the two daughter chromosomes in cells that replicate following a “replication factory” model.

We observed that movement of DnaN/FtsZ is biphasic, tracking with the old (growing) pole in phase I and remaining stationary in phase II; thus, DnaN/FtsZ actively move away from the (non-growing) new pole in phase I and maintain a constant distance from the new pole in phase II until new-end takeoff (NETO). Why do the replisome and division ring track the old pole during phase I? To illustrate why tracking of the old pole might be important, we start

with a simple model for symmetrically growing cells. In cells that follow a “replication factory” model, throughout the period of DNA replication the replisome resides at midcell, which coincides with the future division site. According to this model, no movement of the replisome or division ring is needed for division to occur at midcell, yielding equal-sized daughters (Figure 7a). However, for asymmetrically growing mycobacterial cells, if the replisome does not move, division no longer occurs at midcell and is instead strongly skewed toward the new pole due to old-pole-dominant growth (Figure 7b).

To ensure that division occurs near midcell in asymmetrically growing cells, we considered two possible solutions. First, initiation could occur in close proximity to the old pole and the replisome could gradually shift towards midcell due to old-pole-dominant growth (Figure 7c). *M. smegmatis* might adopt this strategy, at least partially, because the replisome is slightly skewed toward the old pole at initiation (Trojanowski et al., 2015). However, for this strategy alone to ensure that division occurs near midcell, the skew towards the old pole would have to be much more extreme than actually occurs. Second, the replisome could track the old pole as it grows (Figure 7d). However, if tracking persisted throughout the cell’s lifespan, the division site would be strongly skewed towards the old pole, resulting in a small old-pole daughter and a large new-pole daughter. In fact, the opposite is true: division is slightly skewed towards the new cell pole, resulting in the new-pole daughter being somewhat smaller than the old-pole daughter (Aldridge et al., 2012). Thus, neither model alone (Figure 7c,d) can be correct.

As an alternative, we propose a model that combines elements of these two models in order to achieve division near midcell in asymmetrically growing mycobacterial cells (Figure 7e). At the time of initiation, the replisome is slightly skewed towards the old pole (Trojanowski et al., 2015), similar to but less extreme than the model presented in Figure 7c. The replisome then tracks with the old pole as it elongates, initially similar to the model presented in Figure 7d. However, in order to avoid an overly strong skew towards the old pole, replisome movement is biphasic, inasmuch as the replisome tracks with the old pole in phase I but stops tracking with the old pole in phase II. When the division ring appears, which usually occurs in phase I, it colocalizes and moves with the replisome; thus, the movement and final resting position of the replisome relative to the cell length ultimately predicts the site of cell division. This “integrated” model is in good agreement with our experimental observations.

Tracking of the old pole by the replisome during phase I would seem to imply the existence of a physical linkage between the old pole and the replisome. This putative link cannot be direct, because the replisome is always positioned at a significant distance from the old pole. Here, we show that ParB is required for the replisome to track the old pole in phase I. In asymmetrically growing $\Delta parB$ cells, which lack old-pole tracking by the replisome and division ring, division would be strongly skewed toward the new pole (Figure 7b); this prediction is in good agreement with recent observations (Ven, 2019). Furthermore, it was shown previously that the old-pole-proximal ParB focus maintains a relatively constant

distance from the old pole over time (Ginda et al., 2017). However, ParB-dependent tracking of the old pole by the replisome cannot be mediated by direct attachment of ParB to the replisome, because the replisome and the old-pole-proximal ParB focus do not colocalize over time, even when both are tracking the old pole (Ginda et al., 2017).

ParB-dependent old-pole tracking by the replisome could suggest a role for the ParB-binding protein ParA in mediating the old-pole-directed movement of the replisome during phase I. However, in *M. smegmatis*, ParA preferentially localizes to the new pole and is thought to mediate movement of the new-pole-proximal ParB focus towards the new pole; also, ParA is apparently not required for old-pole tracking by the old-pole-proximal ParB focus (Ginda et al., 2017; Pióro et al., 2019). Similarly, in other organisms such as *Vibrio cholera*, *Caulobacter crescentus*, or *Streptomyces coelicolor*, ParA is required specifically for movement of only one ParB focus towards one cell pole (Viollier et al., 2004; Ptacin et al., 2014; Badrinarayanan et al., 2015; Kois-Ostrowska et al., 2016; Fogel and Waldor, 2021). Thus, in *M. smegmatis*, although tracking of the old pole by the replisome during phase I is ParB-dependent, as shown here, it is likely that this movement is independent of ParA.

If ParA is not required for the old-pole-proximal ParB focus and the replisome to track the old pole during phase I, this would suggest the existence of an intermediate linker (or linkers) that remains to be identified (Figure 7f). The putative linker could play a similar role as PopZ in *C. crescentus*, which localizes to the old pole and interacts directly with ParB (Bowman et al., 2008; Ptacin et al., 2014). However, the *M. smegmatis* genome does not encode an obvious PopZ homologue (unpublished observations). Also, it is unclear how a single linker between the old pole and ParB could explain the ParB-dependence of old-pole tracking by the replisome because the replisome and ParB do not colocalize. With sufficient crosslinking, the DNA itself might possibly serve as a flexible physical link between the replisome and the old-pole-proximal ParB focus, although this linker would have to be maintained at a relatively constant length over time despite ongoing DNA replication.

While the nature of the proposed link between the old cell pole and the replisome during phase I remains unclear, it is also unclear how this link is disrupted at the breakpoint between phase I and phase II. One possibility is that, as DnaN/FtsZ track along the cell length in the old-pole direction, they may encounter a region where the cell wall is locally constricted, which can be visualized as a nanoscale “wave trough” on the cell surface (Eskandarian et al., 2017). This local region of minimum cell circumference might represent a minimum energetic point leading to stabilization of the contractile FtsZ ring. Alternatively, the breakpoint between phases I and II might occur when the cell initiates the construction of a division septum. Because the peptidoglycan component of the division septum is continuous with peptidoglycan in the cell’s sidewall (Dahl 2004), it is unlikely that the growing septum would be capable of physically translocating along the cell length. Initiation of septum formation is heralded by the appearance of a nanoscale “pre-cleavage furrow” on the cell surface at the future division site (Eskandarian et al., 2017). Using correlated optical and atomic force

microscopy, it would be interesting to determine whether the breakpoint between phases I and II coincides with the arrival of DnaN/FtsZ at a cell-surface wave trough or appearance of the pre-cleavage furrow.

4.5 Methods

4.5.1 Bacterial strains

Mycobacterium smegmatis mc²155 wild-type and $\Delta parB$ strains expressing mCherry-DnaN (Santi and McKinney, 2015; Santi et al., 2013) were transformed with pND275 expressing an FtsZ-GFP fusion protein under the control of an anhydrotetracycline (ATc)-inducible promoter (Eskandarian et al., 2017). Transformants were selected on solid medium containing 50 $\mu\text{g ml}^{-1}$ hygromycin.

4.5.2 Bacterial culture conditions

Bacterial liquid cultures were grown at 37°C with aeration in minimal M9 medium (Difco) supplemented with 0.2% glucose to mid-log phase, corresponding to an optical density at 600 nm (OD₆₀₀) of 0.2 to 0.5, and stored at -80°C without addition of glycerol. Frozen aliquots were thawed, used once, and discarded.

4.5.3 Time-lapse fluorescence microscopy

Time-lapse microscopy was performed as described (Santi et al., 2013). Briefly, bacterial cultures were grown to OD₆₀₀ 0.2 to 0.5 and agitated to separate single cells from clumps. A 3 μl aliquot was spread on a semipermeable membrane, assembled in a custom-made microfluidic device, and imaged through a glass coverslip. Medium was flowed through the serpentine channels of the device at a speed of 18 $\mu\text{l/min}$. Temperature around the microscope stage was maintained at 37°C. Cells were imaged on phase-contrast and fluorescence channels at 15-minute intervals. Transmitted polarized light exposure was set at 0.1 seconds and 100% or 32% LED power for $\Delta parB$ and wild-type cells, respectively. mCherry LED exposure was set at 0.15 seconds and 5% LED power. GFP LED exposure was set at 0.2 seconds and 50% LED power. Images were acquired using a CoolSnap HQ2 camera with 2x2 binning.

4.5.4 Image analysis

Measurements of cell length and detection of cell division events were performed using a Fiji plugin (Bisquit) developed by O. Mariani. Cell division was manually detected based on the abrupt snapping movement of sibling cells (Hannebelle et al., 2020). Bisquit was also used for tracking lineages, new and old cell poles, and spatial positions of cells. Pole elongation speed was measured on phase-contrast images using cell imperfections as landmarks. The data generated by Bisquit were loaded in Matlab for further analysis. DnaN foci and FtsZ rings were detected using a home-made Matlab graphical user interface based on the *adaptthresh()*

function. mCherry-DnaN foci and FtsZ-GFP rings were assigned to cells based on their spatial positions and the spatial positions of cells. Positions of mCherry-DnaN foci and FtsZ-GFP rings relative to cell length was determined by projecting their spatial position on the midcell ridge using the Matlab *dsearchn()* function.

4.5.5 Selection of mCherry-DnaN foci and FtsZ-GFP rings for trajectory analysis

mCherry-DnaN foci sometimes split and remerge over time (Santi and McKinney, 2015; Trojanowski et al., 2015). Similarly, cells may contain multiple transient FtsZ-GFP rings (Walker et al., 2020). Only mCherry-DnaN foci and FtsZ-GFP rings that displayed a stable trajectory toward the division site were analyzed.

4.5.6 Breaking point and kymograph

Breakpoints between phase I and phase II of the biphasic movement of mCherry-DnaN foci and FtsZ-GFP rings were obtained by performing a bilinear fit on the merged DnaN/FtsZ trajectory, which was found using the Matlab functions *lsqnonlin()* and *fitnlm()* for a bilinear model with four coefficients (the slope before the breakpoint, the slope after the breakpoint, the timing of the breakpoint, and an offset). In order to find the best possible fit, different starting points were tried for the *lsqnonlin()* function and the model providing the smallest sum of squares error when compared to the data was kept. The merged trajectories were obtained by fusing the mCherry-DnaN and FtsZ-GFP data, taking the average distance to the old pole when both markers were present. Distances relative to the old pole were used because the distance to the old pole can be tracked in both the mother cell and daughter cells, whereas the new poles formed by division of the mother cell are present only in the daughters. The DnaN/FtsZ trajectories were then aligned to their temporal breakpoints and the distance to the poles was set to zero. The kymograph was then generated using the Matlab *imagesc()* function.

4.6 Figures

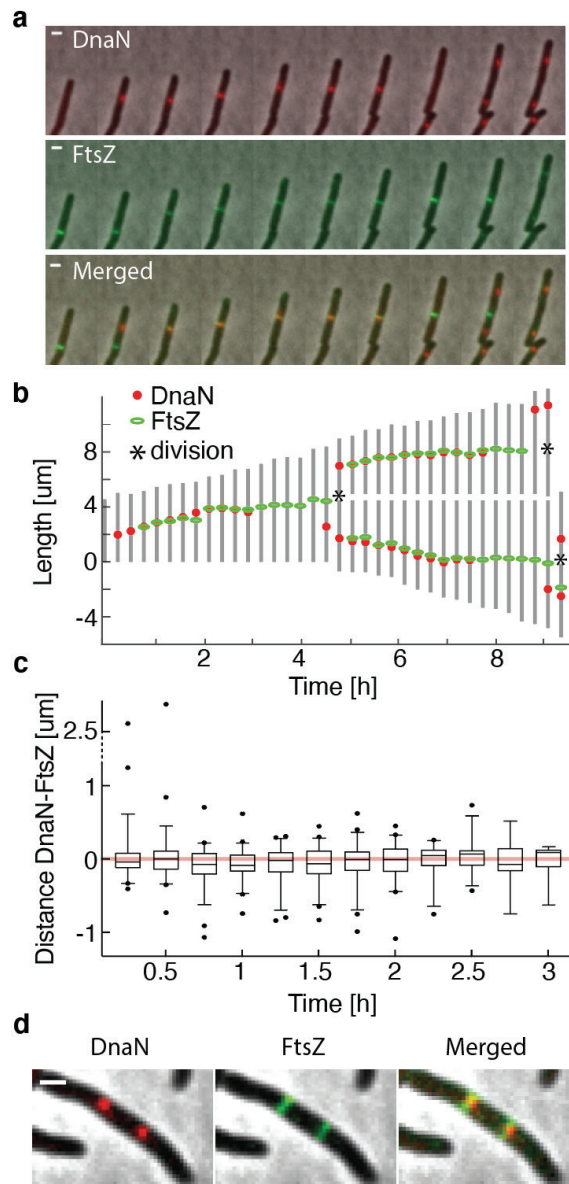


Figure 1. The DNA replisome and cell division ring colocalize in time and space.

(a) Bacteria expressing the mCherry-DnaN replisome marker (upper panels) and the FtsZ-GFP division ring marker (middle panels) were grown in a microfluidic device with a constant flow of M9 medium. Images taken every 15 minutes reveal a close proximity between the replisome and the division ring at all times. Scale bar, 1 μm . **(b)** Schematic representation of time-lapse

images showing growth of two generations of cells from birth to division along with DnaN foci and FtsZ ring positions along the cell length. Cells were aligned to their new pole. The FtsZ ring assembles in close proximity to the DNA replisome and colocalizes with it until the replisome disassembles prior to cell division. **(c)** Distance between DnaN focus and FtsZ ring over time ($n = 56$ cells). Boxplots represent median values with the 25th and 75th percentiles; whiskers represent the 5th and 95th percentiles; symbols represent outliers. **(d)** Representative images of a cell exhibiting a split replisome (DnaN) and two cell division rings (FtsZ). Each replisome colocalizes with a cell division ring (Merged).

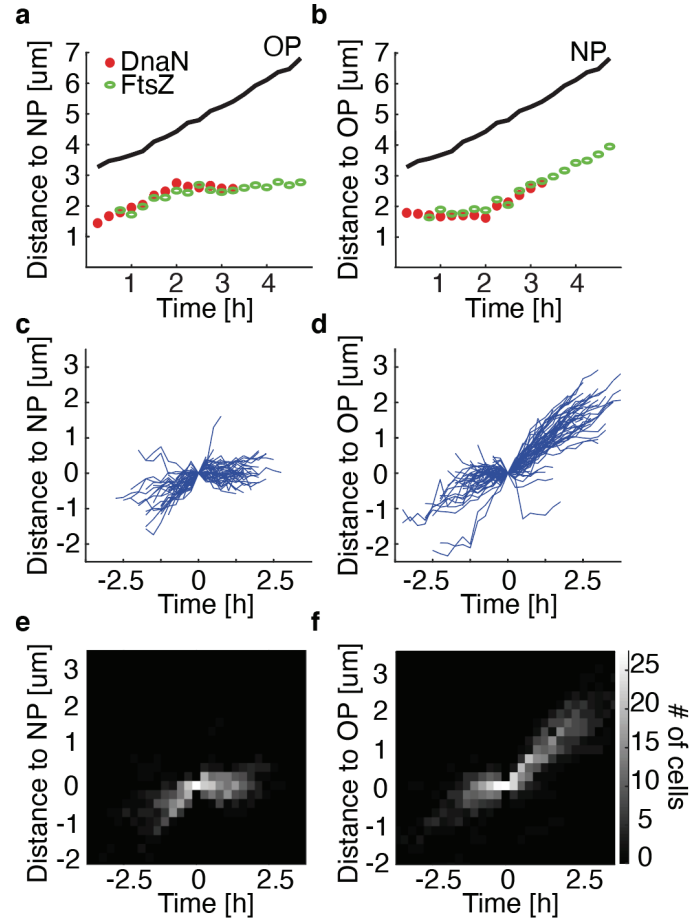


Figure 2. Biphasic trajectory of the DNA replisome and cell division ring towards the future division site.

Bacteria expressing the mCherry-DnaN replisome marker and the FtsZ-GFP division ring marker were grown in a microfluidic device with a constant flow of M9 medium. Images were taken every 15 minutes. **(a,b)** A representative trajectory of DnaN/FtsZ relative to **(a)** the new pole (NP) or **(b)** the old pole (OP). **(c,d)** Line plots of individual DnaN/FtsZ trajectories relative to **(c)** the new pole or **(d)** the old pole. **(e,f)** Kymographs of the movement of DnaN/FtsZ relative to **(e)** the new pole or **(f)** the old pole. **(c-f)** Trajectories were aligned and centered to the breakpoint between phases I and II ($n = 56$ cells).

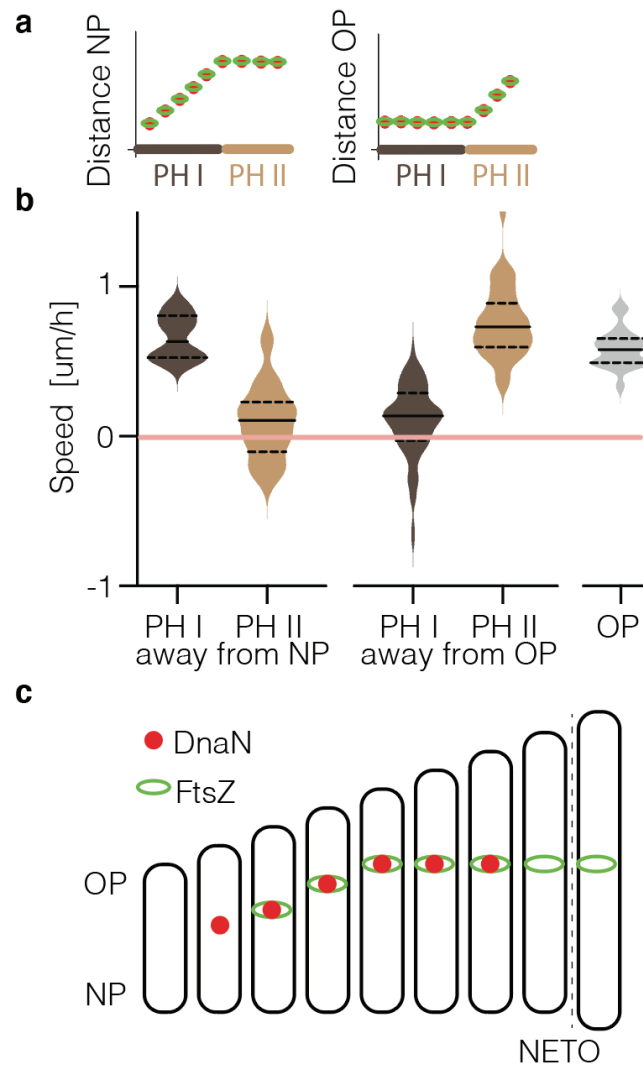


Figure 3. The DNA replisome and cell division ring track the old pole during phase I and the new pole during phase II.

Bacteria expressing the mCherry-DnaN replisome marker and the FtsZ-GFP division ring marker were grown in a microfluidic device with a constant flow of M9 medium. Images were taken every 15 minutes. **(a)** Schematic of the biphasic DnaN/FtsZ trajectory relative to the new pole (NP) or old pole (OP). **(b)** Speed of DnaN/FtsZ movement away from the new pole or old pole during phase I (PH I) and phase II (PH II) compared to the old-pole elongation speed. **(c)** Summary of the biphasic trajectory of DnaN/FtsZ inside a cell. New end take-off (NETO) occurs after the breakpoint between phases I and II at about 90% of the interdivision time.

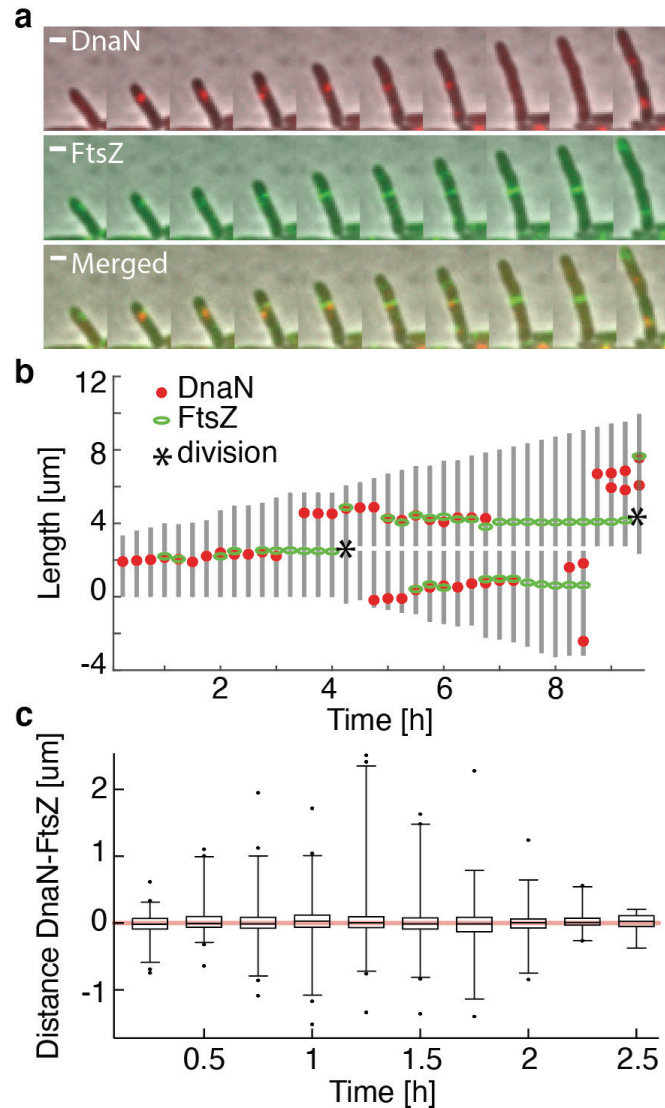


Figure 4. ParB is not required for colocalization of the DNA replisome and cell division ring in time and space.

(a) $\Delta parB$ bacteria expressing the mCherry-DnaN replisome marker (upper panels) and the FtsZ-GFP division ring marker (middle panels) were grown in a microfluidic device with a constant flow of M9 medium. Images taken every 15 minutes reveal a close proximity between the replisome and the division ring at all times. Scale bar, 1 μm . **(b)** Schematic representation of time-lapse images showing growth of two generations of cells from birth to division along with DnaN foci and FtsZ ring positions along the cell length. Cells were aligned to their new pole. The FtsZ ring assembles in close proximity to the DNA replisome and colocalizes with it until the replisome disassembles prior to cell division. **(c)** Distance between DnaN focus and FtsZ ring over time ($n = 60$ cells). Boxplots represent median values with the 25th and 75th percentiles; whiskers represent the 5th and 95th percentiles; symbols represent outliers.

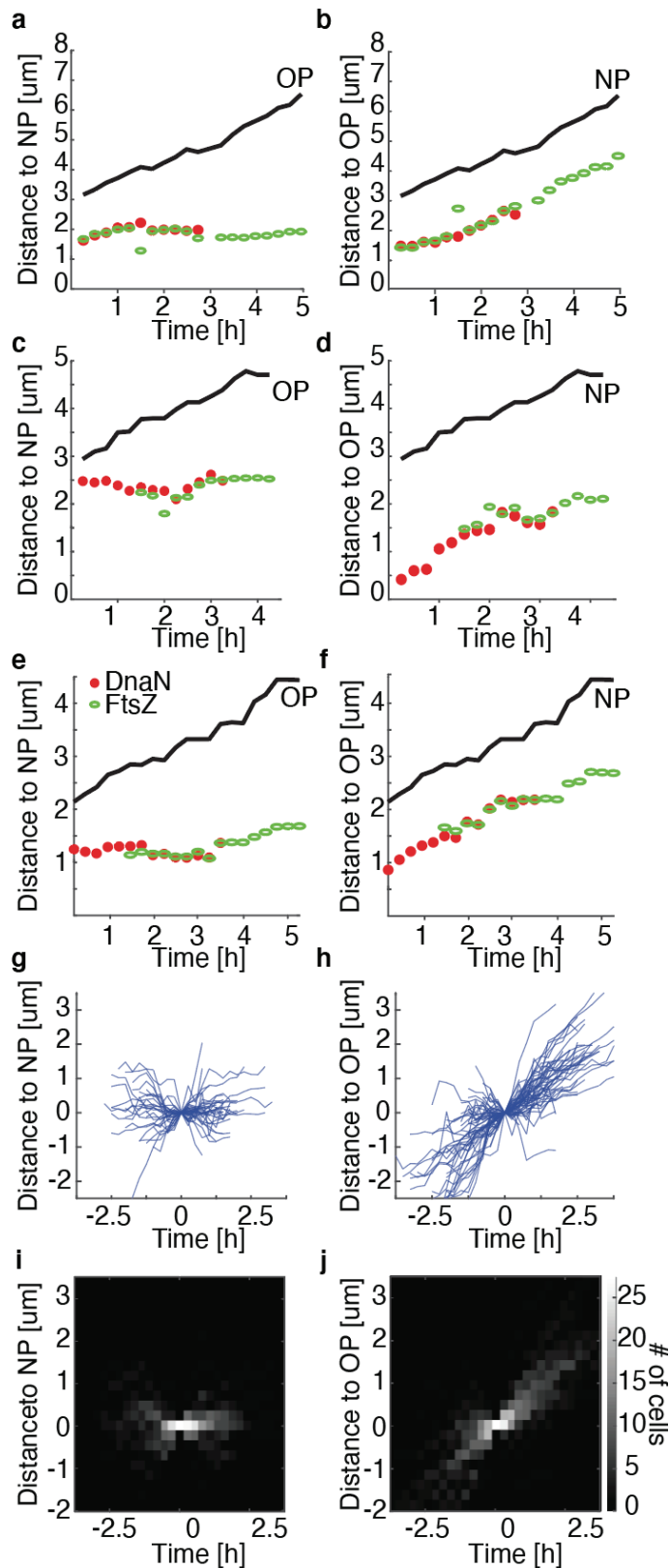


Figure 5. Biphasic trajectory of the DNA replisome and cell division ring towards the future division site is disrupted in $\Delta parB$ cells.

$\Delta parB$ bacteria expressing the mCherry-DnaN replisome marker and the FtsZ-GFP division ring marker were grown in a microfluidic device with a constant flow of M9 medium. Images were taken every 15 minutes. **(a-f)** Examples of trajectories of DnaN/FtsZ relative to **(a,c,e)** the new pole (NP) or **(b,d,f)** the old pole (OP). **(a,b)** DnaN/FtsZ track the old pole during phase I and the new pole during phase II. **(c,d)** DnaN/FtsZ moves towards the new pole in phase I then tracks with the new pole in phase II. **(e,f)** DnaN/FtsZ track the new pole in both phase I and phase II. **(g,h)** Line plots of individual DnaN/FtsZ trajectories relative to **(g)** the new pole or **(h)** the old pole. **(i,j)** Kymographs of the movement of DnaN/FtsZ relative to **(i)** the new pole or **(j)** the old pole. **(c-j)** Trajectories were aligned and centered to the breakpoint between phases I and II ($n = 60$ cells).

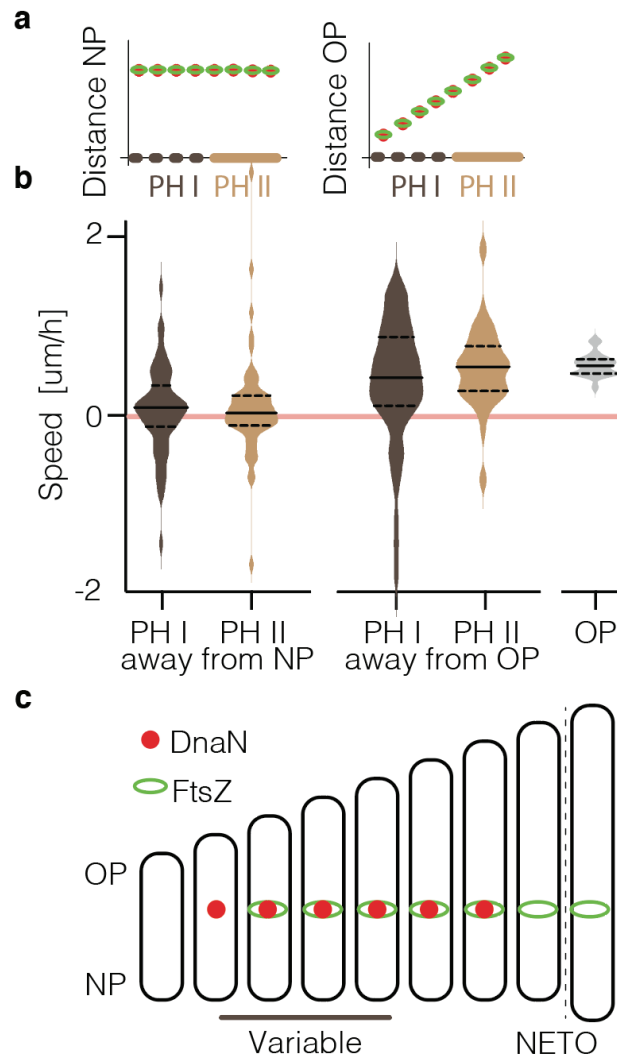


Figure 6. The DNA replisome and cell division ring track the new pole during both phase I and phase II in ΔparB cells.

ΔparB bacteria expressing the mCherry-DnaN replisome marker and the FtsZ-GFP division ring marker were grown in a microfluidic device with a constant flow of M9 medium. Images were taken every 15 minutes. **(a)** Schematic of the DnaN/FtsZ trajectory relative to the new pole (NP) or old pole (OP). **(b)** Speed of DnaN/FtsZ movement away from the new pole or old pole during phase I (PH I) and phase II (PH II) compared to the old-pole elongation speed. **(c)** Summary of the trajectory of DnaN/FtsZ inside a ΔparB cell. New end take-off (NETO) occurs after the breakpoint between phases I and II at about 90% of the interdivision time.

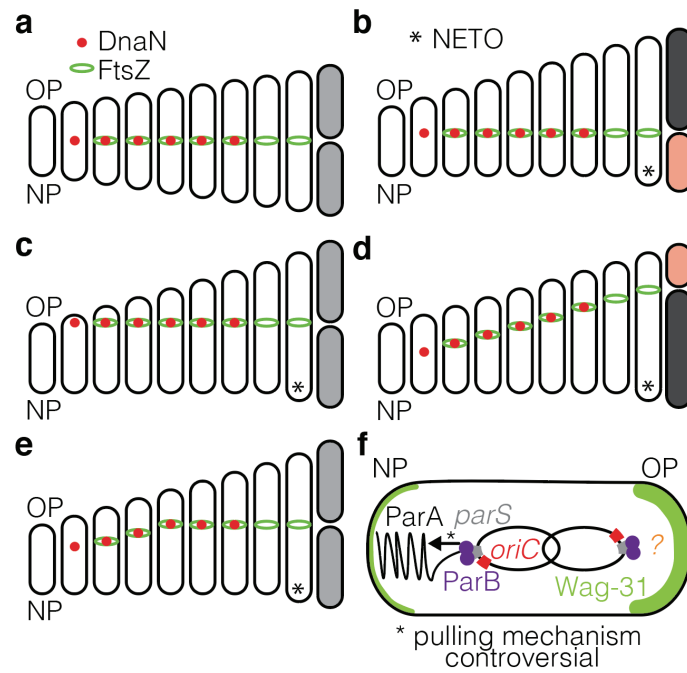


Figure 7. Models for division site selection in bacteria.

(a) Symmetrically growing cell, non-moving replisome appearing midcell. **(b)** Asymmetrically growing cell, non-moving replisome appearing midcell. **(c)** Asymmetrically growing cell, non-moving replisome appearing skewed to the old growing pole. **(d)** Asymmetrically growing cell, replisome appearing midcell tracking the old pole during phase I, non-moving during phase II. **(e)** Model for chromosome segregation **(f)** Asymmetrically growing cell, replisome appearing midcell tracking the old pole during both phase I and phase II.

4.7 Author Contributions

G.V-T., N.D. and J.D.M. conceived the project. G.V-T. performed the experiments and simulations, wrote the Matlab script to analyze the data, analyzed the data and interpreted the results. G.V-T., and J.D.M. wrote the paper. N.D. and J.D.M. supervised the project.

4.8 References

Aldridge, B.B., Fernandez-Suarez, M., Heller, D., Ambravaneswaran, V., Irimia, D., Toner, M., and Fortune, S.M. (2012). Asymmetry and aging of mycobacterial cells lead to variable growth and antibiotic susceptibility. *Science* 335, 100–104.

Badrinarayanan, A., Le, T.B., and Laub, M.T. (2015). Bacterial chromosome organization and segregation. *Annu Rev Cell Dev Biol* 31, 171–199.

Bowman, G.R., Comolli, L.R., Zhu, J., Eckart, M., Koenig, M., Downing, K.H., Moerner, W.E., Earnest, T., and Shapiro, L. (2008). A polymeric protein anchors the chromosomal origin/ParB complex at a bacterial cell pole. *Cell* 134, 945–955.

Dahl, J.L. (2004). Electron microscopy analysis of *Mycobacterium tuberculosis* cell division. *FEMS Microbiology Letters* 240, 15–20.

Dimude, J.U., Stein, M., Andrzejewska, E.E., Khalifa, M.S., Gajdosova, A., Retkute, R., Skovgaard, O., and Rudolph, C.J. (2018). Origins left, right, and centre: Increasing the number of initiation sites in the *Escherichia coli* chromosome. *Genes (Basel)* 9.

Donovan, C., Schauss, A., Krämer, R., and Bramkamp, M. (2013). Chromosome segregation impacts on cell growth and division site selection in *Corynebacterium glutamicum*. *PLoS One* 8, e55078.

Eskandarian, H.A., Odermatt, P.D., Ven, J.X.Y., Hannebelle, M.T.M., Nievergelt, A.P., Dhar, N., McKinney, J.D., and Fantner, G.E. (2017). Division site selection linked to inherited cell surface wave troughs in mycobacteria. *Nature Microbiology* 2, 17094.

Fogel, M.A., and Waldor, M.K. (2021). A dynamic, mitotic-like mechanism for bacterial chromosome segregation. *Genes Dev* 20, 3269–3282.

Ginda, K., Bezulska, M., Ziólkiewicz, M., Dziadek, J., Zakrzewska-Czerwińska, J., and Jakimowicz, D. (2013). ParA of *Mycobacterium smegmatis* co-ordinates chromosome segregation with the cell cycle and interacts with the polar growth determinant DivIVA. *Molecular Microbiology* 87, 998–1012.

Ginda, K., Santi, I., Bousbaine, D., Zakrzewska-Czerwińska, J., Jakimowicz, D., and McKinney, J. (2017). The studies of ParA and ParB dynamics reveal asymmetry of chromosome segregation in mycobacteria: ParAB dynamics in mycobacteria. *Molecular Microbiology* 105, 453–468.

Hajduk, I.V., Rodrigues, C.D.A., and Harry, E.J. (2016). Connecting the dots of the bacterial cell cycle: Coordinating chromosome replication and segregation with cell division. *Seminars in Cell & Developmental Biology* 53, 2–9.

Hannebelle, M.T.M., Ven, J.X.Y., Toniolo, C., Eskandarian, H.A., Vuaridel-Thurre, G., McKinney, J.D., and Fantner, G.E. (2020). A biphasic growth model for cell pole elongation in mycobacteria. *Nature Communications* **11**, 452.

Hett, E.C., and Rubin, E.J. (2008). Bacterial growth and cell division: A Mycobacterial perspective. *Microbiology and Molecular Biology Reviews* **72**, 126–156.

Jakimowicz, D., Brzostek, A., Rumijowska-Galewicz, A., Żydek, P., Dołzbłasz, A., Smulczyk-Krawczyszyn, A., Zimniak, T., Wojtasz, Ł., Zawilak-Pawlik, A., Kois, A., et al. (2007). Characterization of the mycobacterial chromosome segregation protein ParB and identification of its target in *Mycobacterium smegmatis*. *Microbiology* **153**, 4050–4060.

Joyce, G., Williams, K., Robb, M., Noens, E., Tizzano, B., Shahrezaei, V., and Robertson, B. (2012). Cell division site placement and asymmetric growth in mycobacteria. *PloS One* **7**, e44582.

Kang, C.-M., Nyayapathy, S., Lee, J.-Y., Suh, J.-W., and Husson, R.N. (2008). Wag31, a homologue of the cell division protein DivIVA, regulates growth, morphology and polar cell wall synthesis in mycobacteria. *Microbiology* **154**, 725–735.

Kawalek, A., Wawrzyniak, P., Bartosik, A.A., and Jagura-Burdzy, G. (2020). Rules and exceptions: the role of chromosomal ParB in DNA segregation and other cellular processes. *Microorganisms* **8**.

Kois-Ostrowska, A., Strzałka, A., Lipietta, N., Tilley, E., Zakrzewska-Czerwińska, J., Herron, P., and Jakimowicz, D. (2016). Unique function of the bacterial chromosome segregation machinery in apically growing *Streptomyces* - targeting the chromosome to new hyphal tubes and its anchorage at the tips. *PLOS Genetics* **12**, e1006488.

Monahan, L.G., Liew, A.T.F., Bottomley, A.L., and Harry, E.J. (2014). Division site positioning in bacteria: one size does not fit all. *Front. Microbiol.* **5**.

Moriya, S., Rashid, R.A., Rodrigues, C.D.A., and Harry, E.J. (2010). Influence of the nucleoid and the early stages of DNA replication on positioning the division site in *Bacillus subtilis*. *Molecular Microbiology* **76**, 634–647.

Pióro, M., Małecki, T., Portas, M., Magierowska, I., Trojanowski, D., Sherratt, D., Zakrzewska-Czerwińska, J., Ginda, K., and Jakimowicz, D. (2019). Competition between DivIVA and the nucleoid for ParA binding promotes segrosome separation and modulates mycobacterial cell elongation. *Molecular Microbiology* **111**, 204–220.

Ptacin, J.L., Gahlmann, A., Bowman, G.R., Perez, A.M., von Diezmann, A.R.S., Eckart, M.R., Moerner, W.E., and Shapiro, L. (2014). Bacterial scaffold directs pole-specific centromere segregation. *Proc Natl Acad Sci U S A* **111**, E2046-2055.

van Raaphorst, R., Kjos, M., and Veening, J.-W. (2017). Chromosome segregation drives division site selection in *Streptococcus pneumoniae*. *Proc Natl Acad Sci U S A* **114**, E5959–E5968.

Rowlett, V.W., and Margolin, W. (2015). The Min system and other nucleoid-independent regulators of Z ring positioning. *Front. Microbiol.* **6**.

- Santi, I., and McKinney, J.D. (2015). Chromosome organization and replisome dynamics in *Mycobacterium smegmatis*. *MBio* 6, e01999-14.
- Santi, I., Dhar, N., Bousbaine, D., Wakamoto, Y., and McKinney, J.D. (2013). Single-cell dynamics of the chromosome replication and cell division cycles in mycobacteria. *Nature Communications* 4, 2470.
- Trojanowski, D., Ginda, K., Pióro, M., Hołówka, J., Skut, P., Jakimowicz, D., and Zakrzewska-Czerwińska, J. (2015). Choreography of the *Mycobacterium* replication machinery during the cell cycle. *MBio* 6, e02125-14.
- Ven, J.X.Y. (2019). Single-cell studies of *Mycobacterium smegmatis* cell cycle using time-lapse fluorescence microscopy. Ecole Polytechnique Fédérale de Lausanne.
- Viollier, P.H., Thanbichler, M., McGrath, P.T., West, L., Meewan, M., McAdams, H.H., and Shapiro, L. (2004). Rapid and sequential movement of individual chromosomal loci to specific subcellular locations during bacterial DNA replication. *Proc Natl Acad Sci U S A* 101, 9257–9262.
- Walker, B.E., Männik, J., and Männik, J. (2020). Transient membrane-linked FtsZ assemblies precede Z-Ring formation in *Escherichia coli*. *Current Biology* 30, 499-508.e6.
- Wu, L.J., and Errington, J. (2012). Nucleoid occlusion and bacterial cell division. *Nature Reviews Microbiology* 10, 8–12.

Chapter 5 Computational analysis of the mutual constraints between single-cell growth and division control models

Postprint version of the article published in Advanced Biosystems: **DOI: 10.1002/adbi.201900103**

Gaëlle Vuaridel-Thurre*, Ambroise R. Vuaridel, Neeraj Dhar*¹, John D. McKinney*¹

G. Vuaridel-Thurre, A. R. Vuaridel, Dr. N. Dhar, Prof. J. D. McKinney.

School of Life Sciences, Swiss Federal Institute of Technology in Lausanne (EPFL), CH-1015 Lausanne, Switzerland

E-mail: gaelle.thurre@epfl.ch, neeraj.dhar@epfl.ch, john.mckinney@epfl.ch

¹These authors contributed equally.

Keywords: cell size homeostasis, single-cell growth model, timer, sizer, adder

5.1 Abstract

Three models of division control have been proposed to achieve cell size homeostasis: sizer, timer, and adder. However, few published studies of division control take into account the dynamics of single-cell growth and most assume that single-cell growth is exponential. Here, computational simulations considering exponential, linear, and bilinear growth models are performed. These simulations confirm that a timer division control model alone cannot lead to size homeostasis if the single-cell growth model is exponential. Furthermore, timer and adder division control models cannot be distinguished if the single-cell growth model is linear. Models of division control cannot be easily differentiated by analysis of average cell behavior because the birth sizes of the majority of cells are close to the population average. However, the differences between division control models are amplified in outlier cells whose birth size is far from the average. A method is introduced for vector field analysis of the speed of convergence of outlier lineages towards the steady-state birth size, which can help to distinguish between division control models and single-cell growth models.

5.2 Introduction

Cell size and shape are remarkably diverse. Bacterial cell size ranges from a few hundred nanometres for the smallest bacteria to a few hundred micrometers for the largest bacteria.^[1] Eukaryotic cells are typically larger than bacterial cells and can range from a few micrometers to even meters for cells of the nervous system. However, all cells have a limited size window where they function optimally and size control mechanisms may contribute to keeping them within their optimal range.^[2] Thus, the processes of cell growth and division may be coordinated in order to maintain cell size homeostasis over time.

Diverse models have been invoked to explain how individual cells grow and incorporate newly synthesized material. For example, some cells grow by extension of the lateral cell wall (e.g., *Escherichia coli*) while others grow by elongation of the cell poles (e.g., *Mycobacterium* spp.). There have been many attempts to rationalize these growth patterns, such as Daniel and Errington's hypothesis that lateral cell wall extension is inherently *exponential* (because the growth zone expands continuously between birth and division) whereas, by similar reasoning, polar growth is inherently *linear* (because the size of the growth zone remains constant between birth and division).^[3] Other growth models are possible. For example, *Schizosaccharomyces pombe* is thought to grow by polar elongation in a *bilinear* manner, in part because the new cell pole initiates growth later than the old cell pole.^[4–7]

Many studies have converged on **exponential growth** as a model for cell growth based on pulse-labelling of cell populations, optical microscopy, spatial light interference microscopy, and single-cell measurements of buoyant mass obtained with a suspended microchannel resonator.^[8–11] Earlier studies proposed **linear growth** as a general model for cell growth based on measurements made on single cells, synchronized cultures, and population distributions.^[12,13] In a few cases, **bilinear growth** has been invoked as a model to explain the

pattern of single-cell growth observed using optical microscopy.^[4–7] However, it is difficult experimentally to distinguish between these growth models because the shapes of the growth curves generated by exponential, linear, and bilinear growth models are very similar and efforts to distinguish between them are confounded by experimental and biological sources of noise. To illustrate the lack of consensus in the literature, at different times using different methods, single-cell growth of a single species (*E. coli*) has variously been described as exponential, linear, or bilinear.^[11,12,14] The introduction of novel techniques for single-cell size measurements has not ended the debate. For example, although measurements of buoyant cell mass identified exponential growth as the “true” single-cell growth model in *Bacillus subtilis*, the “true” growth model for *E. coli* could not be identified with this technique.^[15]

Cell size homeostasis also requires that growth and division be coordinated. Otherwise, individual cells could become progressively bigger and bigger or smaller and smaller at every generation, eventually resulting in non-viability. When individual cells deviate significantly from the average birth size distribution – for example, following a transient block in cell cycle progression or due to an abnormally asymmetric cell division event – they do eventually return to a “normal” size. This behavior indicates that there must be mechanisms responsible for cell size homeostasis.

In this context, three models for division control have been proposed.^[16] Originally referred to as *sizer*, *clock*, and *incremental* models they are now known as *sizer*, *timer*, and *adder* models, respectively (Figure 1).^[17–19] According to the *sizer* model, cells divide after reaching a certain size. According to the *timer* model, cells divide after a certain amount of time has elapsed since their birth, following an internal clock. According to the *adder* model, cells must increase their size by a fixed amount before they divide, independent of their size at birth. This model seems to be supported by single-cell data for a large variety of organisms.^[20–25] These models for division control, however, are not mutually exclusive, as some studies have reported that combinations of the different mechanisms may operate in a single organism.^[26–32] It is also worth noting that these models (*sizer*, *timer*, *adder*) could be invoked to explain how other cell cycle transitions are controlled, for example, initiation of DNA replication.^[28]

Early studies considered the impact of different single-cell growth models on the control of cell division using a combination of experimental data and mathematical modeling.^[33–38] In more recent studies, the true single-cell growth model is usually assumed to be exponential and the potential consequences of other growth models on division control are seldom explored. Here, we assess the importance of determining the true dynamics of single-cell growth in order to distinguish between alternative division control models operating in the context of cell size homeostasis. We analyze the different methods that are used to identify the growth model based on single-cell growth curves and highlight how difficult it remains to assign the true growth model. We demonstrate that accurate knowledge of the single-cell growth model can, in some cases, eliminate a model of division control from further

consideration. Keeping in mind the constraints imposed by the single-cell growth model, we demonstrate that vector field analysis of the time-dependent behavior of outliers in the size distribution is a useful method to distinguish between different models of division control.

5.3 Results

5.3.1 Boundary conditions for computational simulations of single-cell growth

We consider three possible growth models at the single-cell level: exponential, linear, and bilinear. In studies of single-cell growth it is common to distinguish only between exponential and linear growth. We have included the bilinear growth model in our analysis, in part because an important model organism, *S. pombe*, is thought to grow bilinearly.^[4–7] We implemented a model where cells grow bilinearly and the transition between slow growth and fast growth is size-dependent; under these conditions, linear and bilinear models give different results. The timing of the transition depends on the size at birth such that cells born small make the transition later, in terms of percentage of the interdivision time, than cells born large. Thus, cells following this model are situated somewhere between the exponential and linear models.

For the boundaries of the bilinear model, we define that cells born at an average size exhibit an increase in growth velocity of 35% at 34% of their cell division cycle, as reported for *S. pombe*.^[5] Realistically, cells that are born very small or very large, compared to the average, may not reach the growth rate transition before dividing (small cells) or may not require a lag before making the transition (large cells). Therefore, we define as the lower boundary that cells born smaller than 25% of the average birth size will not increase their growth velocity until the time of division (the transition to fast growth occurs after 100% of the interdivision time). This automatically sets the upper boundary to cells born 137.5% bigger than the average birth size. These large cells grow at their maximal speed during the entire cell cycle from birth until division (the transition to fast growth occurs at 0% of the interdivision time).

5.3.2 Single-cell growth models can be distinguished by residual analysis with Akaike and Bayesian information criteria

The growth model of single cells is usually deduced by fitting exponential, linear, or bilinear functions to the data obtained by time-lapse microscopy or other methods and evaluating the fittings using Pearson's correlation coefficient (r^2) or adjusted r^2 (Figure 2a-c). However, when we fitted each of these functions to simulated exponential, linear, or bilinear growth curves including small Gaussian noise, the adjusted r^2 values were very similar and close to 1, which indicates a very good fit for all of the models at this noise level. These fittings were made by adding Gaussian noise with a standard deviation of 2% of average cell size, which corresponds to the precision of measurement currently achievable with optical microscopy of small cells (e.g., a pixel size of 0.64 μm and an average cell size of 3 μm gives ~2% error).^[20]

Since the adjusted r^2 is based on residuals, we performed an analysis of residuals to increase the discriminatory power (Figure 2d,e,g,i). In the case of adequate fit, residuals are normally distributed around zero; if the distribution falls into a pattern, this suggests the fit is inadequate.^[39] The distinction between different growth models can be further refined by applying the Akaike information criterion (AIC) or the Bayesian information criterion (BIC) to the curve fittings (Figure 2d,f,h,j).^[4,6] These criteria use the principle of parsimony and penalize models that are over-parameterized; BIC penalizes complex models more than AIC and is often preferred.^[40] For example, the bilinear fit is inferior to the exponential fit for a true exponential model (Figure 2f). This distinction is not clear using the adjusted r^2 (Figure 2a) or the residual analysis (Figure 2e) alone, demonstrating the additional discriminatory power of the AIC/BIC criteria. However, this method also has its limitations, and errors in model identification increase with increasing noise, especially for the bilinear model (Figure S1, Supporting Information).

5.3.3 Correct identification of the division control model relies on accurate knowledge of the single-cell growth model

As discussed earlier, three main models for cell division control have been proposed: the *sizer*, *timer*, and *adder* models (Figure 1). Here, we show how these division control models are linked to the single-cell growth models in the context of cell size homeostasis, and how knowing the true growth model can help to distinguish between them. We investigate the exponential, linear, and bilinear models of single-cell growth to understand their stability and behavior in relation to the *sizer*, *timer*, and *adder* models of cell division control.

Exponential cell growth is described as

$$S = S_b \cdot (1 + r)^t \quad (1)$$

where S is the cell size after time t from birth, r is the growth rate (units in time^{-1}), and S_b is the cell size at birth. The cell size after n divisions is given by

$$S_n = S_0 \cdot (1 + r)^{\Delta t \cdot n} \cdot k^n \quad (2)$$

where k is the asymmetry coefficient of division ($k = 0.5$ for symmetric division, $k = 0$ or 1 for totally asymmetric division), S_0 is the initial ancestor cell size at birth, and Δt is the interdivision time. With exponential growth, three solutions of birth size can be realized:

$$\lim_{n \rightarrow \infty} S_n = \begin{cases} +\infty & \text{if } (1 + r)^{\Delta t} \cdot k > 1 \\ 0 & \text{if } (1 + r)^{\Delta t} \cdot k < 1 \\ L_b & \text{if } (1 + r)^{\Delta t} \cdot k = 1 \end{cases} \quad (3)$$

Thus, cells either become larger and larger or smaller and smaller in subsequent generations. The steady-state solution for birth size is reached only in the special case where

$$(1 + r)^{\Delta t} \cdot k = 1 \quad (4)$$

Linear cell growth is described as

$$S = S_b + t \cdot v \quad (5)$$

where v is the growth velocity (units in volume \cdot time⁻¹), and S_b is the cell size at birth. Cell size after n divisions is given by

$$S_n = (S_0 \cdot k^n) + (\Delta t \cdot v \cdot \sum_{i=1}^n k^i) \quad (6)$$

Over many divisions, the birth size of new generations of cells converges toward a unique steady-state solution, which is reached when the birth size becomes equal to

$$\lim_{n \rightarrow \infty} S_n = \frac{\Delta t \cdot v \cdot k}{1 - k} \quad (7)$$

Linear growth therefore yields a stable birth size across cell divisions.

The result is similar for **bilinear cell growth**:

$$\lim_{n \rightarrow \infty} S_n = \frac{(\Delta t_1 \cdot v_1 + \Delta t_2 \cdot v_2) \cdot k}{1 - k} \quad (8)$$

where v_1 is the growth velocity during the first period of the cell cycle Δt_1 , and v_2 is the growth velocity during the second period of the cell cycle Δt_2 . Thus, the sum of Δt_1 and Δt_2 equals the full cell cycle duration.

If we now use these growth model derivations in relation to the control of cell division, we see that cells growing exponentially reach a stable solution for birth size only under a *sizer* model or *adder* model because of an explicit restriction on size, whereas a *timer* model of cell division control results in an unstable birth size over successive generations (Equation 3). Under a *timer* model, if an exponentially growing cell divides asymmetrically, or divides too soon or too late due to noise, cells may become smaller and smaller or larger and larger at each successive division and cell size homeostasis may not be maintained. These results are in good agreement with previous mathematical treatments of this problem.^[19,35–38] Under linear cell growth, no matter if S (*sizer* model), Δt (*timer* model), or $\Delta t \cdot v$ (*adder* model) is fixed, the steady-state solution S_n and thus cell size homeostasis will always be reached (Equation 7). Thus, cells growing linearly can maintain size homeostasis under any of the three division control models: *sizer*, *timer* or *adder*. The same is true for bilinear growth.

In general, for all single-cell growth models, a *sizer* model or *adder* model will prevent cell size from diverging over generational time and Equation 7 is valid for any single-cell growth model, including exponential growth. Since the total added volume is kept constant, the pattern of how it is added does not matter.

To summarize: given that a *timer model* of cell division is unstable with exponential growth, these results underscore the importance of taking into account the model of single-cell growth before assigning models of division control.

5.3.4 The speed at which outliers return to a steady-state birth size is characteristic of each combination of single-cell growth and division models

Under steady-state growth, all three models of cell division control (*sizer*, *timer*, *adder*) are equivalent and not differentiable. Here, we consider a lineage of symmetrically dividing cells to be in steady-state growth if the birth size of all cells in the lineage remains constant over generations in a deterministic manner. Take, for example, a cell born at a volume v that will divide at $2v$, yielding two daughter cells of volume v that will also divide at $2v$. For this lineage, we cannot distinguish between a *sizer* model dictating that cells divide at exactly $2v$, an *adder* model dictating that cells add a volume v , or a *timer* model that allows cells to grow for a certain time, which happens to coincide with a volume of $2v$ at division. Under steady-state growth, all three models are possible and give the same result.

If we now consider outlier cells – for example, cells born at an abnormally small size of only 25% of the steady-state birth size or cells born at an abnormally large size of 200% of the steady-state birth size (Figure 3) – their descendants may eventually reach the steady-state birth size, depending on the single-cell growth model. Crucially, the rate of this convergence is determined by the model of division control (Figure 3), assuming that the descendants of the outlier cells return to a normal behavior.

If the true single-cell growth model is known, in most cases it is possible to distinguish between the models of division control when looking at the number of generations an outlier cell takes to reach the steady-state birth size. The *timer* and *adder* models of division control exhibit the slowest convergence of outlier cells towards steady-state. Cells growing **exponentially** under the control of a *timer* model remain at stable equilibria of large or small size (Figure 3a) because, under deterministic simulations, Equation 4 is satisfied. If Equation 4 were not satisfied, cells growing exponentially following a *timer* model would be born larger and larger or smaller and smaller in each generation, according to Equation 3. If cells grow **linearly**, the rate of convergence will not discriminate between a *timer* or an *adder* model: the two models are strictly equal (Figure 3b) because, during a fixed amount of time, a cell will add a fixed volume independently of its size at birth. Or, stating the case the other way around: adding a fixed volume will take the same amount of time for all cells. Outlier cells growing **bilinearly** under a *timer* model will take slightly more time to reach cell size homeostasis than if they were governed by an *adder* model, because large cells grow faster and will add more volume than small cells in the same amount of time (Figure 3c). As large cells approach the steady-state birth size by becoming smaller and smaller in successive divisions, they will add a little less volume in each generation until the steady-state birth size is reached.

If we combine different models of division control during the cell cycle, the rate of convergence will adapt accordingly. For example, the more dominant the *sizer* model is, in terms of the fraction of the cell cycle it controls, the quicker the convergence will be. We note that this example of a “perfect *sizer* model” is unrealistic, as cells born at $2v$ would instantly divide to form two cells of $1v$ each, with insufficient time to complete DNA replication and segregation. Adding a more realistic “minimum interdivision time” constraint (effectively, a *timer*) reduces the rate of convergence, rendering a pattern somewhat more similar to the *adder* model (Figure 3). This effect is enhanced as the “minimum interdivision time” is increased. In theory, all intermediate convergence curves between the perfect *sizer* model and *adder* model could be found by combining models and adjusting their importance or duration.

Here, we assume that cell division is symmetric (the two daughter cells are equal in size at birth), but our conclusions would be similar for cells that divide asymmetrically. Indeed, in cases of asymmetric division, two steady-state birth sizes would be obtained when following the progeny of outlier cells: one for the smallest daughter cells, and one for the largest daughter cells. Every other cell lineage, between the smallest and largest outliers, will have a steady-state birth size intermediate between those two extremes.

Following a *sizer* model (Figure 4a) or *adder* model (Figure 4c), outlier cells following the three different single-cell growth models converge at the same rate in terms of generations. In the case of a *timer* model, the linear and bilinear models of single-cell growth converge to the steady state at different rates, whereas cells growing exponentially fail to converge (Figure 4b). Rather than looking at the number of generations that it takes for an outlier cell to reach the steady-state birth size, we can instead measure the absolute time. Because exponential growth is size-dependent, abnormally small cells take longer to converge to the steady-state birth size than abnormally large cells even though it takes them the same number of generations. This conclusion is also valid for bilinear growth, albeit to a lesser extent. Therefore, using absolute time as the measure of convergence speed, in theory, it should be possible to differentiate the single-cell growth models (Figure 4d-f). Experimentally, however, this distinction would be challenging due to measurement and biological noise, the latter including asymmetric division, which is common in some bacteria.

To summarize, although it is impossible to distinguish between the different models of cell division control when cells are in steady-state growth, analysis of the convergence rates of outlier cells can, in theory, distinguish between the models because the perturbed system is not in steady state. The only exception is that when single-cell growth follows a linear model, the *adder* model and *timer* model of division control cannot be differentiated.

5.3.5 The correlation between birth size and added size depends on the division control and single-cell growth models

Scatter plots of birth size against added size from birth to division (or variants thereof) have

been widely used to deduce the true model of cell division control.^[17,18] In such plots, cells following a *sizer* model exhibit a slope of -1 (Figure 5b-d, black lines), while cells following an *adder* model exhibit a slope of 0 (Figure 5b-d, blue lines). Cells following these division control models exhibit the same slopes irrespective of the model of single-cell growth. However, the slope of a collection of cells following a *timer* model depends on the growth model: a slope of $s = 1$ if growth is exponential (Figure 5b, red line), $s = 0$ if growth is linear (Figure 5c, red line), or $0 < s < 1$ if growth is bilinear (Figure 5d, red line). In the last scenario, the slope depends on the parameters set for the bilinear model.

In the case of linear growth, the slope of cells following the *timer* model is equal to 0 because a small cell will add the same amount of volume as a large cell during the same interval of time. The *timer* and *adder* models therefore become undistinguishable and a constant added size can represent either model. This point again underscores the importance of identifying the true model of single-cell growth.

5.3.6 Single-cell growth models and division control models can be distinguished by the speed of convergence of outlier cells in vector fields of birth size versus added size

Vector fields superimposed on a graph depicting birth size versus added size (Figure 5a) provide *direct* information about the rate of convergence of outlier cells towards the equilibrium point, defined here as the unique convergence point of the vector field. Thus, vector fields provide a better visualization of the underlying model of division control compared to conventional scatter plots. The vector field shows the direction followed by linear trajectories of cells and their descendants through multiple generations; where the trajectories pass through the equilibrium point, every cell has the same birth size and added size. The arrows indicate the direction of trajectories for successive birth size, under the assumption that the mechanisms responsible for cell growth and cell size homeostasis directly target the equilibrium point. In the “unstable” (cyan) areas the arrows point away from the equilibrium point and cells become progressively smaller or larger in each generation. Conversely, in the “stable” (magenta) areas the arrows point towards the equilibrium point and cells converge progressively towards this point in each generation. The darkness of the colors illustrates the speed at which the birth size of daughter cells becomes larger or smaller than the birth size of their mother cells in successive generations.

Under an **exponential** model of single-cell growth (Figure 5b), convergence towards the equilibrium point is reached the fastest with the *sizer* model of division control, as the trajectory lies within a dark magenta region. Under the *timer* model, cells lie within the extreme border of the “unstable” cyan regions. This region is completely white, indicating that daughter cells and mother cells have the same birth size, and convergence toward the equilibrium point will not occur. However, if noise is added, these cells will tend to fall into the “unstable” cyan region and move away from the equilibrium point. Under an *adder* model, cells that are far from the equilibrium point converge rapidly at the beginning and

more slowly as they approach the equilibrium point, indicated by lightening of the magenta. Under a **linear** model of single-cell growth (Figure 5c), the *sizer* and *adder* models of division control behave exactly the same as for exponentially growing cells (cf. Figure 5b). Under a *timer* model, however, cells growing linearly behave the same as cells growing under an *adder* model. When the growth model is **bilinear** (Figure 5d), the *sizer* and *adder* models of division control behave exactly the same as for cells growing exponentially or linearly (cf. Figure 5b,c). Under a *timer* model, cells smaller than 25% of the average size and cells bigger than 137.5% of the average size grow linearly either at minimal or maximal velocity, respectively, indicated by the dashed regions of the red line in Figure 5d. These cells are too small or too large to exhibit a change in growth velocity and, therefore, they grow linearly and have another theoretical equilibrium point (not shown here).

As already mentioned for Figure 3, during asymmetric division, two extreme steady-state sizes would be obtained when following the lineage of outlier cells (the smallest and the largest cells) through time. Thus, for asymmetrically dividing cells, two vector fields will be obtained, one for each extremum. All other cell lineages will reach a “birth size” and “added size” situated somewhere on the interpolation curve of the two equilibrium points of the two vector fields.

5.4 Conclusion

Here, we highlight the importance of determining single-cell growth models, as the true growth model constrains the possible division control models. We show that conventional methods, such as r^2 analysis, are inadequate to determine the true growth model. Additional discriminating power can be achieved using analysis of residuals, especially when combined with Akaike or Bayesian information criteria.

In steady-state populations, the majority of cells provide little information about the model of division control because their birth sizes are near the population average. However, rare “outlier” cells with birth sizes significantly smaller or larger than the mean can be very informative. If scatter plots are used, we propose that the bulk population should be removed from the analysis, which should focus instead on outliers and their successive generations until the steady-state birth size is reached. We show that the speed (number of generations or absolute time) at which outliers return to a steady-state birth size is characteristic of each combination of single-cell growth model and division control model; only the *timer* and *adder* models are equivalent for cells growing linearly. Experimentally, the speed of convergence to the steady-state birth size could also be studied by reversibly shifting the cell size distribution using mutations, antibiotics, or nutritional conditions that accelerate or delay division.^[41–43] Previously, mechanisms of division control based either on the concentration or absolute number of stimulatory or inhibitory molecules have been proposed.^[44–47] Experimentally, the authors attempted to distinguish between these mechanisms by perturbing the DNA-to-cytoplasm ratio and observing the convergence of interdivision periods back to equilibrium in successive generations. It would be interesting to assess the

compatibility of these “molecular mechanisms” with the *sizer*, *timer* or *adder* models of division control.

Although the *sizer*, *timer*, and *adder* models have been studied extensively in their abstract (mathematical) forms, the underlying and concrete *mechanisms* of size control are not well understood. In the case of a *sizer* model, it has been proposed that a metabolic sensor governs cell size at division in *E. coli* and *B. subtilis*, or that titration of intracellular molecules could serve as a proxy for cell size.^[48–50] This and other potential size-sensing mechanisms that could be used to control the timing of cell division have been reviewed recently.^[2,51–53] In the case of a *timer* model, the time interval could be the result of the sum of multiple processes, each of which requires a specific and finite amount of time^[16]. In some organisms, a *timer* model could also be linked to the organism’s circadian rhythm, as cell size control has been shown to be driven in part by the circadian clock.^[54] In the case of an *adder* model, it was recently proposed that division is triggered by the accumulation of initiators and precursors of division proteins to a fixed threshold, combined with maintenance of their production in proportion to volume growth.^[55] As defined in our analytical analysis, $\Delta t \cdot v$ is fixed in an *adder* model. Thus, mechanistically, the cell could achieve size homeostasis by modulating either Δt (the interdivision time) or v (the cell growth velocity) or both, as proposed by Ginzberg et al.^[56]

Conventionally, division control models are distinguished using scatter plots that correlate the birth size and added size of individual cells. For example, a constant added size irrespective of birth size is often taken to support the *adder* model of division control; however, this relationship also holds true for the *timer* model when single-cell growth is linear. As shown here, scatter plots can be overlaid with vector fields to capture additional parameters, such as cell lineages, speed of convergence to a steady-state birth size, and stability of cell size. Thus, vector fields contain both the information depicted in conventional scatter plots and convergence plots (Figure 3). Scatter plots depict the behavior of actual cells but they cannot predict the behavior of cells following an unstable combination of single-cell growth and division models, for example, cells growing exponentially under a *timer* model. In contrast, vector fields capture the predicted behavior of both stable and unstable combinations of models, which is a useful feature for ruling out unstable combinations without having to perform complex mathematical analyses.

5.5 Figures

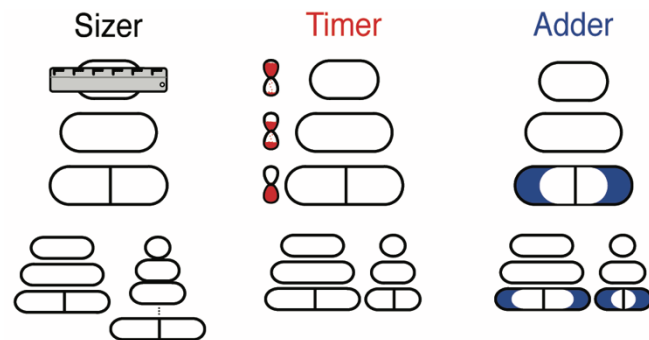


Figure 1. Schematic of three competing cell division control models.

According to the *sizer* model, cells divide after reaching a predetermined size (ruler). In the *timer* model, cells divide after a certain amount of time has elapsed since their birth, following an internal clock (hourglass). In the *adder* model, cells must add a certain fixed amount of volume (blue area) before they divide, independent of their birth size. The contrasting behaviors of a large cell and a small cell are depicted for each scenario. No specific single-cell growth model is assumed.

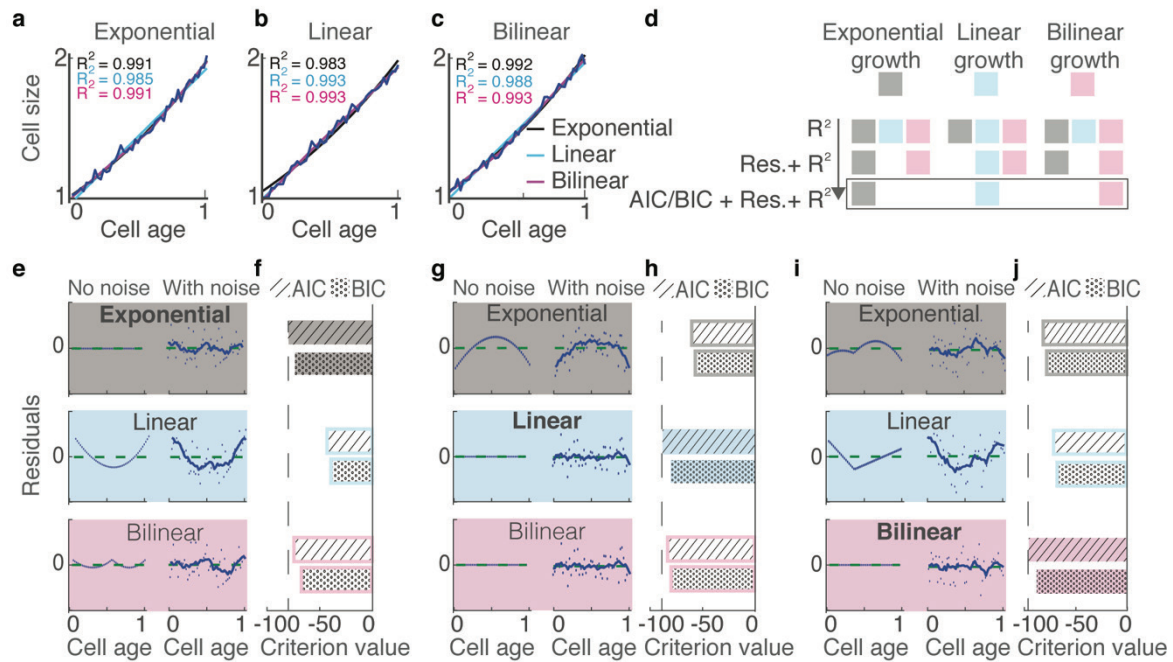


Figure 2. Single-cell growth models can be distinguished by analysis of residuals and AIC/BIC criteria.

(a-c) Fitting of single-cell growth curves at steady-state from a true exponential **(a)**, true linear **(b)**, or true bilinear **(c)** model with added Gaussian noise (standard deviation of 2%). The adjusted r^2 values are very similar for the three fitted models. **(d)** Summary of the model selection using different criteria. Only the combination of r^2 , residuals, and AIC/BIC accurately selects the true model. **(e,g,i)** Residual analysis for all of the fittings of a true exponential **(e)**, true linear **(g)**, or true bilinear **(i)** growth curve fitted with exponential, linear, and bilinear models. The residuals obtained by comparing the true model and the fitted models are shown without (left) or with (right) added noise. The moving average considering sequences of seven values is shown. A good model shows no pattern in the distribution of residuals. **(f,h,j)** AIC and BIC use the principle of parsimony to select the best model by discriminating against models that are too complex. The lowest value is associated with the best model.

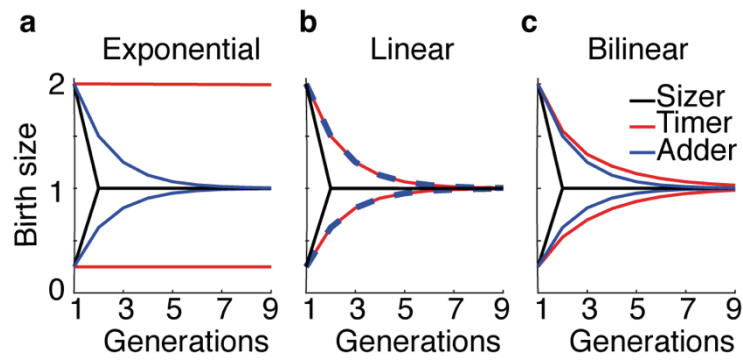


Figure 3. Outlier cells converge on the steady-state birth size at different speeds depending on the single-cell growth and division control models.

The number of generations required for outlier cells to give rise to progeny cells that have a steady-state size at birth defined as “1” depends on the true division control model as well as the true single-cell growth model. **(a-c)** The three division control models considered here are shown in black (*sizer*), red (*timer*), and blue (*adder*). Single-cell growth models were modelled for exponential growth **(a)**, linear growth **(b)**, and bilinear growth **(c)**. Two outlier cells, one small (0.25 times the steady-state birth size of 1) and one large (2 times the steady-state birth size of 1), are shown in each case. See also Figure S2.

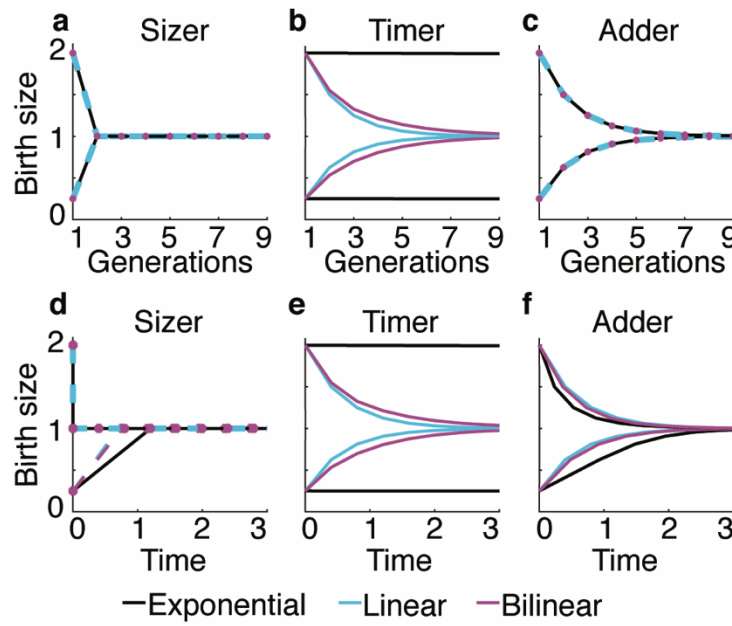


Figure 4. Single-cell growth models can be distinguished by the convergence of outlier cells on the steady-state birth size as a function of time.

In the example shown here, two outlier cells, one small (0.25 times the steady-state birth size of 1) and one large (2 times the steady-state birth size of 1), were simulated. Convergence of these outliers on the steady-state birth size is plotted as a function of generations (**a-c**) or time (**d-f**). Single-cell growth is exponential (black lines), linear (blue lines), or bilinear (pink lines). The timing of cell division was determined according to a *sizer* model (**a,d**), a *timer* model (**b,e**), or an *adder* model (**c,f**). When convergence is plotted as a function of generations (**a-c**), the speed of convergence is equivalent for all single-cell growth models when division is controlled by a *sizer* (**a**) or an *adder* (**c**), but the speed of convergence is different for each single-cell growth model under a *timer* (**b**). When convergence is plotted as a function of time (**d-f**), the speed of convergence can be differentiated for all combinations of single-cell growth models and division control models. These distinctions are blurred by addition of noise, and a “pure” *sizer* is unrealistic for large outlier cells, which divide immediately after birth with no time for DNA replication. See also Figure S3.

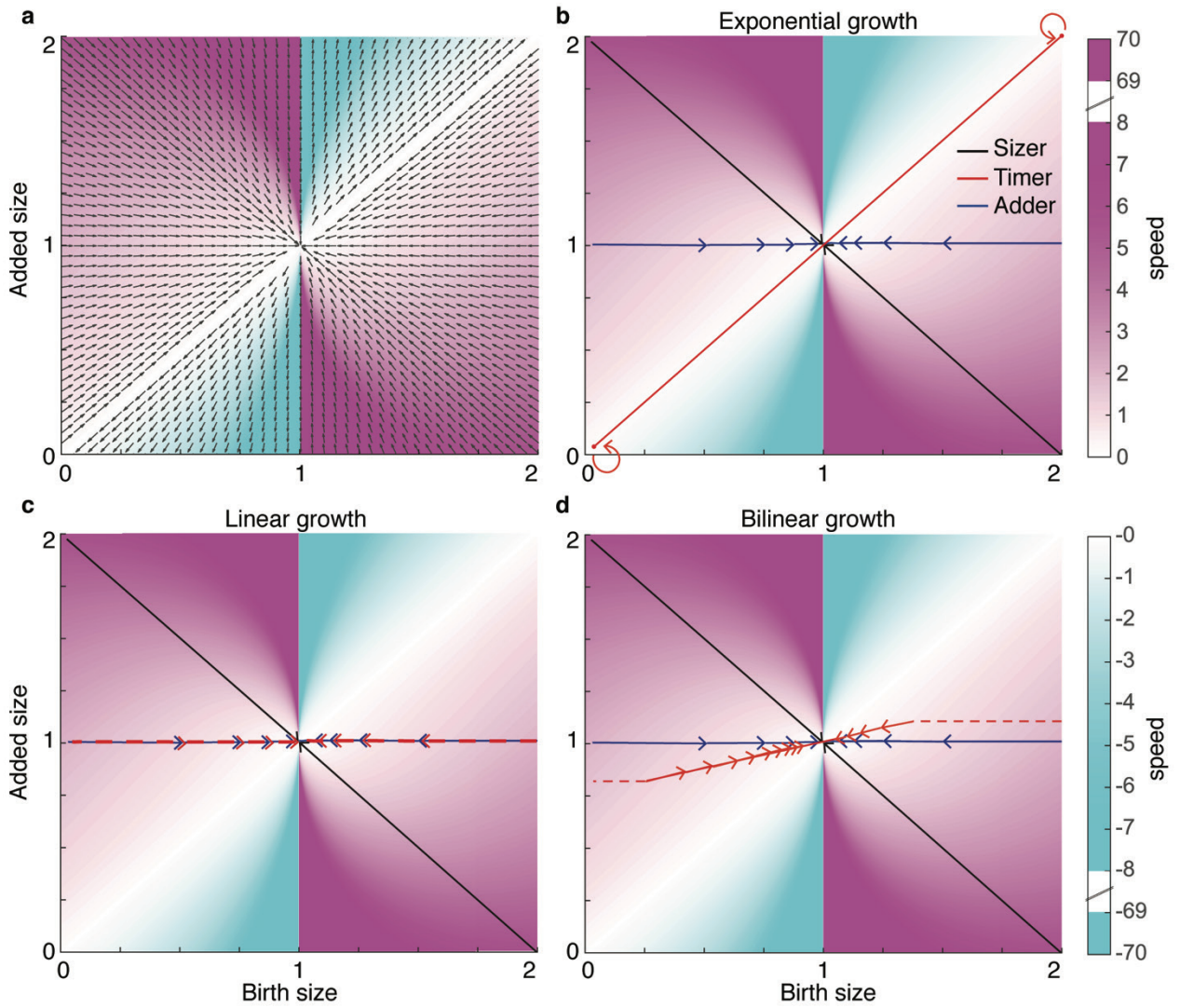


Figure 5. Vector fields of birth size vs. added size show that the speed of convergence of outlier cells towards the equilibrium point depends on both the division control and single-cell growth models.

(a-d) Plots of birth size versus added size show that the correlation between them depends on the underlying single-cell growth and division control and models. Superimposition of vector fields on these plots shows the speed of convergence (in arbitrary units per generation) of outlier cells towards the equilibrium point (1,1). **(a)** Diverging regions of the vector field, where large cells grow larger and small cells grow smaller at every generation, are shown in cyan. Converging regions of the field are shown in magenta. The arrows representing the trajectory of birth size from generation to generation are pointing away from (diverging) or towards (converging) the equilibrium point. Increasing speed of divergence or convergence is indicated by darkening color. Simulated cells are born at specific points on the vector field and follow growth paths (direct trajectory toward the equilibrium point) before the next division following an *adder*, *sizer*, or *timer* model. **(b-d)** Under an *adder* model (blue lines), a cell born at a size $2v$, twice bigger than the equilibrium size ($1v$), grows by $1v$. The cell then divides to generate two daughter cells of $1.5v$, which then grow by $1v$. Consequently,

daughter cells in the next generation will be $1.25v$ at birth. Subsequent generations approach the equilibrium birth size of $1v$ following a horizontal trajectory, independent of the single-cell growth model. Under a *sizer* model (black lines), a cell born at $2v$ in size will not grow, thus giving rise to two daughter cells of $1v$ in size. In this case, the equilibrium birth size is reached within one generation, independent of the single-cell growth model. Under a *timer* model (red lines), the paths approaching the equilibrium point are different depending on whether a cell grows exponentially **(b)**, linearly **(c)**, or bilinearly **(d)**. If cells grow exponentially and double their size during a cell cycle, all mother and daughter cells will retain the same size at birth. This scenario occurs in the white regions of the graphs, where the rate of convergence and divergence is zero. However, this situation becomes unstable if Equation 4 is not satisfied (due to asymmetric division, variable growth rate, or other sources of noise), in which case cells will fall into the unstable region and grow either larger or smaller in successive generations. With linear growth, the trajectory is the same as with an *adder*. When growth is bilinear, the slope is between 0 and 1 and depends on the point when the increase of growth velocity occurs between birth and division.

5.6 Supporting Information

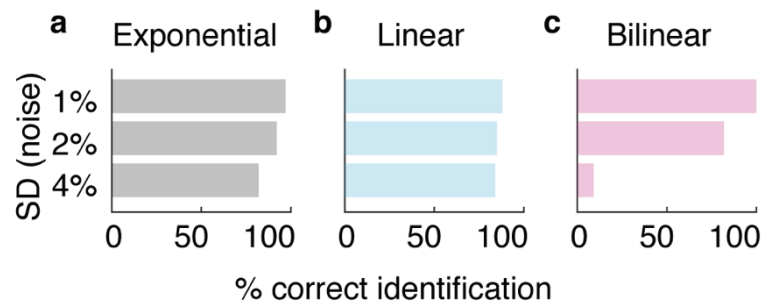


Figure S1. Experimental noise limits the discriminatory power of residual analysis and BIC to differentiate between single-cell growth models.

Correct identification of the true single-cell growth model as **(a)** exponential, **(b)** linear, or **(c)** bilinear, amongst the three fitted models of single-cell growth, becomes less accurate with increasing Gaussian noise of 1%, 2%, or 4% standard deviation (SD). Each bar is the result of 100 simulations of a noisy single-cell growth curve and its identification as belonging to the correct growth model.

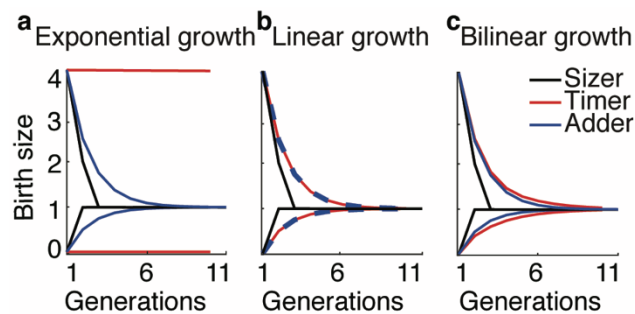


Figure S2. Outlier cells converge on the steady-state birth size at different speeds depending on the single-cell growth and division control models (related to Figure 3).

In the example shown here, two outlier cells were simulated: one small (0.01 times the steady-state birth size of 1) and one large (4 times the steady-state birth size of 1).

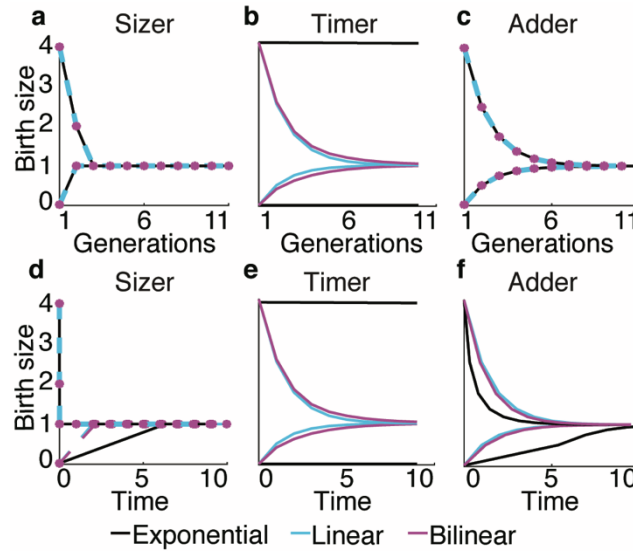


Figure S3. Single-cell growth models can be distinguished by the convergence of outlier cells on the steady-state birth size as a function of time (related to Figure 4).

In the example shown here, two outlier cells were simulated: one small (0.01 times the steady-state birth size of 1) and one large (4 times the steady-state birth size of 1).

5.7 Acknowledgements

We are grateful to Paul Murima, Alexandre Persat, Viesturs Simanis, Virginie Uhlmann, and Yuichi Wakamoto for helpful discussions and feedback. This work was funded in part by a grant to J.D.M. from the Swiss National Science Foundation (310030B_176397).

5.8 Author contributions

G.V. and J.D.M. conceived the project. G.V. created and implemented the models, performed the simulations, and interpreted the results. G.V. and A.V. generated the vector field plots. G.V., N.D., and J.D.M. wrote the paper. N.D. and J.D.M. supervised the project. All authors commented on the manuscript and approved the paper.

5.9 Conflict of Interest

The authors declare no conflict of interest

5.10 References

- [1] K. D. Young, *Microbiol. Mol. Biol. Rev.* **2006**, *70*, 660.
- [2] M. B. Ginzberg, R. Kafri, M. Kirschner, *Science* **2015**, *348*, 1245075.
- [3] R. A. Daniel, J. Errington, *Cell* **2003**, *113*, 767.(Daniel and Errington, 2003)
- [4] S. Baumgartner, I. M. Tolic-Norrelykke, *Biophys. J.* **2009**, *96*, 4336.
- [5] J. M. Mitchison, P. Nurse, *J. Cell Sci.* **1985**, *75*, 357.
- [6] A. Horvath, A. Racz-Monus, P. Buchwald, A. Sveiczer, *Fems Yeast Res.* **2013**, *13*, 635.
- [7] Á. Sveiczer, A. Horváth, *Curr. Genet.* **2017**, *63*, 165.(Sveiczer and Horváth, 2017)
- [8] S. Cooper, *Microbiol.-Uk* **1998**, *144*, 263.
- [9] M. Schaechter, J. P. Williamson, J. R. Hood, A. L. Koch, *Microbiology*, **1962**, *29*, 421.
- [10] S. Iyer-Biswas, C. S. Wright, J. T. Henry, K. Lo, S. Burov, Y. Lin, G. E. Crooks, S. Crosson, A. R. Dinner, N. F. Scherer, *Proc Natl Acad Sci U A* **2014**, *111*, 15912.
- [11] M. Mir, Z. Wang, Z. Shen, M. Bednarz, R. Bashir, I. Golding, S. G. Prasanth, G. Popescu, *Proc Natl Acad Sci U A* **2011**, *108*, 13124.
- [12] H. E. Kubitschek, *Biophys. J.* **1968**, *8*, 792.
- [13] H. E. Kubitschek, *J. Theor. Biol.* **1970**, *28*, 15.
- [14] H. E. Kubitschek, *J. Bacteriol.* **1981**, *148*, 730.
- [15] M. Godin, F. F. Delgado, S. Son, W. H. Grover, A. K. Bryan, A. Tzur, P. Jorgensen, K. Payer, A. D. Grossman, M. W. Kirschner, S. R. Manalis, *Nat. Methods* **2010**, *7*, 387.
- [16] P. A. Fantes, P. Nurse, *Division Timing: Controls, Models and Mechanisms*, Cambridge University Press, Cambridge, **1981**.
- [17] S. Jun, S. Taheri-Araghi, *Trends Microbiol* **2015**, *23*, 4.
- [18] J. T. Sauls, D. Li, S. Jun, *Curr Opin Cell Biol* **2016**, *38*, 38.
- [19] L. Willis, K. C. Huang, *Nat. Rev. Microbiol.* **2017**, *15*, 606.
- [20] M. Campos, I. V. Surovtsev, S. Kato, A. Paintdakhi, B. Beltran, S. E. Ebmeier, C. Jacobs-Wagner, *Cell* **2014**, *159*, 1433.
- [21] M. Deforet, D. van Ditmarsch, J. B. Xavier, *Biophys J* **2015**, *109*, 521.
- [22] I. Soifer, L. Robert, A. Amir, *Curr Biol* **2016**, *26*, 356.
- [23] S. Taheri-Araghi, S. Bradde, J. T. Sauls, N. S. Hill, P. A. Levin, J. Paulsson, M. Vergassola, S. Jun, *Curr. Biol.* **2015**, *25*, 385.

- [24] D. Chandler-Brown, K. M. Schmoller, Y. Winetraub, J. M. Skotheim, *Curr. Biol.* **2017**, 27, 2774.
- [25] C. Cadart, S. Monnier, J. Grilli, P. J. Sáez, N. Srivastava, R. Attia, E. Terriac, B. Baum, M. Cosentino-Lagomarsino, M. Piel, *Nat. Commun.* **2018**, 9, 3275.
- [26] A. Sveiczer, B. Novak, J. M. Mitchison, *J. Cell Sci.* **1996**, 109, 2947.
- [27] M. M. Logsdon, P.-Y. Ho, K. Papavinasasundaram, K. Richardson, M. Cokol, C. M. Sasseti, A. Amir, B. B. Aldridge, *Curr. Biol. CB* **2017**, 27, 3367.
- [28] P. Nurse, *Nature* **1975**, 256, 547.
- [29] M. Delarue, D. Weissman, O. Hallatschek, *PLOS ONE* **2017**, 12, e0182633.
- [30] S. Di Talia, J. M. Skotheim, J. M. Bean, E. D. Siggia, F. R. Cross, *Nature* **2007**, 448, 947.
- [31] M. Osella, E. Nugent, M. Cosentino Lagomarsino, *Proc Natl Acad Sci U A* **2014**, 111, 3431.
- [32] H. Zheng, P.-Y. Ho, M. Jiang, B. Tang, W. Liu, D. Li, X. Yu, N. E. Kleckner, A. Amir, C. Liu, *Proc. Natl. Acad. Sci.* **2016**, 113, 15000.
- [33] J. J. Tyson, O. Diekmann, *J. Theor. Biol.* **1986**, 118, 405.
- [34] R. J. Harvey, A. G. Marr, P. R. Painter, *J. Bacteriol.* **1967**, 93, 605.
- [35] J. J. Tyson, K. B. Hannsgen, *J. Math. Biol.* **1985**, 22, 61.
- [36] G. I. Bell, E. C. Anderson, *Biophys. J.* **1967**, 7, 329.
- [37] E. Trucco, G. I. Bell, *Bull. Math. Biophys.* **1970**, 32, 475.
- [38] G. I. Bell, *Biophys. J.* **1968**, 8, 431.
- [39] F. J. Anscombe, J. W. Tukey, *Technometrics* **1963**, 5, 141.
- [40] E. Gayawan, *Aust. J. Basic Appl. Sci.* **2009**.
- [41] P. Nurse, P. Thuriaux, *Genetics* **1980**, 96, 627.
- [42] S. S. Justice, D. A. Hunstad, L. Cegelski, S. J. Hultgren, *Nat. Rev. Microbiol.* **2008**, 6, 162.
- [43] M. Schaechter, O. MaalOe, N. O. Kjeldgaard, *J. Gen. Microbiol.* **1958**, 19, 592.
- [44] P. A. Fantes, W. D. Grant, R. H. Pritchard, P. E. Sudbery, A. E. Wheals, *J. Theor. Biol.* **1975**, 50, 213.
- [45] P. E. Sudbery, W. D. Grant, *Exp. Cell Res.* **1975**, 95, 405.
- [46] P. E. Sudbery, W. D. Grant, *J. Cell Sci.* **1976**, 22, 59.
- [47] J. Tyson, G. Garcia-Herdugo, W. Sachsenmaier, *Exp. Cell Res.* **1979**, 119, 87
- [48] N. S. Hill, P. J. Buske, Y. Shi, P. A. Levin, *PLOS Genet.* **2013**, 9, e1003663.

- [49] R. B. Weart, A. H. Lee, A.-C. Chien, D. P. Haeusser, N. S. Hill, P. A. Levin, *Cell* **2007**, *130*, 335.
- [50] K. M. Schmoller, J. M. Skotheim, *Trends Cell Biol.* **2015**, *25*, 793.
- [51] A. A. Amodeo, J. M. Skotheim, *Cold Spring Harb. Perspect. Biol.* **2016**, *8*, a019083.
- [52] A. C. Lloyd, *Cell* **2013**, *154*, 1194.
- [53] W. F. Marshall, *Annu. Rev. Biophys.* **2016**, *45*, 49.
- [54] B. M. C. Martins, A. K. Tooke, P. Thomas, J. C. W. Locke, *Proc. Natl. Acad. Sci.* **2018**, *115*, E11415.
- [55] F. Si, G. Le Treut, J. T. Sauls, S. Vadia, P. A. Levin, S. Jun, *Curr. Biol.* **2019**, *29*, 1760.
- [56] M. B. Ginzberg, N. Chang, H. D'Souza, N. Patel, R. Kafri, M. W. Kirschner, *eLife* **2018**, *7*, e26957.

Conclusion

Despite a general agreement that *M. smegmatis* grows exclusively by insertion of new cell wall material near the cell poles, the exact pattern of pole elongation has been vigorously debated for some time. According to the **unipolar model**, *M. smegmatis* grows exclusively from the old pole, with the new pole initiating growth only after division and separation of the daughter cells (Aldridge et al., 2012). According to the **bipolar model**, both poles grow at equal speed following the separation of daughter cells (Santi et al., 2013). More recently, Hannebelle et al., 2020 proposed a unifying **biphasic model** in which mycobacteria grow in a biphasic manner that resembles the “new end take-off” (NETO) dynamics of fission yeast. According to this model, the lag between cell birth and NETO determines the degree of single-cell growth asymmetry.

In this thesis, we extend the biphasic model by showing that the lag before NETO changes with the cell growth speed and I propose a model where the timing of NETO covaries with the growth speed of the poles to optimize the overall cell growth speed. A consequence of the variability in the timing of NETO is that the pole growth dynamics change as a function of single-cell growth speed and, consequently, the single-cell growth model appears to vary from cell to cell. Thus, single-cell growth can appear to be **monophasic** (only one pole grows between birth and division), **biphasic** (only one pole grows initially but both poles grow following a NETO event), or even **triphasic** (this occurs when a NETO event is delayed until after division of the mother cell, resulting in two NETO events occurring in the same daughter cell). These findings shed light on the variability of the NETO timing and explain the apparent cell-to-cell differences in growth models at the single-cell level, which was previously unexplained.

Our findings are based on the comparison of the NETO timing in cell populations grown in different culture media. However, we also observe a high variability of the NETO timing between individual cells under the same growth condition, and it would be of interest to map the NETO timing with the pole growth speed at the single-cell level in order to generalize the relationship between these two parameters.

In apparent contradiction to our results showing that slow-growing cells have a later NETO than fast-growing cells, it was shown that slower-growing species of mycobacteria, such as *M. tuberculosis*, have an *earlier* NETO (in proportion to the interdivision time) than *M. smegmatis* (Hannebelle et al., 2020). It would be interesting to put these results within the perspective of our finding that the timing of NETO covaries along with the growth speed of the poles to optimize the overall cell growth speed. We speculate that the timing of NETO is dictated by the pole growth speed that is physiologically “allowed” in slow-growing mycobacterial species, which may differ from *M. smegmatis*.

Cell-cycle periods are usually well defined in *M. smegmatis*, with a second cycle of DNA replication often initiating after termination of the previous replication cycle but prior to division when cells are grown in rich medium (Santi et al., 2013). It has been shown that individual cells that are larger than average at birth initiate DNA replication earlier in the cell cycle compared to cells that are smaller than average at birth. It has also been shown that larger cells grow faster than smaller cells (Santi et al., 2013; Logsdon et al., 2017). However, no direct link has been demonstrated at the single-cell level between growth speed and cell cycle progression, neither within a single growth condition nor between different growth conditions.

In this thesis, we show that single-cell growth speed is a good predictor of cell cycle progression. Indeed, cell-cycle progression is similar when comparing cells growing at the same speed under different environmental conditions but different when comparing cells growing at different speeds under the same environmental conditions. We also showed that earlier initiation of DNA replication (due to overexpression of the DnaA initiator protein) leads to an increase in growth speed. The mechanism linking DNA replication and growth speed is currently unknown. It would be interesting to determine whether earlier replication of the ribosomal RNA locus, located near the origin of replication, is responsible for the observed increase in growth speed in cells that initiate replication prematurely, since ribosome activity is commonly thought to be rate-limiting for cell growth in bacteria.

Multifork replication is a well-known phenomenon occurring in fast-growing bacteria in order to allow an interdivision time smaller than the time needed for DNA replication. However, a recent study identified multifork replication events in *M. smegmatis*, which has, on average, an interdivision time longer than the time required for replication of its chromosome (Trojanowski et al., 2017). These findings pose a challenge to the presumed link between fast growth and multifork replication.

By studying multifork replication at the single-cell level, we show in this thesis that multifork replication occurs when the time between successive DNA replication initiation events is shorter than the time required for DNA replication, which may occur even in slowly growing cells with interdivision times exceeding the time required for DNA replication. We were able to increase the frequency of multifork replication experimentally by either decreasing the time between DNA replication initiation events (by engineering cells to overexpress DnaA) or by increasing the time required for DNA replication (by treating cells with hydroxyurea). We also find that multifork replication and interdivision time are linked between generations, inasmuch as cells that undergo multifork replication have normal or longer-than-average interdivision times but give rise to daughters with shorter-than-average interdivision times.

Cell division needs to be spatially and temporally regulated to ensure an equal partitioning of chromosomes to the daughter cells. The FtsZ division ring is thought to be first protein to localize to the future division site and is therefore considered to be the earliest division marker (Monahan et al., 2014). In mycobacteria, this view has been challenged by the

discovery of cell-surface wave troughs, which are inherited from the mother cell and correspond to future division sites (Eskandarian et al., 2017). In this thesis, we show that the DNA replisome and the FtsZ division ring colocalize and that the replisome is an even earlier protein marker for the division site than the FtsZ ring. Mycobacteria lack the Minicell (Min) and nucleoid occlusion (Noc) systems, which ensure that cell division occurs midcell in many other bacteria. How the division site is selected in mycobacteria remains unknown. In this thesis, we show that the replisome and FtsZ ring move together in a biphasic trajectory toward the future division site. In phase I, they move towards the old cell pole at a speed that matches the pole's elongation speed, thereby maintaining a constant distance from the old pole; in phase II, they stop moving and remain stationary until cell division. Their coordinated movement (but not their colocalization) is ParB-dependent, which explains why disruption of ParB results in aberrant division site selection. We propose a model in which ParB-dependent movement of the replisome and division ring ultimately determines the site of cell division.

In future experiments, analysis of the movement of the replisome and division ring should be performed in a ParA-knockout strain. If our hypothesis is correct that their movement during phase I is ParB-dependent but ParA-independent, which would suggest the existence of an as-yet-unidentified linker between ParB and the old cell pole, then tracking of the old pole by the replisome and FtsZ ring during phase I should not be affected by the absence of ParA.

Three main models of division control have been proposed to achieve cell size homeostasis: sizer, timer, and adder. However, few published studies of division control take into account the dynamics of single-cell growth and most assume that single-cell growth is exponential. Using computational simulations, we show in this thesis the importance of knowing the true single-cell growth model before considering any model of division control. For example, we confirm that a timer division control model alone cannot lead to size homeostasis if the single-cell growth model is exponential. Furthermore, we show that timer and adder division control models cannot be distinguished if the single-cell growth model is linear. In addition to linear and exponential single-cell growth models, we consider bilinear growth and verify that cell size homeostasis can be achieved under this single-cell growth model.

The contributions on cell growth, cell cycle progression, and cell division presented in this thesis are summarized in [Figure 1](#).

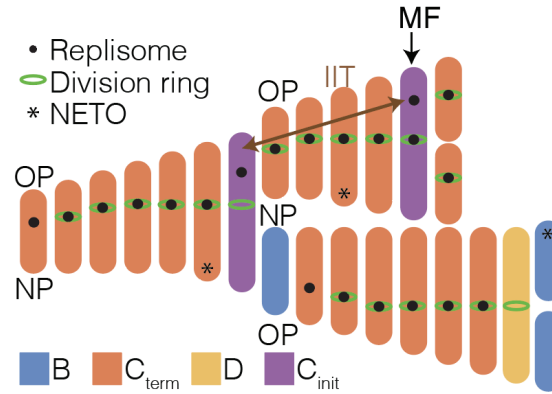


Figure 1. Summary of cell growth, cell cycle progression, and cell division in *M. smegmatis*.

Fast-growing cells execute NETO earlier than slow-growing cells. The timing of NETO results in apparently different single-cell growth models. Fast-growing cells have a faster cell cycle progression (shorter B period, longer C_{init}). Multifork replication (MF) occurs when the inter-initiation time (IIT) is shorter than the C period ($C_{init} + C_{term}$). The replisome and the FtsZ division ring colocalize and move in a biphasic trajectory toward the future division site.

To conclude this thesis, I would like to propose a model that potentially explains cell size in *M. smegmatis*. According to the mathematical definition of cell size (Cell size = length at birth + growth speed * interdivision time), cell size is directly affected by changes in growth speed and interdivision time. Based on this dogma, my hypothesis is that growth speed is more sensitive than interdivision time to nutrient upshifts, which result in a bigger increase in growth speed than decrease in interdivision time (Figure 2a). Likewise, cell size does not change in response to temperature upshifts or downshifts, suggesting an equal effect on growth speed and interdivision time (Figure 2b).

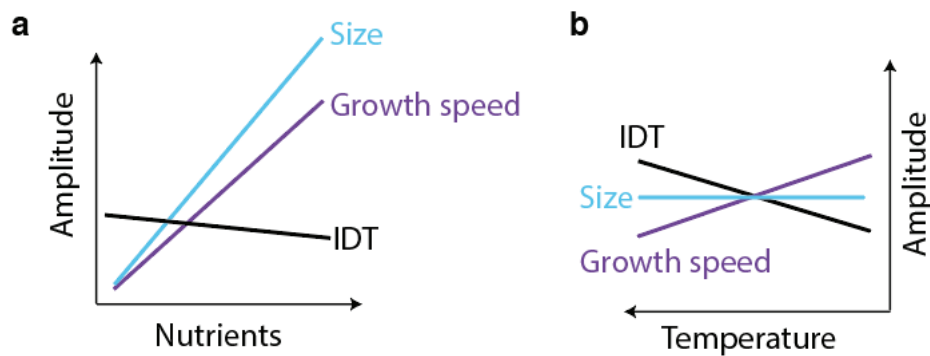


Figure 2. Schematic of cell size dependency on growth speed and interdivision time. Effects of (a) nutrient availability or (b) temperature on interdivision time (IDT), growth speed, and cell size.

In order to understand what the drivers of growth speed and interdivision time are, we illustrate in [Figure 3](#) the possible couplings between nutrients, growth speed, chromosome cycle, and division cycle in *M. smegmatis*. Nutrients from the environment provide energy and building blocks for cellular processes. However, the availability of energy and building blocks *inside* the cell may depend on the single-cell nutrient uptake capacity. Therefore, individuals with a low intrinsic uptake capacity grown in nutrient-rich conditions could potentially have the same intracellular supplies of energy and building blocks as individuals with a high intrinsic uptake capacity grown in nutrient-poor conditions. Thus, cell-to-cell differences in the intracellular levels of energy and building blocks could determine the speed of single-cell growth and cell-cycle progression. It is unlikely that the kinetics of both of these parameters vary equally in response to nutrient changes. However, single-cell growth speed and cell-cycle progression seem to be tightly intertwined, because we showed that single-cell growth speed is a good predictor of the duration of each cell cycle period, and that earlier initiation of DNA replication results in increased growth speed (see chapter 2). Focusing on division-site selection, we showed that DNA replication is linked to cell division by the apparent coupling and coordinated movement of the replisome and the FtsZ division ring. Moreover, it has been shown previously that DNA damage results in delayed cell division ([Erill et al., 2007](#); [Modell et al., 2014](#)) and that blocking initiation of DNA replication blocks cell division ([Dewachter et al., 2018](#)), further suggesting that the chromosome replication/segregation cycle has a direct effect on the timing and position of cell division. Growth speed may also have an effect on the timing of cell division, but whether this effect is direct or indirect is currently unclear, since growth speed and cell-cycle progression are so tightly intertwined at the single-cell level. Assuming a direct link between chromosome cycle, cell-cycle progression, and interdivision time, the relative changes in growth speed and cell-cycle progression in response to environmental changes could also drive changes in cell size.

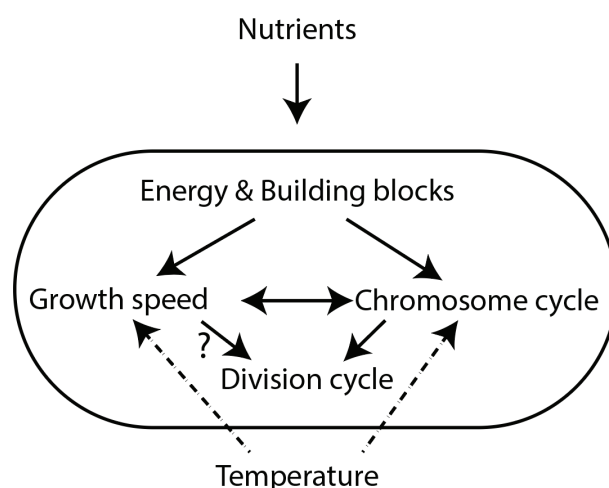


Figure 3. Possible couplings between growth speed, chromosome cycle, and cell division cycle in *M. smegmatis*

In summary, my hypothesis is that cell size is determined by the coupling between growth speed, which controls cell elongation, and the chromosome cycle, which controls cell division. Changes in intracellular levels of energy and building blocks affect the growth speed more than the chromosome cycle, resulting in changes in cell size. Changes in temperature affect the growth speed and the chromosome cycle equally, resulting in unchanged cell size. To further test this hypothesis, I would suggest building a mathematical simulation to test whether this model is able to provide cell size homeostasis under different growth conditions. Furthermore, the relationship between the chromosome cycle and the interdivision time should be assessed in greater detail. For example, do individual cells with similar interdivision times have the same length of the B, C, and D periods? Moreover, it would be interesting to experimentally test the effect of growth speed on both cycles (chromosome cycle and cell division cycle), for example, by limiting the rate of cell wall biosynthesis to slow the rate of cell growth independent of nutrient availability.

References

References

- Adams, D.W., and Errington, J. (2009). Bacterial cell division: assembly, maintenance and disassembly of the Z ring. *Nature Reviews Microbiology* 7, 642–653.
- Adiciptaningrum, A., Osella, M., Moolman, M.C., Lagomarsino, M.C., and Tans, S.J. (2015). Stochasticity and homeostasis in the *E. coli* replication and division cycle. *Scientific Reports* 5, 18261.
- Aldridge, B.B., Fernandez-Suarez, M., Heller, D., Ambravaneswaran, V., Irimia, D., Toner, M., and Fortune, S.M. (2012). Asymmetry and aging of mycobacterial cells lead to variable growth and antibiotic susceptibility. *Science* 335, 100–104.
- Amir, A. (2017). Is cell size a spandrel? *ELife* 6, e22186.
- Amodeo, A.A., and Skotheim, J.M. (2016). Cell-size control. *Cold Spring Harbor Perspectives in Biology* 8, a019083.
- Anscombe, F.J., and Tukey, J.W. (1963). The examination and analysis of residuals. *Technometrics* 5, 141–160.
- Atlung, T., Clausen, E.S., and Hansen, F.G. (1985). Autoregulation of the *dnaA* gene of *Escherichia coli* K12. *Molec. Gen. Genet.* 200, 442–450.
- Avery, S.V. (2006). Microbial cell individuality and the underlying sources of heterogeneity. *Nature Reviews Microbiology* 4, 577–587.
- Badrinarayanan, A., Le, T.B., and Laub, M.T. (2015). Bacterial chromosome organization and segregation. *Annu Rev Cell Dev Biol* 31, 171–199.
- Baumgartner, S., and Tolic-Norrelykke, I.M. (2009). Growth pattern of single fission yeast cells is bilinear and depends on temperature and DNA synthesis. *Biophys J* 96, 4336–4347.
- Bell, G.I. (1968). Cell growth and division: III. conditions for balanced exponential growth in a mathematical model. *Biophysical Journal* 8, 431–444.
- Bell, G.I., and Anderson, E.C. (1967). Cell growth and division. I. A mathematical model with applications to cell volume distributions in mammalian suspension cultures. *Biophys. J.* 7, 329–351.
- Belliveau, N.M., Chure, G., Hueschen, C.L., Garcia, H.G., Kondev, J., Fisher, D.S., Theriot, J.A., and Phillips, R. (2020). Fundamental limits on the rate of bacterial growth. *BioRxiv* 2020.10.18.344382.
- Bennett, M.R., and Hasty, J. (2009). Microfluidic devices for measuring gene network dynamics in single cells. *Nat Rev Genet* 10, 628–638.
- Bisson-Filho, A.W., Hsu, Y.-P., Squyres, G.R., Kuru, E., Wu, F., Jukes, C., Sun, Y., Dekker, C., Holden, S., VanNieuwenhze, M.S., et al. (2017). Treadmilling by FtsZ filaments drives peptidoglycan synthesis and bacterial cell division. *Science* 355, 739–743.

- Botella, H., Yang, G., Ouerfelli, O., Ehrt, S., Nathan, C.F., and Vaubourgeix, J. (2017). Distinct spatiotemporal dynamics of peptidoglycan synthesis between *Mycobacterium smegmatis* and *Mycobacterium tuberculosis*. *MBio* 8, e01183-17.
- Bowman, G.R., Comolli, L.R., Zhu, J., Eckart, M., Koenig, M., Downing, K.H., Moerner, W.E., Earnest, T., and Shapiro, L. (2008). A polymeric protein anchors the chromosomal origin/ParB complex at a bacterial cell pole. *Cell* 134, 945–955.
- Brauer, M.J., Huttenhower, C., Airoidi, E.M., Rosenstein, R., Matese, J.C., Gresham, D., Boer, V.M., Troyanskaya, O.G., and Botstein, D. (2007). Coordination of growth rate, cell cycle, stress response, and metabolic activity in yeast. *MBoC* 19, 352–367.
- Cadart, C., Monnier, S., Grilli, J., Sáez, P.J., Srivastava, N., Attia, R., Terriac, E., Baum, B., Cosentino-Lagomarsino, M., and Piel, M. (2018). Size control in mammalian cells involves modulation of both growth rate and cell cycle duration. *Nature Communications* 9, 3275.
- Campos, M., Surovtsev, I.V., Kato, S., Paintdakhi, A., Beltran, B., Ebmeier, S.E., and Jacobs-Wagner, C. (2014). A constant size extension drives bacterial cell size homeostasis. *Cell* 159, 1433–1446.
- Chandler-Brown, D., Schmoller, K.M., Winetraub, Y., and Skotheim, J.M. (2017). The adder phenomenon emerges from independent control of pre- and post-start phases of the budding yeast cell cycle. *Current Biology* 27, 2774-2783.e3.
- Cooper, S. (1998). Length extension in growing yeast: is growth exponential? Yes. *Microbiol-Uk* 144, 263–265.
- Cooper, S. (2006). Distinguishing between linear and exponential cell growth during the division cycle: single-cell studies, cell-culture studies, and the object of cell-cycle research. *Theoretical Biology & Medical Modelling* 3, 10.
- Cooper, S., and Helmstetter, C.E. (1968). Chromosome replication and the division cycle of *Escherichia coli* B/r. *J. Mol. Biol.* 31, 519–540.
- Dahl, J.L. (2004). Electron microscopy analysis of *Mycobacterium tuberculosis* cell division. *FEMS Microbiology Letters* 240, 15–20.
- Daniel, R.A., and Errington, J. (2003). Control of cell morphogenesis in bacteria. *Cell* 113, 767–776.
- Deforet, M., van Ditmarsch, D., and Xavier, J.B. (2015). Cell-size homeostasis and the incremental rule in a bacterial pathogen. *Biophysical Journal* 109, 521–528.
- Delarue, M., Weissman, D., and Hallatschek, O. (2017). A simple molecular mechanism explains multiple patterns of cell-size regulation. *PLOS ONE* 12, e0182633.
- Delincé, M.J., Bureau, J.-B., López-Jiménez, A.T., Cosson, P., Soldati, T., and McKinney, J.D. (2016). A microfluidic cell-trapping device for single-cell tracking of host–microbe interactions. *Lab on a Chip* 16, 3276–3285.
- Dewachter, L., Verstraeten, N., Fauvart, M., and Michiels, J. (2018). An integrative view of cell cycle control in *Escherichia coli*. *FEMS Microbiology Reviews* 42, 116–136.

- Di Talia, S., Skotheim, J.M., Bean, J.M., Siggia, E.D., and Cross, F.R. (2007). The effects of molecular noise and size control on variability in the budding yeast cell cycle. *Nature* 448, 947–U12.
- Dimude, J.U., Stein, M., Andrzejewska, E.E., Khalifa, M.S., Gajdosova, A., Retkute, R., Skovgaard, O., and Rudolph, C.J. (2018). Origins left, right, and centre: Increasing the number of initiation sites in the *Escherichia coli* chromosome. *Genes (Basel)* 9.
- Donovan, C., Schauss, A., Krämer, R., and Bramkamp, M. (2013). Chromosome segregation impacts on cell growth and division site selection in *Corynebacterium glutamicum*. *PLoS One* 8, e55078.
- Ducet, A., Quardokus, E.M., and Brun, Y.V. (2016). MicrobeJ, a tool for high throughput bacterial cell detection and quantitative analysis. *Nat Microbiol* 1, 16077.
- Duffy, D.C., McDonald, J.C., Schueller, O.J.A., and Whitesides, G.M. (1998). Rapid prototyping of microfluidic systems in poly(dimethylsiloxane). *Anal. Chem.* 70, 4974–4984.
- Ehrenberg, M., Bremer, H., and Dennis, P.P. (2013). Medium-dependent control of the bacterial growth rate. *Biochimie* 95, 643–658.
- Ehrt, S., Guo, X.V., Hickey, C.M., Ryou, M., Monteleone, M., Riley, L.W., and Schnappinger, D. (2005). Controlling gene expression in mycobacteria with anhydrotetracycline and Tet repressor. *Nucleic Acids Research* 33, e21–e21.
- Erill, I., Campoy, S., and Barbé, J. (2007). Aeons of distress: an evolutionary perspective on the bacterial SOS response. *FEMS Microbiology Reviews* 31, 637–656.
- Eskandarian, H.A., Odermatt, P.D., Ven, J.X.Y., Hannebelle, M.T.M., Nievergelt, A.P., Dhar, N., McKinney, J.D., and Fantner, G.E. (2017). Division site selection linked to inherited cell surface wave troughs in mycobacteria. *Nature Microbiology* 2, 17094.
- Eswara, P.J., and Ramamurthi, K.S. (2017). Bacterial cell division: Non-models poised to take the spotlight. *Annu Rev Microbiol* 71, 393–411.
- Fantes, P.A., and Nurse, P. (1981). Division timing: controls, models and mechanisms (Cambridge University Press, Cambridge).
- Fantes, P.A., Grant, W.D., Pritchard, R.H., Sudbery, P.E., and Wheals, A.E. (1975). The regulation of cell size and the control of mitosis. *Journal of Theoretical Biology* 50, 213–244.
- Fazeli, E., Roy, N.H., Follain, G., Laine, R.F., von Chamier, L., Hänninen, P.E., Eriksson, J.E., Tinevez, J.-Y., and Jacquemet, G. (2020). Automated cell tracking using StarDist and TrackMate. *F1000Res* 9.
- Fogel, M.A., and Waldor, M.K. (2021). A dynamic, mitotic-like mechanism for bacterial chromosome segregation. *Genes Dev* 20, 3269–3282.
- Gayawan, E. (2009). A comparison of Akaike, Schwarz and R square criteria for model selection using some fertility models. *Australian Journal of Basic and Applied Sciences*.
- Ginda, K., Bezulska, M., Ziółkiewicz, M., Dziadek, J., Zakrzewska-Czerwińska, J., and Jakimowicz, D. (2013). ParA of *Mycobacterium smegmatis* co-ordinates chromosome

segregation with the cell cycle and interacts with the polar growth determinant DivIVA. *Molecular Microbiology* 87, 998–1012.

Ginda, K., Santi, I., Bousbaine, D., Zakrzewska-Czerwińska, J., Jakimowicz, D., and McKinney, J. (2017). The studies of ParA and ParB dynamics reveal asymmetry of chromosome segregation in mycobacteria. *Molecular Microbiology* 105, 453–468.

Ginzberg, M.B., Kafri, R., and Kirschner, M. (2015). On being the right (cell) size. *Science* 348, 1245075–1245075.

Ginzberg, M.B., Chang, N., D'Souza, H., Patel, N., Kafri, R., and Kirschner, M.W. (2018). Cell size sensing in animal cells coordinates anabolic growth rates and cell cycle progression to maintain cell size uniformity. *ELife* 7, e26957.

Godin, M., Delgado, F.F., Son, S., Grover, W.H., Bryan, A.K., Tzur, A., Jorgensen, P., Payer, K., Grossman, A.D., Kirschner, M.W., et al. (2010). Using buoyant mass to measure the growth of single cells. *Nature Methods* 7, 387–390.

Grant, N.A., Abdel Magid, A., Franklin, J., Dufour, Y., and Lenski, R.E. (2021). Changes in cell size and shape during 50,000 generations of experimental evolution with *Escherichia coli*. *J Bacteriol* 203.

Greendyke, R., Rajagopalan, M., Parish, T., and Madiraju, M.V.V.S. (2002). Conditional expression of *Mycobacterium smegmatis dnaA*, an essential DNA replication gene. *Microbiology*, 148, 3887–3900.

Grigorian, A.V., Lustig, R.B., Guzmán, E.C., Mahaffy, J.M., and Zyskind, J.W. (2003). *Escherichia coli* cells with increased levels of DnaA and deficient in recombinational repair have decreased viability. *J Bacteriol* 185, 630–644.

Hajduk, I.V., Rodrigues, C.D.A., and Harry, E.J. (2016). Connecting the dots of the bacterial cell cycle: Coordinating chromosome replication and segregation with cell division. *Seminars in Cell & Developmental Biology* 53, 2–9.

Hannebelle, M.T.M., Ven, J.X.Y., Toniolo, C., Eskandarian, H.A., Vuaridel-Thurre, G., McKinney, J.D., and Fantner, G.E. (2020). A biphasic growth model for cell pole elongation in mycobacteria. *Nature Communications* 11, 452.

Hansen, M.T., Pato, M.L., Molin, S., Fill, N.P., and von Meyenburg, K. (1975). Simple downshift and resulting lack of correlation between ppGpp pool size and ribonucleic acid accumulation. *J. Bacteriol.* 122, 585–591.

Harvey, R.J., Marr, A.G., and Painter, P.R. (1967). Kinetics of growth of individual cells of *Escherichia coli* and *Azotobacter agilis*. *J Bacteriol* 93, 605–617.

Hendrickson, H., and Lawrence, J.G. (2007). Mutational bias suggests that replication termination occurs near the *dif* site, not at Ter sites. *Molecular Microbiology* 64, 42–56.

Hett, E.C., and Rubin, E.J. (2008). Bacterial growth and cell division: a Mycobacterial perspective. *Microbiology and Molecular Biology Reviews* 72, 126–156.

Hill, N.S., Buske, P.J., Shi, Y., and Levin, P.A. (2013). A moonlighting enzyme links *Escherichia coli* cell size with central metabolism. *PLOS Genetics* 9, e1003663.

- Horvath, A., Racz-Monus, A., Buchwald, P., and Sveicz, A. (2013). Cell length growth in fission yeast: an analysis of its bilinear character and the nature of its rate change transition. *Fems Yeast Res* 13, 635–649.
- Hutchings, M.I., Truman, A.W., and Wilkinson, B. (2019). Antibiotics: past, present and future. *Current Opinion in Microbiology* 51, 72–80.
- Iyer-Biswas, S., Wright, C.S., Henry, J.T., Lo, K., Burov, S., Lin, Y., Crooks, G.E., Crosson, S., Dinner, A.R., and Scherer, N.F. (2014). Scaling laws governing stochastic growth and division of single bacterial cells. *Proceedings of the National Academy of Sciences* 111, 15912–15917.
- Jakimowicz, D., Brzostek, A., Rumijowska-Galewicz, A., Żydek, P., Dołzbłasz, A., Smulczyk-Krawczyszyn, A., Zimniak, T., Wojtasz, Ł., Zawilak-Pawlik, A., Kois, A., et al. (2007). Characterization of the mycobacterial chromosome segregation protein ParB and identification of its target in *Mycobacterium smegmatis*. *Microbiology* 153, 4050–4060.
- Jani, C., Eoh, H., Lee, J.J., Hamasha, K., Sahana, M.B., Han, J.-S., Nyayapathy, S., Lee, J.-Y., Suh, J.-W., Lee, S.H., et al. (2010). Regulation of polar peptidoglycan biosynthesis by Wag31 phosphorylation in mycobacteria. *BMC Microbiol* 10, 327.
- Jensen, R.B., Wang, S.C., and Shapiro, L. (2001). A moving DNA replication factory in *Caulobacter crescentus*. *The EMBO Journal* 20, 4952–4963.
- Jonas, K. (2014). To divide or not to divide: control of the bacterial cell cycle by environmental cues. *Current Opinion in Microbiology* 18, 54–60.
- Joyce, G., Williams, K., Robb, M., Noens, E., Tizzano, B., Shahrezaei, V., and Robertson, B. (2012). Cell division site placement and asymmetric growth in mycobacteria. *PloS One* 7, e44582.
- Jun, S., and Taheri-Araghi, S. (2015). Cell-size maintenance: universal strategy revealed. *Trends in Microbiology* 23, 4–6.
- Jun, S., and Wright, A. (2010). Entropy as the driver of chromosome segregation. *Nat Rev Microbiol* 8, 600–607.
- Jun, S., Si, F., Pugatch, R., and Scott, M. (2018). Fundamental principles in bacterial physiology—history, recent progress, and the future with focus on cell size control: a review. *Rep. Prog. Phys.* 81, 056601.
- Justice, S.S., Hunstad, D.A., Cegelski, L., and Hultgren, S.J. (2008). Morphological plasticity as a bacterial survival strategy. *Nature Reviews Microbiology* 6, 162.
- Kaiser, M., Jug, F., Julou, T., Deshpande, S., Pfohl, T., Silander, O.K., Myers, G., and van Nimwegen, E. (2018). Monitoring single-cell gene regulation under dynamically controllable conditions with integrated microfluidics and software. *Nat Commun* 9.
- Kang, C.-M., Nyayapathy, S., Lee, J.-Y., Suh, J.-W., and Husson, R.N. (2008). Wag31, a homologue of the cell division protein DivIVA, regulates growth, morphology and polar cell wall synthesis in mycobacteria. *Microbiology* 154, 725–735.
- Katayama, T., Ozaki, S., Keyamura, K., and Fujimitsu, K. (2010). Regulation of the replication cycle: conserved and diverse regulatory systems for DnaA and *oriC*. *Nature Reviews Microbiology* 8, 163–170.

- Kawalek, A., Wawrzyniak, P., Bartosik, A.A., and Jagura-Burdzy, G. (2020). Rules and exceptions: the role of chromosomal ParB in DNA segregation and other cellular processes. *Microorganisms* 8.
- Kieser, K.J., and Rubin, E.J. (2014). How sisters grow apart: mycobacterial growth and division. *Nat Rev Microbiol* 12, 550–562.
- Koc, A., Wheeler, L.J., Mathews, C.K., and Merrill, G.F. (2004). Hydroxyurea arrests DNA replication by a mechanism that preserves basal dNTP pools. *Journal of Biological Chemistry* 279, 223–230.
- Kois-Ostrowska, A., Strzałka, A., Lipietta, N., Tilley, E., Zakrzewska-Czerwińska, J., Herron, P., and Jakimowicz, D. (2016). Unique function of the bacterial chromosome segregation machinery in apically growing *Streptomyces* - targeting the chromosome to new hyphal tubes and its anchorage at the tips. *PLOS Genetics* 12, e1006488.
- Kubitschek, H.E. (1968). Linear cell growth in *Escherichia coli*. *Biophysical Journal* 8, 792–804.
- Kubitschek, H.E. (1970). Evidence for the generality of linear cell growth. *Journal of Theoretical Biology* 28, 15–29.
- Kubitschek, H.E. (1981). Bilinear cell growth of *Escherichia coli*. *Journal of Bacteriology* 148, 730–733.
- Kuru, E., Velocity Hughes, H., Brown, P.J., Hall, E., Tekkam, S., Cava, F., de Pedro, M.A., Brun, Y.V., and VanNieuwenhze, M.S. (2012). In situ probing of newly synthesized peptidoglycan in live bacteria with fluorescent D-amino acids. *Angew Chem Int Ed Engl* 51, 12519–12523.
- Lane, N. (2015). The unseen world: reflections on Leeuwenhoek (1677) “Concerning little animals.” *Philos Trans R Soc Lond B Biol Sci* 370.
- Lemon, K.P., and Grossman, A.D. (2000). Movement of replicating DNA through a stationary replisome. *Molecular Cell* 6, 1321–1330.
- Levin, P.A., and Angert, E.R. (2015). Small but mighty: Cell size and bacteria. *Cold Spring Harb Perspect Biol* 7, a019216.
- Lewin, G.R., Carlos, C., Chevrette, M.G., Horn, H.A., McDonald, B.R., Stankey, R.J., Fox, B.G., and Currie, C.R. (2016). Evolution and ecology of *Actinobacteria* and their bioenergy applications. *Annual Review of Microbiology* 70, 235–254.
- Lloyd, A.C. (2013). The regulation of cell size. *Cell* 154, 1194–1205.
- Løbner-Olesen, A., Skarstad, K., Hansen, F.G., von Meyenburg, K., and Boye, E. (1989). The DnaA protein determines the initiation mass of *Escherichia coli* K-12. *Cell* 57, 881–889.
- Lock, R.L., and Harry, E.J. (2008). Cell-division inhibitors: new insights for future antibiotics. *Nature Reviews Drug Discovery* 7, 324–338.
- Locke, J.C.W., and Elowitz, M.B. (2009). Using movies to analyse gene circuit dynamics in single cells. *Nat Rev Microbiol* 7, 383–392.

- Logsdon, M.M., and Aldridge, B.B. (2018). Stable regulation of cell cycle events in mycobacteria: insights from inherently heterogeneous bacterial populations. *Front. Microbiol.* 9.
- Logsdon, M.M., Ho, P.-Y., Papavinasasundaram, K., Richardson, K., Cokol, M., Sassetti, C.M., Amir, A., and Aldridge, B.B. (2017). A parallel adder coordinates mycobacterial cell-cycle progression and cell-size homeostasis in the context of asymmetric growth and organization. *Curr. Biol.* 27, 3367–3374.e7.
- Mahone, C.R., and Goley, E.D. (2020). Bacterial cell division at a glance. *Journal of Cell Science* 133.
- Marshall, W.F. (2016). Cell geometry: how cells count and measure size. *Annual Review of Biophysics* 45, 49–64.
- Martins, B.M.C., Tooke, A.K., Thomas, P., and Locke, J.C.W. (2018). Cell size control driven by the circadian clock and environment in cyanobacteria. *PNAS* 115, E11415–E11424.
- Meniche, X., Otten, R., Siegrist, M.S., Baer, C.E., Murphy, K.C., Bertozzi, C.R., and Sassetti, C.M. (2014). Subpolar addition of new cell wall is directed by DivIVA in mycobacteria. *Proc Natl Acad Sci U S A* 111, E3243–E3251.
- Messer, W. (2002). The bacterial replication initiator DnaA. DnaA and oriC, the bacterial mode to initiate DNA replication. *FEMS Microbiol Rev* 26, 355–374.
- Mir, M., Wang, Z., Shen, Z., Bednarz, M., Bashir, R., Golding, I., Prasanth, S.G., and Popescu, G. (2011). Optical measurement of cycle-dependent cell growth. *Proceedings of the National Academy of Sciences of the United States of America* 108, 13124–13129.
- Mitchison, J.M. (2003). Growth during the cell cycle. *Int. Rev. Cytol.* 226, 165–258.
- Mitchison, J.M. (2005). Single cell studies of the cell cycle and some models. *Theor Biol Med Model* 2, 4.
- Mitchison, J.M., and Nurse, P. (1985). Growth in cell length in the fission yeast *Schizosaccharomyces pombe*. *Journal of Cell Science* 75, 357–376.
- Modell, J.W., Kambara, T.K., Perchuk, B.S., and Laub, M.T. (2014). A DNA damage-induced, SOS-independent checkpoint regulates cell division in *Caulobacter crescentus*. *PLoS Biol* 12.
- Monahan, L.G., Liew, A.T.F., Bottomley, A.L., and Harry, E.J. (2014). Division site positioning in bacteria: one size does not fit all. *Front. Microbiol.* 5.
- Moriya, S., Rashid, R.A., Rodrigues, C.D.A., and Harry, E.J. (2010). Influence of the nucleoid and the early stages of DNA replication on positioning the division site in *Bacillus subtilis*. *Molecular Microbiology* 76, 634–647.
- Murray, H., and Koh, A. (2014). Multiple regulatory systems coordinate DNA replication with cell growth in *Bacillus subtilis*. *PLOS Genetics* 10, e1004731.
- Nurse, P. (1975). Genetic control of cell size at cell division in yeast. *Nature* 256, 547–551.
- Nurse, P., and Thuriaux, P. (1980). Regulatory genes controlling mitosis in the fission yeast *Schizosaccharomyces pombe*. *Genetics* 96, 627.

- Odermatt, P.D., Hannebelle, M.T.M., Eskandarian, H.A., Nievergelt, A.P., McKinney, J.D., and Fantner, G.E. (2020). Overlapping and essential roles for molecular and mechanical mechanisms in mycobacterial cell division. *Nat Phys* 16, 57–62.
- Osella, M., Nugent, E., and Cosentino Lagomarsino, M. (2014). Concerted control of *Escherichia coli* cell division. *Proceedings of the National Academy of Sciences of the United States of America* 111, 3431–3435.
- de Pedro, M.A., Quintela, J.C., Höltje, J.V., and Schwarz, H. (1997). Murein segregation in *Escherichia coli*. *J Bacteriol* 179, 2823–2834.
- Pióro, M., Małecki, T., Portas, M., Magierowska, I., Trojanowski, D., Sherratt, D., Zakrzewska-Czerwińska, J., Ginda, K., and Jakimowicz, D. (2019). Competition between DivIVA and the nucleoid for ParA binding promotes segrosome separation and modulates mycobacterial cell elongation. *Molecular Microbiology* 111, 204–220.
- Ptacin, J.L., Gahlmann, A., Bowman, G.R., Perez, A.M., von Diezmann, A.R.S., Eckart, M.R., Moerner, W.E., and Shapiro, L. (2014). Bacterial scaffold directs pole-specific centromere segregation. *Proc Natl Acad Sci U S A* 111, E2046–2055.
- van Raaphorst, R., Kjos, M., and Veening, J.-W. (2017). Chromosome segregation drives division site selection in *Streptococcus pneumoniae*. *Proc Natl Acad Sci U S A* 114, E5959–E5968.
- Reyes-Lamothe, R., Possoz, C., Danilova, O., and Sherratt, D.J. (2008). Independent positioning and action of *Escherichia coli* replisomes in live cells. *Cell* 133, 90–102.
- Reyrat, J.-M., and Kahn, D. (2001). *Mycobacterium smegmatis*: an absurd model for tuberculosis? *Trends in Microbiology* 9, 472–473.
- Riber, L., Olsson, J.A., Jensen, R.B., Skovgaard, O., Dasgupta, S., Marinus, M.G., and Løbner-Olesen, A. (2006). Hda-mediated inactivation of the DnaA protein and *dnaA* gene autoregulation act in concert to ensure homeostatic maintenance of the *Escherichia coli* chromosome. *Genes Dev.* 20, 2121–2134.
- Rothfield, L., Taghbalout, A., and Shih, Y.-L. (2005). Spatial control of bacterial division-site placement. *Nature Reviews Microbiology* 3, 959–968.
- Rowlett, V.W., and Margolin, W. (2015). The Min system and other nucleoid-independent regulators of Z ring positioning. *Front. Microbiol.* 6.
- Santi, I., and McKinney, J.D. (2015). Chromosome organization and replisome dynamics in *Mycobacterium smegmatis*. *MBio* 6, e01999-14.
- Santi, I., Dhar, N., Bousbaine, D., Wakamoto, Y., and McKinney, J.D. (2013). Single-cell dynamics of the chromosome replication and cell division cycles in mycobacteria. *Nature Communications* 4, 2470.
- Sargent, M.G. (1975). Control of cell length in *Bacillus subtilis*. *Journal of Bacteriology* 123, 7–19.
- Sauls, J.T., Li, D., and Jun, S. (2016). Adder and a coarse-grained approach to cell size homeostasis in bacteria. *Current Opinion in Cell Biology* 38, 38–44.

- Schaechter, M., MaalOe, O., and Kjeldgaard, N.O. (1958). Dependency on medium and temperature of cell size and chemical composition during balanced growth of *Salmonella typhimurium*. *Journal of General Microbiology* 19, 592–606.
- Schaechter, M., Williamson, J.P., Hood, J.R., and Koch, A.L. (1962). Growth, cell and nuclear divisions in some Bacteria. *Microbiology*, 29, 421–434.
- Schaus, N., O'Day, K., Peters, W., and Wright, A. (1981). Isolation and characterization of amber mutations in gene *dnaA* of *Escherichia coli* K-12. *J Bacteriol* 145, 904–913.
- Schmoller, K.M., and Skotheim, J.M. (2015). The biosynthetic basis of cell size control. *Trends in Cell Biology* 25, 793–802.
- Si, F., Le Treut, G., Sauls, J.T., Vadia, S., Levin, P.A., and Jun, S. (2019). Mechanistic origin of cell-size control and homeostasis in bacteria. *Current Biology* 29, 1760-1770.e7.
- Singh, B., Nitharwal, R.G., Ramesh, M., Pettersson, B.M.F., Kirsebom, L.A., and Dasgupta, S. (2013). Asymmetric growth and division in *Mycobacterium* spp.: compensatory mechanisms for non-medial septa. *Molecular Microbiology* 88, 64–76.
- Skarstad, K., and Katayama, T. (2013). Regulating DNA replication in bacteria. *Cold Spring Harb Perspect Biol* 5.
- Soifer, I., Robert, L., and Amir, A. (2016). Single-cell analysis of growth in budding yeast and bacteria reveals a common size regulation strategy. *Current Biology: CB* 26, 356–361.
- Sudbery, P.E., and Grant, W.D. (1975). The control of mitosis in *Physarum polycephalum*: The effect of lowering the DNA: Mass ratio by UV irradiation. *Experimental Cell Research* 95, 405–415.
- Sudbery, P.E., and Grant, W.D. (1976). The control of mitosis in *Physarum polycephalum*: The effect of delaying mitosis and evidence for the operation of the control mechanism in the absence of growth. *Journal of Cell Science* 22, 59–65.
- Su'etsugu, M., and Errington, J. (2011). The replicase sliding clamp dynamically accumulates behind progressing replication forks in *Bacillus subtilis* cells. *Molecular Cell* 41, 720–732.
- Sveiczer, Á., and Horváth, A. (2017). How do fission yeast cells grow and connect growth to the mitotic cycle? *Curr Genet* 63, 165–173.
- Sveiczer, A., Novak, B., and Mitchison, J.M. (1996). The size control of fission yeast revisited. *Journal of Cell Science* 109, 2947–2957.
- Sveiczer, Á., Horváth, A., and Buchwald, P. (2014). Is there a universal rule for cellular growth? – Problems in studying and interpreting this phenomenon. *FEMS Yeast Research* 14, 679–682.
- Taheri-Araghi, S., Bradde, S., Sauls, J.T., Hill, N.S., Levin, P.A., Paulsson, J., Vergassola, M., and Jun, S. (2015). Cell-size control and homeostasis in bacteria. *Current Biology* 25, 385–391.
- Thanbichler, M., and Shapiro, L. (2006). MipZ, a spatial regulator coordinating chromosome segregation with cell division in *Caulobacter*. *Cell* 126, 147–162.

- Thanky, N.R., Young, D.B., and Robertson, B.D. (2007). Unusual features of the cell cycle in mycobacteria: Polar-restricted growth and the snapping-model of cell division. *Tuberculosis* 87, 231–236.
- Trojanowski, D., Ginda, K., Pióro, M., Hołowka, J., Skut, P., Jakimowicz, D., and Zakrzewska-Czerwińska, J. (2015). Choreography of the *Mycobacterium* replication machinery during the cell cycle. *MBio* 6, e02125-14.
- Trojanowski, D., Hołowka, J., Ginda, K., Jakimowicz, D., and Zakrzewska-Czerwińska, J. (2017). Multifork chromosome replication in slow-growing bacteria. *Scientific Reports* 7, 43836.
- Trucco, E., and Bell, G.I. (1970). A note on the dispersionless growth law for single cells. *Bulletin of Mathematical Biophysics* 32, 475–483.
- Trueba, F.J., van Spronsen, E.A., Traas, J., and Woldringh, C.L. (1982). Effects of temperature on the size and shape of *Escherichia coli* cells. *Arch. Microbiol.* 131, 235–240.
- Tyson, J.J., and Diekmann, O. (1986). Sloppy size control of the cell division cycle. *J. Theor. Biol.* 118, 405–426.
- Tyson, J.J., and Hannsgen, K.B. (1985). Global asymptotic stability of the size distribution in probabilistic models of the cell cycle. *J. Math. Biology* 22, 61–68.
- Tyson, J., Garcia-Herdugo, G., and Sachsenmaier, W. (1979). Control of nuclear division in *Physarum polycephalum*: Comparison of cycloheximide pulse treatment, UV irradiation, and heat shock. *Experimental Cell Research* 119, 87–98.
- Vadia, S., and Levin, P.A. (2015). Growth rate and cell size: a re-examination of the growth law. *Current Opinion in Microbiology* 24, 96–103.
- Ven, J.X.Y. (2019). Single-cell studies of *Mycobacterium smegmatis* cell cycle using time-lapse fluorescence microscopy. *Ecole Polytechnique Fédérale de Lausanne*.
- Viollier, P.H., Thanbichler, M., McGrath, P.T., West, L., Meewan, M., McAdams, H.H., and Shapiro, L. (2004). Rapid and sequential movement of individual chromosomal loci to specific subcellular locations during bacterial DNA replication. *Proc Natl Acad Sci U S A* 101, 9257–9262.
- Vuaridel-Thurre, G., Vuaridel, A.R., Dhar, N., and McKinney, J.D. (2020). Computational analysis of the mutual constraints between single-cell growth and division control models. *Advanced Biosystems* 4, 1900103.
- Wakamoto, Y., Dhar, N., Chait, R., Schneider, K., Signorino-Gelo, F., Leibler, S., and McKinney, J.D. (2013). Dynamic persistence of antibiotic-stressed *Mycobacteria*. *Science* 339, 91–95.
- Walker, B.E., Männik, J., and Männik, J. (2020). Transient membrane-linked FtsZ assemblies precede Z-Ring formation in *Escherichia coli*. *Current Biology* 30, 499-508.e6.
- Wallden, M., Fange, D., Lundius, E.G., Baltekin, Ö., and Elf, J. (2016). The synchronization of replication and division cycles in individual *E. coli* cells. *Cell* 166, 729–739.
- Wang, J.D., and Levin, P.A. (2009). Metabolism, cell growth and the bacterial cell cycle. *Nature Reviews Microbiology* 7, 822–827.

- Weart, R.B., Lee, A.H., Chien, A.-C., Haeusser, D.P., Hill, N.S., and Levin, P.A. (2007). A metabolic sensor governing cell size in bacteria. *Cell* 130, 335–347.
- Weitzman, J.B. (2003). Growing without a size checkpoint. *J Biol* 2, 3.
- Westfall, C.S., and Levin, P.A. (2017). Bacterial cell size: multifactorial and multifaceted. *Annual Review of Microbiology* 71, 499–517.
- Willis, L., and Huang, K.C. (2017). Sizing up the bacterial cell cycle. *Nature Reviews Microbiology* 15, 606–620.
- Winder, F.G., and Barber, D.S. (1973). Effects of hydroxyurea, nalidixic acid and zinc limitation on DNA polymerase and ATP-dependent deoxyribonuclease activities of *Mycobacterium smegmatis*. *J. Gen. Microbiol.* 76, 189–196.
- Witz, G., van Nimwegen, E., and Julou, T. (2019). Initiation of chromosome replication controls both division and replication cycles in *E. coli* through a double-adder mechanism. *ELife* 8, e48063.
- Woong Park, S., Klotzsche, M., Wilson, D.J., Boshoff, H.I., Eoh, H., Manjunatha, U., Blumenthal, A., Rhee, K., Barry, C.E., Aldrich, C.C., et al. (2011). Evaluating the sensitivity of *Mycobacterium tuberculosis* to Biotin Deprivation Using Regulated Gene Expression. *PLoS Pathog* 7.
- Wu, L.J., and Errington, J. (2012). Nucleoid occlusion and bacterial cell division. *Nature Reviews Microbiology* 10, 8–12.
- Xu, Y.-C., and Bremer, H. (1988). Chromosome replication in *Escherichia coli* induced by oversupply of DnaA. *Mol Gen Genet* 211, 138–142.
- Young, K.D. (2006). The selective value of bacterial shape. *Microbiol Mol Biol Rev* 70, 660–703.
- Zheng, H., Ho, P.-Y., Jiang, M., Tang, B., Liu, W., Li, D., Yu, X., Kleckner, N.E., Amir, A., and Liu, C. (2016). Interrogating the *Escherichia coli* cell cycle by cell dimension perturbations. *PNAS* 113, 15000–15005.

Curriculum Vitae

Gaëlle Vuaridel-Thurre

| | | | |
|----------------------|-----------------------------------|--------------|-------------------------|
| Address | Route de Cossonay 39, 1008 Prilly | Email | gaelle.thurre@gmail.com |
| Nationality | Swiss | Phone | 079 275 36 48 |
| Date of Birth | September 22nd, 1989 | | |

About me

My strengths are in data analysis, data visualization and synthetic thinking. My interests lie in finding trends and models to describe data and design experiments accordingly.

Academic Record

| | |
|----------------|--|
| 2015 - present | PhD in Bioengineering , Laboratory of Microbiology and Microsystems, Global Health Institute, Prof. J. D. McKinney, Swiss Federal Institute of Technology (EPFL), Lausanne. Including teaching duties in biology, chemical biology and probability and statistics. <i>Coordination between growth, division and chromosome replication cycles in mycobacteria.</i> |
| 2013 - 2015 | MSc in Bioengineering , (EPFL) Grade 5.60/6. Mention of Excellence. <u>Master Project</u> : <i>Development of a microfluidic device for culture and observation of fission yeast cell division.</i> Co-supervised by Prof. P. Renaud and by Prof. V. Simanis. <u>Semester Project</u> : <i>Stochastic Growth Models of the Influenza Virus.</i> Supervised by Prof. J. D. Jensen. |
| 2009 - 2013 | BSc in Life Science and Technologies , (EPFL) Grade: 4.98/6. <u>Bachelor Project</u> : <i>Geometry reconstruction and computational fluid dynamics from 3D MRI datasets of the human aorta.</i> Supervised by Prof N. Stergiopoulos (EPFL). |
| 2004 - 2008 | Gymnasial maturity in Economy and Law , Collège Claparède, Genève. |

Scientific Background & Skills

- **Data management**: Data analysis, statistics, pattern & trend identification, modelling.
- **Programming**: Matlab, Javascript, C++, R.
- **Informatics**: MS office, Illustrator, Prism, ImageJ.
- **Microscopy**: long-term time-lapse microscopy with live cells.
- **Cell handling**: *Mycobacterium smegmatis*, *Schizosaccharomyces pombe*.
- **Microfluidics**: PDMS chip design and fabrication.

Professional Experience

| | |
|-------------------|---|
| Summer 2014 | Internship at Debiopharm Development of a custom-made database to help traceability. |
| 2013 - 2014 | Co-founder of STIL (Salon des Technologies et de l'Innovation de Lausanne) Management of three people in the logistic section. Communication with the exhibitors. |
| Summers 2011 & 12 | Internship at the Center of Phenogenomics (EPFL) Maintenance and welfare of mouse lines. |
| 2008 - 2009 | Desk helper at Prest Services Info (9 months full-time) Taught me hard work and scrupulosity. Funded 6 months in Australia to improve my English skills. |

Publications

- **Computational analysis of the mutual constraints between single-cell growth and division control models**, Vuaridel-Thurre G, Vuaridel AR, Dhar N, McKinney JD. Adv. Biosyst. 2020;4(2):1900103.
- **A biphasic growth model for cell pole elongation in mycobacteria**, Hannebelle MTM, Ven JXY, Toniolo C, Eskandarian HA, Vuaridel-Thurre G, McKinney JD & Fantner GE. Nat Commun. 2020 Jan 23;11(1):452.

Project supervision

| | |
|------|---|
| 2019 | Studying the impact of growth rate variation on “new end take-off” (NETO) dynamics in mycobacteria. Aimie Dulac (bachelor student in Life Sciences), Bachelor project. |
| 2016 | A two-piecewise regression model for bacterial growth. Kenneth Nguyen (bachelor student in Mathematics), summer project. |

Languages

| | |
|----------------|----------------------------------|
| French | Native |
| English | Full professional proficiency |
| German | Limited professional proficiency |

Personal Interests

Sewing, mushroom hunting, gardening, renovate my house with my husband but most importantly, accompany my two daughters in their discovery of the world.